2015

TRANSIENT THERMOELECTRIC SUPERCOOLING: ISOSCELES CURRENT PULSES FROM A RESPONSE SURFACE PERSPECTIVE AND THE PERFORMANCE EFFECTS OF PULSE COOLING A HEAT GENERATING MASS

Alfred Piggott
Michigan Technological University, ajpiggot@mtu.edu

TRANSIENT THERMOELECTRIC SUPERCOOLING: ISOSCELES CURRENT PULSES FROM A RESPONSE SURFACE PERSPECTIVE AND THE PERFORMANCE EFFECTS OF PULSE COOLING A HEAT GENERATING MASS

By

Alfred J. Piggott III

A THESIS

Submitted in partial fulfillment of the requirements for the degree of

MASTER OF SCIENCE

In Mechanical Engineering

MICHIGAN TECHNOLOGICAL UNIVERSITY

2015

This thesis has been approved in partial fulfillment of the requirements for the Degree of MASTER OF SCIENCE in Mechanical Engineering.

Department of Mechanical Engineering – Engineering Mechanics

Thesis Advisor: *Prof. Jeffrey S. Allen*

Committee Member: *Prof. Craig Friedrich*

Committee Member: *Dr. Douglas T. Crane*

Department Chair: *Dr. William Predebon*

Dedication

To my family

Thank you for very patiently waiting for the completion of this work.

Contents

List of Figures

List of Tables

Acknowledgments

I would like to thank my advisor, Professor Jeffery S. Allen. Professor Allen provided a wealth of knowledge, kept me on the right track, provided a formidable challenge and maintained confidence throughout this exciting project.

I would also like to thank Dr. Douglas T. Crane. Dr. Crane provided encouragement, a great deal of expertise in thermoelectrics, a detailed eye and many thought provoking and interesting ideas for future work.

Nomenclature

`.ic`	Syntax for an initial condition in LTSPICE
`.op`	Syntax for a SPICE directive in LTSPICE
`.param`	Syntax used in LTSPICE to crease variables
α	Seebeck coefficient for a thermocouple
α_n	Seebeck coefficient for an n thermoelement
α_p	Seebeck coefficient for an p thermoelement
ΔT	Difference in temperature between the hot side of the couple and the cold side
ΔT_{max}	Maximum temperature difference that can be sustained across a thermoelectric cooler at steady state operating conditions
$\Delta T_{postpulse}$	Maximum temperature difference that can be sustained across a thermoelectric cooler after a current pulse
ΔT_{Pulse}	Maximum temperature difference that can be sustained across a thermoelectric cooler during a current pulse
$\dot{Q}_h$	Rate of heat released at the hot side of a thermoelectric device
$\dot{Q}_{\text{Conductance}}$	Amount of heat transferred through a thermoelement due to thermal conduction from the hot side to the cold side
$\dot{Q}_{Joule}$	Amount of heat transferred to the hot or cold side due to internal Joule heating in the thermoelement
$\dot{Q}_{Peltier}$	Amount of heat absorbed by the cold side of the device due to Peltier cooling
$\dot{W}_n$	Rate of work / Power input to the thermoelectric device
ρ	Electrical resistivity of the thermoelement
ρ	Density of the thermoelement
1D	One dimensional
2D	Two dimensional
3D	Three dimensional
A	Heat transfer area where the mass, heatsink or insulation contacts ambient air

A	Cross sectional area normal to heat flow in a thermoelement
A_t	Area of a thermoelement normal to current flow multiplied by two
A_{yz}	Area normal to heat flow in x-direction of a thermoelement
ANSYS	Analysis System
C_p	Specific heat capacity
C_{th}PerSegment	Total thermal capacitance of the thermoelement divided by the number of segments in the model
C_{th2}	Total thermal capacitance of the thermoelement divided by 2
C_{th4}	Total thermal capacitance of the thermoelement divided by 4
CapAluminaCold	Thermal capacitance of the alumina on the cold side of the module per capacitor
CapAluminaHot	Thermal capacitance of the alumina on the hot side of the module per capacitor
CapCopperCold	Thermal capacitance of the copper interconnects on the cold side per capacitor
CapCopperHot	Thermal capacitance of the copper interconnects on the hot side per capacitor
CapInsul	Thermal capacitance of the insulation per capacitor
CapMass	Thermal capacitance of the mass per capacitor
CapSpread	Thermal capacitance of the heat spreader per capacitor
COP	Coefficient of performance
GreaseContactResistanceCold	Interface resistance of the grease per resistor between the grease and the alumina and grease and mass on the cold side.
GreaseContactResistanceHot	Interface resistance of the grease per resistor between the grease and the alumina on the hot side.
h	Convective heat transfer coefficient
HeatGen	Heat generation per node in the mass
I	Electrical current
$I_{\max}$	Electrical current at ΔT_{max}
I_{opt}	Electrical current at max Q_c

$I_{optimal}$	Electrical current at max Q_c
I_P	Max electrical current during a current pulse
InsulContact	Interface resistance per resistor between the mass and the insulation
k	thermal conductivity
K	thermal conductance
k_x	thermal conductivity of the mass in the x-direction
L	Thermoelement Length
L_x	length of the mass in the x-direction
LTSPICE	Linear Technology Simulation Program With Integrated Circuit Emphasis
n	N-type semiconductor
N	Number of couples
$N_{parastrings}$	Number of parallel strings of resistors in a mass model
n-type	N-type semiconductor
NumberOfSegments	the number of "finite elements" in the model
p	P-type semiconductor
P	Ratio of peak electrical current during a pulse to electrical current I_{max}
P_{in}	Power / Rate or work input to a thermoelectric device
p-type	P-type semiconductor
PWL	Piecewise Linear
Q_c	Heat absorbed by the cold side of a thermoelectric device
Q_{max}	Heat absorbed at the cold side of a thermoelectric device while operating at I_{opt}
Q_{pc}	Heat absorbed by the cold side of a thermoelectric device due to Peltier cooling
Q_{ph}	Heat released by the hot side of a thermoelectric device due to Peltier heating
R	electrical resistance of the thermoelement
$R_{convection}$	Thermal resistance due to convection
R_m	Electrical resistance of the couple or module
R_{th}	Total thermal resistance of the thermoelement
R_{th2}	Thermal resistance per resistor in the thermoelement model
$R_{thermalx}$	Thermal resistance on the mass in the x-direction

RConInBottom	Thermal convection resistance on the bottom of the insulation per resistor
RConInFac	Thermal convection resistance on the vertical face of the insulation per resistor
RConInSide	Thermal convection resistance on the vertical side of the insulation per resistor
RConInTop	Thermal convection resistance on the top of the insulation per resistor
RconvecMassBottom	Thermal convection resistance on the bottom on the mass per resistor
RconvecMassSide	Thermal convection resistance on the side of the mass per resistor
RconvecMassTop	Thermal convection resistance on the top of the mass per resistor
RConvSpreadBottom	Thermal convection resistance on the bottom of the spreader per resistor
RConvSpreadSide	Thermal convection resistance on the side of the heat spreader per resistor
RConvSpreadTop	Thermal convection resistance on the top of the heat spreader per resistor
RCopperCold	Thermal resistance per resistor of the copper on the cold side
RCopperHot	Thermal resistance per resistor of the copper on the hot side
reltol	SPICE accuracy control
RInsulX	Thermal resistance of the insulation in the x direction per resistor
RInsulY	Thermal resistance of the insulation in the y direction per resistor
RInsulZ	Thermal resistance of the insulation in the z direction per resistor
RinterconnectCold	Thermal resistance of the copper interconnect on the cold side per resistor
RinterconnectHot	Thermal resistance of the copper interconnect on the hot side per resistor

RmassX	Thermal resistance of the mass in the x direction per resistor
RmassY	Thermal resistance of the mass in the y direction per resistor
RmassZ	Thermal resistance of the mass in the z direction per resistor
RmPerSegment	Per segment electrical resistance
RSolderCold	Thermal resistance per resistor of the solder on the cold side
RSolderHot	Thermal resistance per resistor of the solder on the hot side.
RspreadX	Thermal resistance of the heat spreader in the x direction per resistor
RspreadY	Thermal resistance of the heat spreader in the y direction per resistor
RspreadZ	Thermal resistance of the heat spreader in the z direction per resistor
S	Seebeck coefficient
S_m	Module or couple level Seebeck coefficient
SinkCnt	Thermal interface resistance between the heat sink and the mass per resistor
SPICE	Simulation Program with Integrated Circuit Emphasis
T_c	Temperature at the cold side of the device
T_h	Temperature at the hot side of the device
t_{return}	The time required for T_c to return to where it started after a current pulse is started
TINA	Toolkit for Interactive Network Analysis
TRM	Time to Reach Minimum temperature
V	Volts
V_{max}	Voltage at I_{max}
Z	Thermoelectric material figure of merit
Z_m	Thermoelectric material figure of merit
ZT	Thermoelectric dimensionless material figure of merit

Abstract

With increased public interest in protecting the environment, scientists and engineers aim to improve energy conversion efficiency. Thermoelectrics offer many advantages as thermal management technology. When compared to vapor compression refrigeration, above approximately 200 to 600 watts, cost in dollars per watt as well as COP are not advantageous for thermoelectrics. The goal of this work was to determine if optimized pulse supercooling operation could improve cooling capacity or efficiency of a thermoelectric device. The basis of this research is a thermal-electrical analogy based modeling study using SPICE. Two models were developed. The first model, a standalone thermocouple with no attached mass to be cooled. The second, a system that includes a module attached to a heat generating mass. With the thermocouple study, a new approach of generating response surfaces with characteristic parameters was applied. The current pulse height and pulse on-time was identified for maximizing Net Transient Advantage, a newly defined metric. The corresponding pulse height and pulse on-time was utilized for the system model. Along with the traditional steady state starting current of I_{max}, I_{opt} was employed. The pulse shape was an isosceles triangle. For the system model, metrics new to pulse cooling were Q_c, power consumption and COP. The effects of optimized current pulses were studied by changing system variables. Further studies explored time spacing between pulses and temperature distribution in the thermoelement. It was found net Q_c over an entire pulse event can be improved over I_{max} steady operation but not over steady I_{opt} operation. Q_c can be improved over I_{opt} operation but only during the early part of the pulse event. COP is reduced in transient pulse operation due to the different time constants of Q_c and P_{in}. In some cases lower performance interface materials allow more Q_c and better COP during transient operation than higher performance interface materials. Important future work might look at developing innovative ways of biasing Joule heat to T_h.

Chapter 1. Introduction

1.1 Introduction and Motivation

Thermoelectric devices are solid state heat pumps. These devices are used in a range of automotive heated and cooled products that include temperature controlled seats, cup holders and mini refrigerators. Recent research has investigated integration of thermoelectric modules into hybrid vehicle battery packs for distributed thermal management [1] as well as using thermoelectric devices for zonal HVAC heating and cooling [2]. There are also a wide range of non-automotive thermoelectric applications like medical thermal therapy devices [3], electronic kiosk coolers [4], and electronics and CPU cooling applications [5].

Advantages of using thermoelectric devices include heating and cooling from the same unit, precise temperature control within 0.01 °C, ability to cool to temperatures below ambient, COP greater than one during heating mode, ability to provide spot cooling, no moving parts, high reliability, silent operation, mountable in any orientation and no fluorocarbon usage.

Thermoelectric coolers have cooling capacities as low as 0.15 watts [6]. There is no upper threshold. However, above 200 to 600 watts [1, 7] a better mix of cost and efficiency is available from vapor compression refrigeration. It should be noted, this is a generalization and depends on the value of the benefits relative to cost and efficiency. If higher amounts of thermoelectric cooling could be achieved at the same or lower than the present cost, all of the benefits of thermoelectric cooling could be obtained for use in a broader range of higher cooling power applications.

The majority of the effort to improve thermoelectric device performance is focused on materials research. Complimentary research activities may provide additional performance enhancement. One such complimentary research path is pulsed current thermoelectric device operation.

Commercial thermoelectric devices operate on steady state DC current and steady state operation has been studied extensively. The body of literature for transient pulsed current operation is much smaller. A key finding in regard to pulsed current studies is the ability to achieve colder temperatures for a short time than those possible during steady current operation. In transient studies this temperature reduction is called Supercooling. In studies that use a square wave current pulse, supercooling

is always followed by a period of superheating that has a temperature increase greater than the temperature reduction in supercooling. The duration of the superheating event is longer than the supercooling event. Therefore, the average temperature during a transient pulse event is higher than the temperature during steady current operation. Manno et al. [8] observed an isosceles triangle shaped current pulse and reported that the advantage during supercooling was greater than the penalty during superheating. This observation suggests that a greater transient supercooling advantage exists and therefore there is an implied advantage of using transient operation. The average temperature of the cold side will be lower than during steady current operation. Therefore cooling capacity could be increased by operating a device with continuous isosceles shaped current pulses.

Chapter 2. Background

Thermoelectric coolers are solid-state heat pumps. These heat pumps utilize the thermoelectric effect. The thermoelectric effect is direct conversion of electric current to a temperature difference and vice versa. The former is used for heating and cooling which is the main focus of this paper. The latter is used in thermoelectric generators [9, 10] for power generation. The thermoelectric effect is a generalized term that comprises three different effects. These effects are, the Peltier effect, the Seebeck effect and the Thomson effect [11].

In 1834 Jean Peltier discovered what we now call the Peltier effect. When two different metals are connected at one point, called a junction, and a voltage difference is applied across the free ends of the metals, current flow in the metals induces cooling at the junction. Current flow in the opposite direction induces heating at the junction [11].

In 1821,Thomas Seebeck [12] discovered when two dissimilar metals were connected end to end and then the free ends also connected to each other, a magnetic field appeared when one of the junctions was heated. At the time, Seebeck called this the thermomagnetic effect because a nearby compass would deflect during the experiment. It was later discovered, the heating had induced a current, then by Amperes law induced a magnetic field. This direct conversion of heat into electricity is called the Seebeck effect.

In 1854, William Thomson (later Lord Kelvin), discovered what is known as the Thomson effect. The Thomson effect takes place in a circuit made of a single material. When an electrical current travels through a circuit that has a temperature gradient changing in the direction of current flow, heat will be absorbed or released by the material. The direction of heat flow is dependent on if the current is flowing from hot to cold or cold to hot [13]. Although the Thomson effect is important in very detailed calculations, in typical calculations it is negligible [14]. Lord Kelvin, also discovered that the Peltier, Seebeck and Thomson effect were all manifestations of one effect that can be characterized by the Seebeck coefficient [15].

Thermoelectric devices are currently used in a range of automotive heated and cooled products that include temperature controlled seating [16], cup holders and mini in-vehicle refrigerators, [17]. Home and office products include small refrigerators [18], mattresses [19] and office chairs [20]. These devices are also used in medical products

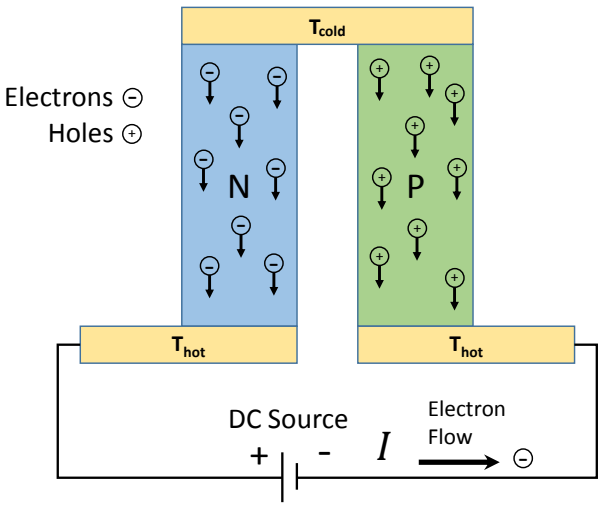

Figure 2.1. Thermocouple

that provide thermal therapy [3]. Thermoelectric air conditioners maintain enclosure temperatures for many different industries like medical, hazardous environment, telecommunications, health care, military, laboratory, outdoor kiosk, and electronics cooling [4]. Recent research has focused on use of these devices for hybrid vehicle battery thermal management [1] and zonal heating and cooling of passenger vehicles [2].

Thermoelectric devices of today use semiconductors and provide much higher heating and cooling performance than the metals studied by Peltier, Seebeck and Thomson. The higher performance is due to a more advantageous mix of material properties over metals.

The construction of a thermoelectric device begins with a semiconductor couple as shown in Figure 2.1. A couple consists of one p-type and one n-type semiconductor block connected by metallic strips. These semiconductor blocks are also called thermoelements. The p and n semiconductor blocks are connected electrically in series and thermally in parallel. The metal strip serves as a junction between the two semiconductors. When DC current is passed through the couple, heat is absorbed at the cold side junction and heat is released at the hot side junction, which is opposite the couple. To create a thermoelectric module, many couples are typically placed electrically in series to increase the cooling capacity. Sometime modules connect many couples in parallel or series and parallel to increase cooling capacity. Connecting couples in parallel leads to reduced electrical resistance and increased operating current.

Thermoelectric semiconductor behavior can be explained with charge carrier analysis. In thermoelectric materials, charge carriers are electrons and holes. Electrons carry a negative charge and holes carry a positive charge. In n-type materials, the charge carriers are electrons and in p-type materials, the charge carriers are holes. Holes are empty spaces in a crystal lattice that an electron could occupy. These holes are free to move about within the lattice [21]. When charge carriers move they take heat with them [22]. From a physics standpoint, energy absorbed and liberated can be accounted for by a change in energy level of electrons. Electrons that move to a higher energy level absorb heat and electrons that move to a lower energy level release heat. The material characteristics and polarity of the DC source relative to the p and n arrangement makes possible energy absorption and release in a controlled manner [23].

2.1 Steady State Equations

Equations for steady state cooling performance are well known and understood. The cooling power at T_c for n couples is expressed as

$$\dot{Q}_c = n\left[\alpha T_c I - \left(\frac{1}{2}\right) I^2 R - K\Delta T\right] \tag{2.1}$$

Equation 2.1 can be described as the net impact of the physical processes that make up each of three terms in the equation. The first term is the Peltier term.

$$\dot{Q}_{Peltier} = \alpha T_c I \tag{2.2}$$

In the Peltier term, α is the Seebeck coefficient [V/K] and is defined as

$$\alpha = \alpha_p - \alpha_n\,, \tag{2.3}$$

where α_p and α_n are intrinsic material properties of n-type and p-type materials. N-type materials have a negative Seebeck coefficient and p-type materials have a positive Seebeck coefficient. T_c is the temperature of the cold side of each thermoelement. I is the electric current through the couple. Equation 2.2 describes the amount of cooling power in watts that can be obtained at a given electrical current and cold side temperature from a material of a certain Seebeck coefficient. If equation 2.2 was alone in equation 2.1, cooling power would be linearly proportional to current through the couple and could be increased indefinitely by increasing the current. This is not the case due to the remaining two terms in equation 2.1. The remaining terms have opposite signs of the Peltier term and therefore subtract from the cooling power. See figure 2.3

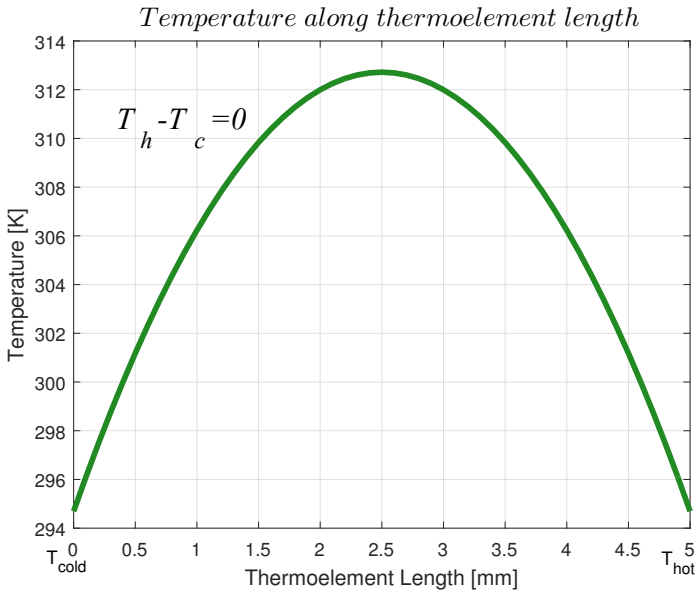

Figure 2.2. Temperature Distribution in a Thermoelement

The second term is the Joule heating term.

$$\dot{Q}_{Joule} = -\left(\frac{1}{2}\right) I^2 R \tag{2.4}$$

I is again the current through couple as it was in the Peltier term. R is the electrical resistance of the couple in units of ohms. R is defined as

$$R = \left(\frac{\rho_p L_p}{A_p}\right) + \left(\frac{\rho_n L_n}{A_n}\right) \tag{2.5}$$

The p and n terms are separated because the material properties differ. In equation 2.5, ρ is the electrical resistivity $[\Omega\, m]$, L is the length of the thermoelement in the direction of current flow [m]. A is the cross sectional area of the thermoelement that is normal to current flow.

The Joule heating term quantifies the rate of volumetric heat generation within the couple. The 1/2 coefficient signifies that half of the heat generated is conducted to the cold side of the couple. The reason half of the conduction moves to the cold side can be explained by thermal conduction and the volumetric nature of the Joule heating. During steady state operation, the temperature gradient between T_h and T_c is an upside down parabola (see figure 2.2) where T_h is the temperature of the hot side of the thermoelement. This places the center of each thermoelement at the maximum temperature of the couple. The driving force for conduction is a temperature gradient and since the temperature difference is the same in either direction from the center

to either end of the thermoelement, one half of the Joule heat conducts to the hot side and one half to the cold side.

In contrast to the Peltier term, current in the Joule heating term is squared. This means that at some level of current, depending on the magnitude of R, α and T_C, the Joule heating term will overtake the Peltier term. By this observation, there will be a maximum current that produces maximum Q_c.

The third term in equation 2.1 is the thermal conductance term. By Fourier's law we have,

$$\dot{Q}_{\text{Conductance}} = -K\left(T_h - T_c\right) \tag{2.6}$$

where K is the thermal conductance [W/K]. K can be calculated using the following equation.

$$K = \left(\frac{k_p A_p}{L_p}\right) + \left(\frac{k_n A_n}{L_n}\right) \tag{2.7}$$

Here k is equal to the thermal conductivity of the p or n-type semiconductor block, A is the cross sectional area normal to heat flow of each block and L is the length of each semiconductor block which is the length that electric current must flow through a single thermoelement.

As in the Joule heating term, the conductance term has negative sign which makes this term parasitic to the Peltier cooling term. If the temperature difference between T_h and T_c is continuously increased, eventually the conductance term will reduce Q_C to zero or negative. Negative represents the direction of heat flow with the thermoelectric cooler turned off.

Equation 2.1 can also be used to help understand desirable semiconductor material properties. Referring to equation 2.1, $\dot{Q}_c$ can be maximized by altering the material properties. Maximizing the Seebeck coefficient α, minimizing the electrical resistivity ρ, and minimizing the thermal conductivity k will increase $\dot{Q}_c$.

When thermoelectric materials are characterized and compared, the thermoelectric figure of merit Z in units of K^{-1} is used.

$$Z = \frac{\alpha^2}{\rho k} \tag{2.8}$$

A higher magnitude of Z represents a material with improved performance. It was seen in equation 2.1 that maximizing α, and minimizing ρ and k improved performance of the couple. This same strategy follows when improving the thermoelectric

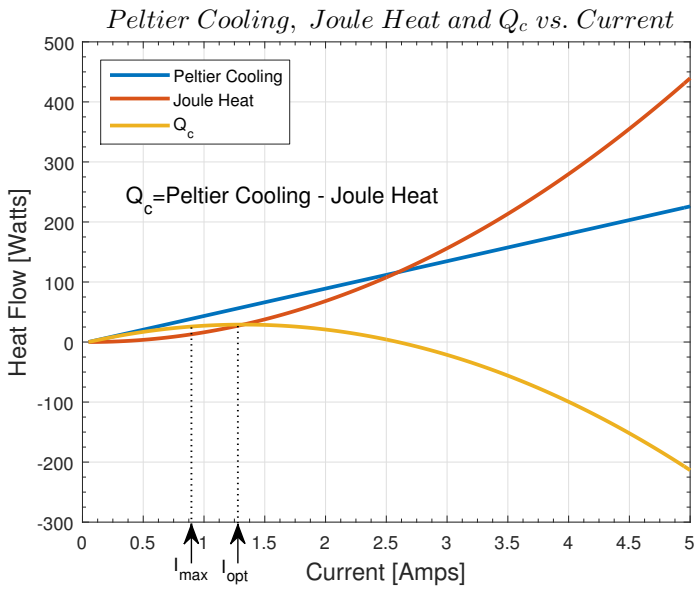

Figure 2.3. Peltier Cooling, Joule Heat and Q_c vs. Current

figure of merit Z in equation 2.8. When the figure of merit is normalized for temperature, it is called ZT. This dimensionless figure of merit is found by multiplying the absolute temperature of the materials during the measurement of properties by the figure of merit Z.

$$ZT = \frac{\alpha^2 T}{\rho k} \tag{2.9}$$

A ZT of 1 is the highest ZT currently commercially available [24]. The highest reported ZT is 3 [25]. High figure of merit materials that have been reported in the last 10 years range from approximately 0.95 to 2.2 [25]. The ZT of seven out of nine of these materials are reported at a temperature much higher than commercial heating and cooling applications. The temperature ranges from 550K to 800K. These materials are intended for high temperature thermoelectric generators. The materials reported at 298K had a ZT of 1.25 and 1.27 [24]. At a ZT of 2, thermoelectric air conditioners may become practical [26]. To match the efficiency of vapor compression air conditioners, ZT would need to be increased to 4 [24].

2.2 Steady State Operating Current

There are two steady state device operating values of current that are of interest for this study. The first is the value of current that generates maximum Q_C. The second is the current that produces maximum ΔT across the thermoelements. The current that produces maximum cooling is slightly higher than the current that produces the maximum temperature difference. See figure 2.3

The naming convention of the two current values of interest vary from reference to reference. For this work, the electrical current that sustains the maximum temperature difference between the hot and the cold side of the device will be called $I_{\max}$. The electrical current that creates maximum Q_C will be called $I_{optimal}$. $I_{optimal}$ will be abbreviated as I_{opt}.

$I_{\max}$ can be characterized with the figure of merit Z, the hot side temperature T_h, the Seebeck coefficient α and the electrical resistance of the couple R as follows.

$$I_{\max} = \frac{\alpha}{R}\left[\left(T_h + \frac{1}{Z}\right)^2 - T_h^2\right]^{1/2} - \frac{1}{Z} \tag{2.10}$$

I_{opt} can be characterized with α, T_h and R.

$$I_{\text{opt}} = \frac{\alpha T_h}{R} \tag{2.11}$$

Here α and R are defined per equation 2.3 and 2.5. Equation 2.5 is valid for a couple or a module as long as all couples in the module are electrically connected in series.

In a similar manner as equation 2.1 that defines the heat absorbed by the cold side ($\dot{Q}_c$) of the thermoelement due to Peltier cooling, equation 2.12 defines the heat released by the hot side ($\dot{Q}_h$) due to Peltier heating.

$$\dot{Q}_h = n\left(\alpha T_h I + \frac{1}{2}I^2 R - K\Delta T\right) \tag{2.12}$$

Thermoelectric devices are heat engines. An energy balance with a boundary around the couple or device gives the rate work done by the power input to the couple or device as follows

$$\dot{W}_n = \dot{Q}_h - \dot{Q}_c \tag{2.13}$$

By substituting equation 2.1 and equation 2.12 into equation 2.13 we have

$$\dot{W}_n = n\Big[\alpha I(T_h - T_c) + I^2 R\Big] \tag{2.14}$$

When cooling is of interest, then the coefficient of performance (COP) is:

$$COP = \frac{\dot{Q}_c}{\dot{W}_n} \tag{2.15}$$

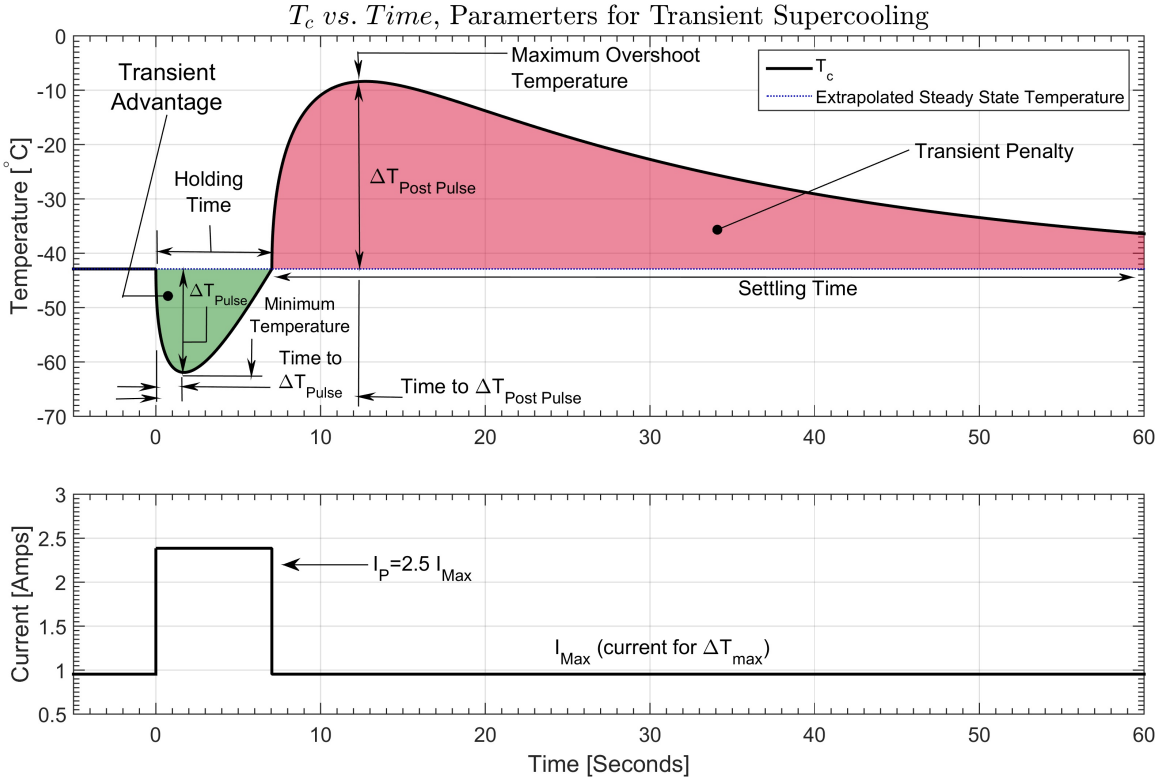

Figure 2.4. Cold side temperature, T_c, During a Transient Pulse (Square Wave)

2.3 The Transient Effect

In the preceding section, it was discussed that there is a steady state operating current that will produce maximum ΔT across the thermoelectric device called $I_{\max}$. Referring to figure 2.4, while operating at this steady current, if a current pulse of magnitude greater than $I_{\max}$ is applied, an instantaneous lower temperature at T_c will be achieved. This is called supercooling. After reaching minimum temperature at the cold side, temperature will start to recover with time back toward the steady state temperature that existed before the current pulse was applied. At the point, T_c returns to the steady state temperature, there is no longer a benefit to continuing the current pulse. The current pulse is turned off. T_c then overshoots the $I_{\max}$ steady temperature and reaches a maximum. After the maximum temperature is reached, T_c exponentially decays back to steady state.

The transient effect occurs when a current pulse greater than the steady state $I_{\max}$ current is applied to a device. This transient supercooling effect happens due to a combination of two different mechanisms; Peltier cooling and Joule heating. Increased Peltier cooling happens instantly and continuously at the junction. Joule heating happens instantly throughout the volume of the thermoelement. The change

in temperature at the cold side due to Joule heat that is delayed by thermal diffusion through the thermoelement.

Snyder et al. [27] defines a method in equation 2.16 to normalize the magnitude of the current pulse with respect to $I_{\max}$. This allows for normalization of pulsed current for different $I_{\max}$ values.

$$P = \frac{I_{\text{pulse}}}{I_{\max}} \tag{2.16}$$

2.4 Previous Transient Operation Observations

The following is a chronological list of previous work found in the literature. The purpose is to serve as a brief historical overview, to help set the context for the originality of work performed herein and show this area of work is still an active and relevant topic. Some of these works are cited later with further direct relevance to the work herein

The early work studied ways to further reduce minimum temperature obtained by a massless couple. Mass loads were later added to couple studies. A basic set of cooling parameters was established. Several applications have been proposed and a move toward module level rather than couple level studies has been seen. A logical next step is optimization work and system level studies that are presented herein. Further details are below.

In 1958 Stilbans and Fedorovich [28] first reported transient pulsed supercooling with a standalone couple.

Early work from 1960 to 1974 [29–34] studied the behavior theoretically and experimentally using a single couple and single pulse with no connected mass.

In the first study of its kind, Field and Blum [35] (1979) researched adding a passive mass load and thermal interface resistance to a single couple with a single pulse.

Twenty two years later in 1999, Miner et al. [36] built and tested a hybrid pulsed massless couple and mechanical device. This device mechanically connected a small mass to the cold side of a couple during supercooling and mechanically disconnected the mass from the couple during superheating. In this way, most of the Joule heat exited the hot side of the couple. The air gap between the mass and the cold side during superheating acted in a sense as a thermal diode. The performance of the device in terms of equivalent ZT value was between 2 and 3. The work herein in

regard to response surfaces can be used to further improve the performance of this device with optimized pulse height and pulse on-time.

Kumar et al. [37] (2000) did experiments with single pulse using thin film devices with attached passive mass. A heat generating mass was used for the work herein.

Snyder et al. [27] (2002) took the approach of establishing a basic set of parameters to describe pulse cooling and the dependencies of each parameter. A linear approximation to the heat equation was derived that describes thermoelectric pulsed transient behavior. The parameters established in this work are used extensively in the work herein.

The first research of transient supercooling from a thermodynamic approach was done by Chakraborty [38] (2006) in which they created a temperature entropy (T-S) diagram for a pulse cooler using Gibbs law.

Another approach to studying transient pulse supercooling was taken by Zhou et al. [39] (2007) by studying inhomogeneous graded thermoelectric materials with pulse cooling.

Gupta et al. [40] (2011) did a computational study of a thin cooler on a chip with heatsink and found single pulse cooling to be effective on removing hot spots.

Shen et al. [41] (2012) used a computational model to study voltage pulses, heat transfer coefficients of the hot side of the device and the impacts of steady cooling load on a passive heat sink.

In most recent research Bezsudnov and Snarskii [42] (2014) studied pulse cooling on a rotating device

Ma [43] (2014) developed a numerical model to investigated the impact of using an off the shelf cooler module with ceramic plates and metal interconnects on each side of the couples with single square wave pulse. The mass connected was very small. The work herein differs because interface resistance, Joule heat generation in the metallic strips, heat generation within the mass, a large mass and an isosceles triangle pulse are used.

Manno et al. [8] (2014) looked at pulse cooling a chip however took the approach of integrating the chip into the cooler by making the chip one of the thermoelements of the cooler. Manno et al. [8] defined the new metrics Transient Advantage and

Transient Penalty. These metrics were extensively used for the work herein.

Shen [44] (2014) investigated a miniature thermoelectric module for pulse laser cooling.

2.5 Characteristic Behavior during Pulsed Current Operation

The behavior of a thermoelement during pulsed current operation is complex. Physical mechanisms and responses of the thermoelement are often referred to by names that are not consistent between journal articles. This section defines the various terms used to describe the physical mechanisms and responses shown in Figure 2.4.

2.5.1 Supercooling

The supercooling event is characterized in different ways in the literature. One characterization is called "Minimum Temperature Achievable", others are "Maximum Temperature Difference" and Pulse Cooling enhancement [8]. Maximum Temperature Difference is also known as ΔT_{pulse} [27].

As mentioned before, operating at steady state $I_{\max}$ produces a steady state temperature difference ΔT_{max}. Often the hot side of the device is constrained by a thermal reservoir. Therefore the cold side temperature will be dependent on the ΔT produced by the device and T_h. This same situation applies to transient operation. The minimum temperature achieved during transient operation will be a function of not only the hot side temperature but the steady state ΔT for which the device was operating prior to the pulse. Different experiments may use different hot side temperatures. They may also use different devices that produce different steady state ΔT_{max}. "Maximum temperature difference", "ΔT_{pulse}" and "Pulse Cooling Enhancement" metrics allow normalization of these factors. "Maximum temperature difference" and "ΔT_{pulse}" are both temperature differences between T_c operating at steady state $I_{\max}$ and T_c at the minimum temperature achieved. "Pulse Cooling Enhancement" is the ratio of T_c at the minimum achievable temperature and T_c at $I_{\max}$.

2.5.2 Time to Reach Minimum Temperature

Time to Reach Minimum Temperature (TRM) is the metric used to describe the amount of time between the start of the transient current pulse and when the minimum temperature (or ΔT_{pulse}) is reached.

2.5.3 Holding Time

Holding Time [8], Time while Cooled [27], and T_{return} [27] are all terms used to describe the amount of time T_c spends below the steady state temperature after the pulse is applied. All of these terms characterize supercooling time. For this work, the term Holding Time will be used

2.5.4 Superheating

Similarly to Supercooling, Superheating is characterized in two different ways. One way is called Maximum Overshoot Temperature [27] and the other $\Delta T_{postpulse}$ [27]. Maximum temperature overshoot happens after a rapid rise in temperature above steady state due to Joule heat reaching the cold side after diffusion through the thermoelement. This is the maximum temperature T_c reaches after the pulse has been turned off. Similarly to ΔT_{pulse}, $\Delta T_{postpulse}$ normalizes the superheating event with respect T_c at $I_{\max}$ steady operation.

2.5.5 Time to Maximum Temperature Overshoot

Time to maximum temperature overshoot is a new metric defined herein as the time required to reach maximum transient temperature starting from time zero at the start of the current pulse.

2.5.6 Settling Time

Settling Time [45] is the time required for T_c to exponentially decay back to the steady state temperature after reaching the holding time after the pulse is switched off. In some cases the pulse is switched off after holding time.

2.5.7 Transient Advantage

Transient advantage [8] combines the metrics of "Minimum Temperature Achieved" and "Holding Time" into to one metric. Transient advantage is defined as the area between two curves. The area can be found by first drawing a straight line extended horizontally for a time period of an entire pulse event at the same temperature as the steady temperature prior to the pulse. Next the area under this straight line is found only for the holding time. Finally, subtract from this the area under the T_c curve during holding time. This difference represents the area between the two curves and is defined as the Transient Advantage.

2.5.8 Transient Penalty

Similarly to Transient Advantage, Transient Penalty [8] combines the metrics of "Maximum Temperature Overshoot" and "Settling Time" into one metric. The straight line used to find transient advantage can also be used to find "Transient Penalty". "Transient Penalty" is defined as the area between this straight line and T_c between the end of Holding time and the end of settling time.

2.5.9 Transient Advantage Over Transient Penalty

Manno et al. [8] defined Advantage Over Penalty as the "Transient Advantage" divided by the "Transient Penalty" to show the relative magnitude of "Transient Advantage" to "Transient Penalty".

2.5.10 Net Transient Advantage

This is a new metric defined herein as the Net Transient Advantage. This metric is Transient Advantage minus Transient Penalty. A positive value means a net advantage and and negative value is a net penalty.

2.6 Parameters Affecting Pulsed Supercooling

2.6.1 Thermoelement Length

Snyder et al. [27] noted all characteristic times (time to reach minimum temperature, time while cooled, time to return to steady state) are proportional to the square of the thermoelectric element length.

2.6.2 Current Pulse Amplitude

Snyder et al. [27] studied transient supercooling using a square wave and noted as current pulse amplitude increases, the minimum cold junction temperature becomes lower, but lower for a shorter time. Manno et al. [8] showed the rate of temperature reduction increases with increased current magnitude. There were however diminishing returns with increased current pulse amplitude. As current was continually increased, current pulse amplitude was not a one to one relationship with lower temperature. It was also confirmed maximum temperature overshoot is increased with current pulse magnitude.

2.6.3 Pulse Duration

Manno et al. [8] studied pulse duration of a square wave and found no reduction in supercooling temperature with pulse duration. Maximum temperature overshoot and transient penalty however increased up to a maximum for a pulse duration that left the pulse on continuously.

2.6.4 Pulse Shape

Lv et al. [46] summarized the work that has been done related to pulse shape. The pulse shapes that have been studied are predominately step current (square wave, t^0), with 18 of 20 cited references either using it for the entire study or in part. Other shapes that were investigated were $t^{1/3}$, $t^{1/2}$, t^1 , t^2, t^3 and the horizontal mirror images, e^t, $t^{-0.5}$, $t^{0.5}$, sine, arcsine, cosine, arccosine, saw tooth, negative saw tooth, ramp up, ramp down and isosceles. Thonhauser et al. [47] studied pulse shapes and found some shapes were more efficient and prevented extensive heating after Supercooling. It was concluded the temperature after the pulse was for the most part a function of the energy input to the thermal element during the pulse. Manno et al. [8] studied several different pulse shapes and found for the Isosceles triangle shape, the Transient Advantage is larger than the Transient Penalty.

2.6.5 Time between Pulses

Ma et al. [48] researched pulsing a thermoelectric device prior to T_c completing full temperature overshoot. It was found that if the second pulse is applied prior to T_c reaching the full temperature overshoot, T_c of the next pulse will be higher than T_c of the first pulse but it appears the characteristic transient shape of T_c remains the same. If pulses are continued at the same interval which is less than full overshoot, the average temperature of T_c in time increases initially and then stabilizes. The temperature rise then stabilization seen was due to Joule heat that was not fully dissipated before the next pulse was applied.

2.6.6 Thermoelectric Figure of Merit

Snyder et al. [27] found the thermoelectric figure of merit Z to be the only material parameter that affects the minimum temperature achieved.

2.6.7 Thermal Diffusivity

From the Snyder linear approximation model [27], increasing thermal diffusivity did not change ΔT_{pulse} however it did reduce the time to ΔT_{pulse} and reduced Holding Time.

2.6.8 Element Shape

Hoyos et al. [49] designed conical shaped thermoelements. This shape allowed for thermal resistance to increase toward the cold smaller diameter end and preferentially send Joule heat to the hot side. Thermal capacitance was increased which allowed an increase in delay of Joule heating to reach the cold side. The electrical resistance was however increased at the cold end which made the concentration of Joule heat higher. The net effect was a colder temperature at the cold side of the thermoelement. Yan [50] investigated using conical shaped thermoelements with the large diameter at the cold side rather than the small diameter as previously studied. Yang was able to increase Holding Time with the design.

2.7 Transient Modeling

Often in modeling, analogies are used to help solve problems that are intensely difficult and prohibitively time consuming. When it comes to thermal modeling, electrical analogies are used [51]. There are many analogies between conduction heat transfer and electrical conduction, see Table 2.1. The driving force for electrical flow is a voltage difference. Likewise, the driving force for heat flow is a temperature difference.

In the 1970's, as electrical circuits became more complex, a need to be able to simulate circuits with a computer arose. Researchers developed a numerical software to make this possible [52]. SPICE (Simulation Program with Integrated Circuit Emphasis) is an open source analog integrated circuit simulator. SPICE was developed at the Electronics Research Laboratory of the University of California, Berkeley. SPICE has been commercialized by various companies that add proprietary features like user interfaces and convergence aids. Some commercialized versions like Linear Technology LTSPICE and Texas instruments TINA are free. These electrical circuit simulators can be used to solve complex transient thermal problems.

SPICE models have been developed to simulate thermoelectric coolers. Chavez et al. [53] designed a steady state SPICE electrical-thermal analogy model of thermoelectric cooler. Lin [54] created a steady state SPICE model designed to accept inputs from thermoelectric cooler manufacture data sheets. Lineykin and Ben-Yaakov [55] developed a semi-lumped / semi-distributed mass transient SPICE model. Mitrani et al. [56] devised a 1D distributed mass model suitable for simulating transient pulsed cooling using SPICE.

Other approaches have been used to model transient pulsed thermoelectric devices. Hoyos and Jerger [57] created a hand coded electrical analogy model of a couple with no attached mass. Snyder et al. [27] derived a linear approximation model of a couple

that was fast and easy to use.

Three dimensional models that use ANSYS [58] or Cosmol [59] have been used but these models require expensive licenses. Sullivan et al. [60] compared SPICE model results with a finite volume Fluent model. There was a good agreement of results between the two models, however the SPICE model was up to 430% faster in one scenario. These 3D packages are also known to have a steep learning curve.

For this study, the SPICE model was chosen because it was expandable in terms of adding mass, boundary conditions and thermal interface resistances. Furthermore it is free, fast, accurate and for LTSPICE, has a large and helpful on-line support community.

Table 2.1. Thermal Electrical Analogies

Thermal Quantity	**Electrical Analogy**
Temperature [K]	Voltage [V]
Absolute Zero [0 K]	Ground [0 V]
Heat Flow Rate, $\dot{Q} = \left(\frac{\Delta T}{R_{th}}\right)[W]$	Current Flow, $I = \left(\frac{\Delta V}{R}\right)[A]$
Heat, $Q = \left(\frac{\Delta T}{R_{th}}\right)[J]$	Charge, $C = \left(\frac{\Delta V t}{R}\right)[As]$
Thermal Conductivity, $k[\,\left(\frac{W}{mK}\right)\,]$	Electrical Conductivity, $\sigma[\,\left(\frac{1}{\Omega m}\right)\,]$
Thermal Mass, $C_{th}[\,\left(\frac{J}{K}\right)\,]$	Electrical Capacitance, $C = \left(\frac{As}{V}\right)[F]$
Thermal Resistance, $R_{th}[\,\left(\frac{K}{W}\right)\,]$	Electrical Resistance, $R = \left(\frac{V}{I}\right)[\Omega]$

Chapter 3. Model Development

Two models have been developed for investigating transient pulsed cooling. The first model is a standalone thermocouple without an attached mass. The term massless thermocouple is sometimes used. This term is used to denote a lack of an attached mass to be cooled. The internal mass of the thermoelement is taken into account. The second model developed is of a system that includes many thermocouples that form a module. This module is attached to a heat spreader which attached to a mass with internal heat generation. Thus, the model is of a system with a mass and the first is "massless".

3.1 Thermocouple Model

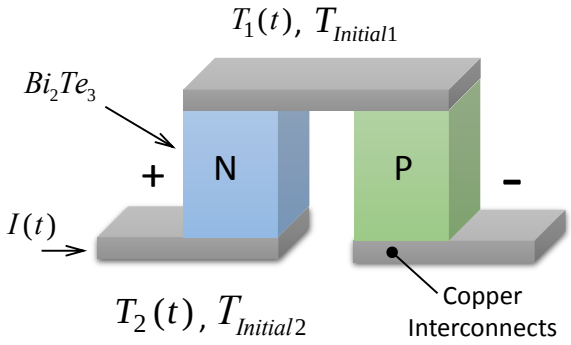

Figure 3.1. Thermocouple

The thermoelectric thermoelement model development started with choosing a model that was best suited for the task. The model selected for the study was developed by Mitrani et al. [56]. This model is a scalable 1D model of a thermoelectric couple and made up of two portions. One portion is the thermal model and the other is the electrical model. Both portions of the model are made up of networked electrical components and modeled in SPICE software designed for simulating electrical circuits. For the thermal portion of the model, electrical-thermal analogies were used to decide the input values for each electrical component. The electrical-thermal analogy circuit portion and the pure electrical circuit portion of the model are linked to capture the combined electrical and thermal nature of a thermoelectric device. The two circuit networks are then numerically solved simultaneously for transient responses. For simplicity, the model combines the P and N thermoelements into one thermoelement.

This is acceptable due to the properties of the P and N being very similar. This combination is common with thermoelectric modeling.

This model takes care to capture all of the physics associated with the thermoelectric device. These physics include the variables of Peltier cooling, Peltier heating, Joule heating, thermal resistance, thermal capacitance, electrical resistance and Seebeck voltage. Each of the thermal items are integrated into the model by use of its thermal-electrical analog. See table 2.1. The electrical items are directly input with no analogy.

The networking of these physics brings together all of these effects where a solver can then find the cumulative result. This allows for the study of interaction between the Peltier effect, Joule heating and thermal conduction under different transient input currents, initial conditions and boundary conditions.

Although not used for this study, the electrical analogy approach also lends itself naturally to simulating the thermal effect of electronic control circuits. These controls are designed with SPICE software and the thermal analogies allow them to be combined in one SPICE model.

The main feature of the Mitrani et al. [56] model that makes it exceptional is the distributed approach. This distributed approach captures the time separation between the Peltier effect, Joule heating effect, the Seebeck effect and transient thermal conduction throughout the thermoelement. The Peltier effect is a localized effect that happens at the junctions of the thermoelement. Joule heating is a volumetric effect that happens throughout the thermoelement. Thermal conduction is a transient effect dependent on the temperature distribution, mass and thermal resistance of the thermoelement.

In the model, the thermoelement is broken down into discreet parts that are analogous to many finite elements. In this case, fifty finite elements are used. In the thermal-electrical portion of the model, each finite element has mass, internal joule heat generation and thermal resistance.

In the thermal-electrical analogy model, mass is analogous to a capacitor. Joule heat generation is analogous to current flow in a current source. Thermal resistance is analogous to electrical resistance. This distributed approach over many finite elements allows this model to capture the delay in volumetrically generated joule heat reaching the cold side of the device after a current pulse has completed. This delay in Joule heat is the signature effect of transient pulsed thermoelectric cooling and would not be accounted with a lumped mass model.

Unlike the volumetric joule heating effect that happens throughout the thermoelement, Peltier cooling happens only at the cold junction. Peltier heating only happens at the hot junction. To capture the Peltier effect, current sources, which are analogous to heat flow are placed on each end of the thermal-electric analogy model to capture the location of where the effect naturally occurs. At one end of the thermoelement model, a current source pulls heat from a node to simulate Peltier cooling. At the opposite end of the thermoelement model a current source pushes heat into a node to simulate Peltier heating.

The electrical model in the SPICE software consists of a separate circuit on the same schematic as the thermal analogy model. Both of these models are solved simultaneously. The electrical circuit model contains one current source. This is where the input electrical current for the model is defined. The electrical circuit also contains a voltage source and resistor for each finite element of the model.

Unlike the thermal model that simulates heat flow with the analogy of a current source, the electrical model simulates current directly with a current source. No analogy is needed. The voltage sources in the electrical model simulate the Seebeck voltage generated at each finite element in the thermal analogy model. The voltage sources in the electrical model are linked to the thermal model. These voltage sources are dependent on the temperature difference across each finite element of the thermoelement model multiplied by the Seebeck coefficient. The electrical model reads these temperature differences as a voltage differences because it has no knowledge of the thermal analogies being used.

The resistors in the electrical model simulate the electrical resistance of each finite element of the thermoelement. All components of the electrical model are placed in series with one another since the sum of all Seebeck voltages and electrical resistances of each finite element total to the Seebeck voltage and electrical resistance of the entire thermoelement. This summation works the same way for the finite elements in the thermal model. The difference for the thermal-electrical analogy portion is that thermal capacitance, Joule heating and thermal resistances are being summed rather than Seebeck voltages and electrical resistances.

Boundary and initial conditions are also used for this model. A voltage source is connected to the hot side of the device. The thermal analogy of a voltage source is a temperature source. The voltage source in this model acts as a constant temperature thermal reservoir that maintains the hot side temperature. In physical thermoelectric device applications, the hot side is kept at a constant temperature by use of a heat exchanger that is cooled by the ambient thermal reservoir.

Each connection between two or more electrical components is defined as a node. Initial conditions are set for each node of the model. These initial conditions are specified as voltages in the SPICE model but are analogous to initial temperatures. Initial temperatures were used to study the behavior of the device starting at a higher temperature than the quasi-steady state cool down stabilized cold side temperature.

The physics of a thermoelectric device dictate thermal behavior is a function of electrical current through the couple. Peltier heating and cooling as well as Joule heating are dependent on electrical current. The heat pumped by Peltier cooling is equal to the electrical current times the Seebeck coefficient times the temperature at the cold side. The heat pumped by Peltier heating is equal to the electrical current times the Seebeck coefficient times the temperature at the hot side. The heat generated by Joule heating is equal to the electrical current squared times the resistance of the thermoelement. For this model, formulas are used in the current dependent thermal-electrical analogy components. This allows heat pumping and Joule heat generation to be proportional to current flow as the real physics dictate. These formulas are linked to the electrical model current. The current dependent electrical-thermal analogy component formulas take their values of current from the electrical model portion at every time step.

3.2 Modeling Process

The modeling process is categorized into four main steps. The first step is the model build step. This is the step where the Mitrani et al. [56] model is built in the SPICE software. The second step is the preprocessing step. This is the step where the inputs to the SPICE model are calculated in Matlab and entered into the SPICE model. This includes all variables for all components and the PWL (Piece-wise Linear) electrical current text file which dictates the electrical current profile used. The third step is running the SPICE model and exporting the data. This can be done manually or by using a third party automation software. The fourth step is post processing the exported data. Matlab is also used for this post processing step.

Step 1: Model Build

For the model build step, LTSPICE is used. LTSPICE can be downloaded for free. http://www.linear.com. Once the program is installed, a new schematic can be started by selecting "File", "New schematic". Components can be added to the schematic by first pushing the "component" button and selecting the components needed for the model from the menu. Each component is a pictorial schematic representation of an electrical component. After a component is selected, it will "attach" to the mouse curser. After moving the mouse curser to the desired location, a click on the schematic "detaches" the component to the schematic.

Once the components are arranged and placed, each component can be connected by "Wires" which are drawn on the schematic by dragging the mouse curser between components after clicking the "Wire" button. The "Wire" button contains an icon that looks like a pencil.

Grounds need to be added or the model will not run. In the thermal-electrical analogy model, a ground acts as an absolute zero temperature in Kelvin. For the electrical portion of the model, a ground is an electrical ground, no analogy is applied. Add a ground by clicking the "Ground" button, dragging the ground symbol to ground side of the circuit and connecting it to the circuit with a wire. Once the components, wires and grounds are placed, the model is ready for inputs. These numerical inputs describe the behavior of components of the model. The SPICE model ties these inputs together proportionally and mimics the dynamic device behavior. Each component receives an input that is calculated in the preprocessing step. The preprocessing will be discussed in the next section.

The component inputs values can be entered as a number or a variable in each component. Much time can be saved by entering the inputs as variables. The variables can be named to represent the components for which they are used. This allows hundreds of components with the same value to be changed from a central location rather than one component at a time.

To associate variable names with the components, start by right-clicking on the component of interest. This will open a dialog box which contains all of the component attributes. In the "Value" box, enter the variable name surrounded by curly brackets "VariableName". Do not add the quotation marks.

After the variable names are associated, assign a value to each variable. Do this by first creating a SPICE directive. The SPICE directive is created by clicking on the ".op" button and dragging it to an open space on the schematic. This is done in the same fashion as placing the components. Once the SPICE directive is placed, a right-click on the SPICE directive opens a dialog box where variables need to be inserted. The syntax used for creating the variables is a ".param" statement. This statement is entered followed by the variable name, then an equal sign and then the numeric value for the variable. An example is (.param VariableName= 45.65). The parenthesis should not be entered.

Initial temperature/voltage conditions for the model are set by using the SPICE directive as described above. With initial conditions, rather than using the ".param" statement, an ".ic" statement is used. Initial conditions are specified at each node.

The ".ic" statements can also be specified with variables. Unlike the ".param" statement, the ".ic" statement must also contain information that specifies which node is to receive the initial condition. As an example, ".ic V(n001)=VariableName". This statement reads "The initial voltage at node one is equal to the value stored in VariableName." It is important to remember the initial voltage is analogous to temperature in Kelvin when initial conditions are specified for the thermal-electrical analogy model.

After the variables calculated in the preprocessing are entered into the components and SPICE directive, the formula variables must be entered. In this case, rather than entering variables into each SPICE component, formulas are entered. When formulas are used in this model, it is because one or more of the variables is dependent on another part of the model. For the thermal-electrical analogy portion of the model, the calculated variables are the current sources used for Joule heat, the Peltier cooling current source, and the Peltier heating current source. For the electrical portion of the model, voltage sources that simulate the Seebeck voltages are dependent on the temperature deltas across each finite element of the thermal-electrical analogy portion of the model.

Joule heating is calculated with the thermal-electrical analogy model current sources using the formula I^2R, where R is the electrical resistance in one finite element of the thermoelement. This is calculated in the preprocessing step. In the SPICE model, "I" must be made dependent on the electrical model current source using a link. To add a link, right click on the thermal-electrical analogy Joule heat current source. The "component attribute editor" dialog box opens. In the value box, enter $I = ((I(b54))^2 * R$. This equation reads "The current in this current source is equal to the current at current source b54 (in electrical model) squared, multiplied by the electrical resistance in that specific finite element.

Peltier cooling and Peltier heating are also dependent on current. In the thermal-electrical analogy model, formulas are used within the Peltier cooling and heating current source to link the current in the electrical model. The formula for Peltier cooling is electrical current times the Seebeck coefficient times the temperature at the cold side. For Peltier heating the formula is electrical current times the Seebeck coefficient times the temperature at the hot side.

In this model, material properties for the Seebeck coefficient in the Peltier sources are non-temperature dependent, the Seebeck term is lumped together with the temperature term in the preprocessing step. As described, the electrical current portion of these equations comes from the electrical current source within the electrical portion

of the model. Therefore the lumped Seebeck coefficient and temperature are multiplied by the current in the electrical model at every time step of the spice simulation. In the electrical-thermal analogy portion of the SPICE model, the Joule heat source is a current source and specified as $I = Q_{pc} * (I(\text{B54}))$. The statement reads "current / heat flow for this current source is equal to the variable Q_{pc} times the current in the electrical current source B54 in the electrical model. Here Q_{pc} is the lumped temperature and Seebeck coefficient. The variable Q_{pc} in this model is named for the heat transfer by Peltier cooling. The variable for Peltier heating is Q_{ph}. Q_{ph} is specified the same way in the SPICE model as Q_{pc} however the value is different due to the difference in hot and cold side temperature in the lumped calculation during preprocessing.

The Seebeck voltage in a thermoelement is defined by the temperature difference between the hot side and cold side of the thermoelement times the Seebeck coefficient. The units of Seebeck coefficient are V/K. Multiplying the Seebeck coefficient by the temperature difference gives the Seebeck voltage. In the SPICE model, the Seebeck voltage is calculated across every finite element of the thermal-electrical analogy model. To enter the formula for the Seebeck voltage in the electrical model voltage sources, start by right clicking on one of the voltage sources in the electrical portion of the model. This brings up the "component attribute editor". In the "Value box enter $V = (V(\text{n002}) - V(\text{n001})) * S$. This statement reads, "Voltage at this voltage source is equal to the voltage at node two minus the voltage at node one all multiplied by the Seebeck coefficient. This formula is entered once for every voltage source in the electrical model. The number of voltage sources in the electrical model is specified by the number of finite elements in the thermoelement model. In this case there are fifty finite elements in the thermal-electrical portion of the model and fifty in the electrical model. The voltage difference will change depending on which finite element voltage difference in the thermal model is being specified. It is important to remember the voltage difference is coming from the thermal model so it is actually a temperature difference.

In the electrical model, electrical current is specified by the user. This electric current can be specified in several different ways. A constant value or a time varying value can be used. The time varying value can be input by either using logical formulas of by using a Piecewise Linear (PWL) text file. For a small portion of this work logical operators were used. The transient pulse current was specified to turn on when steady state temperature was reached. The current was set to turn off after Holding Time was reached and then turn back on after Settling Time. For the majority of this modeling work, a PWL text file was used to specify electrical current. This PWL file consists of a column of time values associated with a column of electrical current values. The development of compiling these PWL files is covered in the next section.

Before the model can be run, the simulation parameters need to be setup. Set these parameters by clicking on the "Simulate" menu and then clicking in the "Edit Simulation Cmd." When the "Edit Simulation Cmd." dialog box appears, click on the "Transient" tab. On this tab, enter the "Stop Time". This the amount of real world time desired for the model to simulate. The next input is the "Time to Start Saving Data" input. This input was used for "long" simulation time transient modeling that contains a quasi-steady state and that quasi-steady state is the only area of interest in the model output. This input allows the full simulation to be run, but only saves the data for the time period of interest. If this option is not used, the output data file size could be prohibitively large and hard to work with. There are many settings in the LTSPICE control panel that can help with model convergence. For this work the default LTSPICE settings were used.

Step 2: Preprocessing

The preprocessing step consists of calculating values to use for all of the variables set in the LTSPICE model components. Preprocessing also includes calculations for the transient electrical current PWL file. Both of these calculations were performed in Matlab however they were separate scripts. The variables calculated in Matlab are the Peltier Cooling term (Q_{pc}), the Peltier heating term (Q_{ph}), the thermal capacitance of the thermoelement (Cth2 and Cth4), the thermal resistance of the thermoelement (Rth2), the electrical resistance of the thermoelement (R), the Seebeck coefficient (S) and the transient current profile.

The input variables were calculated in two different ways. This was done as a cross check to improve accuracy. The first calculation method uses intrinsic material property data to calculate the thermoelectric variables. This method is a more ideal method as it does not account factors which may reduce performance on a module level. These module level factors are thermal radiation, thermal convection, manufacturing variation in the thermoelements, solder joint and copper interconnect electrical and thermal resistance, and solder and copper interconnect joule heat generation. In effect the intrinsic calculations only account for the thermoelement in an ideal state.

The second method of calculation was done using vendor data [61] The results of the two calculation methods were within 4 to 6% of each other. Since ultimately the results of the using the intrinsic properties were used here, the details of the vendor data calculations will not be shown. The physical properties of the thermoelement model are specified in Table 3.1

Resistivty, thermal conductivty and Seebeck coefficent data was utilized from [62]. The material property data from [62] is specified at various temperatures. An Excel sixth order polynominal curve fit on this data was used to interpolate to 308.15K.

The data found by interpolation is listed in Table 3.1. 308.15K was chosen because it is the target temperature for T_h and T_c at steady state.

Table 3.1. Thermoelement Properties

Property	Value	Units	Reference
Length	1	mm	[56]
Width	1	mm	[56]
Height	5	mm	[56]
Resistivity	9.54E-06	Ω m	[62]
Thermal Conductivity	1.5718	W/m K	[62]
Seebeck Coefficient	1.97E-04	V/K	[62]
Density	7530	kg/m^3	[62]
Specific Heat	544	J/kg K	[62]

Model Inputs

The following are inputs to the SPICE model that were calculated in the prepossessing step.

1. Electrical current

Steady state electrical current was calculated for two conditions needed for the studies. One was $I_{optimal}$ and the other was I_{max}.

$$I_{opt} = \frac{S_m T_h}{R_m} \tag{3.1}$$

S_m is the module or couple level Seebeck coefficient and is calculated by,

$$S_m = 2SN \tag{3.2}$$

S is the materials based Seebeck coefficient, the 2 coefficient accounts for two thermoelements in series that make one couple. N is the number of couples. N is 1 for the massless thermocouple studies.

R_m is the electrical resistance of the couple or module and is calculated by,

$$R_m = N\frac{2\rho L}{A} \tag{3.3}$$

N is again the number of couples, A is the area normal to current flow for one thermoelement. L is the length for which current flows through one thermoelment. The 2 accounts for two thermoelements in the couple. ρ is the electrical resistivity of the thermoelement.

I_{max} [63] was calculated as follows,

$$I_{max} = \frac{S_m}{R_m}(((T_h + \frac{1}{Z_m})^2 - (T_h)^2)^{\frac{1}{2}} - \frac{1}{Z_m}) \tag{3.4}$$

S_m, R_m, and T_h were defined previously. Z_m is the figure of merit for the material and is defined as,

$$Z_m = \frac{S^2}{\rho k} \tag{3.5}$$

S is the Seebeck coeffient, ρ is electrical resistivty and k is the thermal conductivity. These are all material properties of the thermoelement and given in table 3.1.

2. Peltier Cooling

Peltier cooling was calculated partially in the preprocessing step. The portion left out was multiplying the preprocessing result by the current. This step happens in the SPICE model.

Peltier cooling is calculated as follows,

$$Q_{pc} = T_c S_m \tag{3.6}$$

Target steady T_c is stated in table 3.5 and S_m was defined above.

3. Peltier Heating

Similarly to Peltier cooling, the electrical current multiplication step is done in the SPICE model.

Peltier heating is calculated as follows,

$$Q_{ph} = T_h S_m \tag{3.7}$$

T_h is stated in table 3.5 and S_m was defined above.

4. Joule Heating

Joule heating per current source is handled in the model. Current is squared and then multiplied by the per segment electrical resistance.

$$RmPerSegment = \frac{R_m}{NumberOfSegments} \tag{3.8}$$

R_m is calculated per equation 3.3 and $NumberOfSegments$ is 50. This is equal to the number of "finite elements" in the model.

5. Thermal Capacitance

For the Mitrani et al. [56] model, capacitance is divided by the 50 segments / "finite elements" and then sub-divided within those segments. This is done to evenly distribute the thermal capacitance throughout the model.

The sub-divisions are,

$$C_{th2} = \frac{C_{th}PerSegment}{2} \tag{3.9}$$

and

$$C_{th4} = \frac{C_{th}PerSegment}{4} \tag{3.10}$$

$C_{th}PerSegment$ is the total capacitance of the thermoelement dived by the number of segments, which is 50 in this case.

$$C_{th}PerSegment = \frac{C_{th}}{NumberOfSegments} \tag{3.11}$$

The total thermal capacitance of the thermoelement is the product of the volume, density and specific heat capacity of the thermoelement in equation 3.12. The density and specific heat capacity can be found in table 3.1

$$C_{th} = V\rho C_p \tag{3.12}$$

6. Thermal Resistance

In the Mitrani et al. [56] model, there are two thermal resistors per segment. R_{th2} is the thermal resistance per resistor and defined by,

$$R_{th2} = \frac{1}{2}\frac{R_{thI}}{NumberOfSegments} \tag{3.13}$$

The $NumberOfSegments$ was previously defined. The $\frac{1}{2}$ accounts for the two resistors per segment and the total thermal resistance of the thermoelement R_{th} is defined as follows,

$$R_{th} = \frac{L}{NkA_t} \tag{3.14}$$

L has been previously defined, k is the thermal conductivty of the thermoelement per table 3.1, N is the number of thermocouples and A_t is the area of a thermoelement normal to current flow multipled by two, as follows,

$$A_t = 2A \tag{3.15}$$

After these calculations were completed in Matlab, they were conveniently output

as text to the Matlab Command Window. The outputs of Matlab can be combined with the .param statements using Matlab "fprintf" functions. This allows the output text to be copied directly into the SPICE directive window. This saved much time. Without this, the output from Matlab would need to be copied one value at a time to each existing .param statement on the SPICE directive.

3.2.0.1 Calculation of Transient Electrical Current Profile

As mentioned above, the PWL file is a text file with a column of time values that correspond to a column of electrical current values. For this work, isosceles triangle shaped current pulses were studied. A Matlab scripts was created to calculate the transient current PWL file. The height of these isosceles triangles is the peak pulse-height. The base of the triangle is the pulse on-time. These two variables and the variable of time between pulses were also studied. This required the Matlab script to have an option to vary pulse-height, pulse on-time and pulse spacing. These pulses need to start from some steady state current so the base steady state current was also made as a variable. In this study I_{max} and I_{opt} were used as the base steady current. The start of pulsing in time was also designed as a variable for additional simulation flexibility.

In this work, response surfaces were studied. This required 2025 combinations of pulse-height and pulse on-time to be simulated. This means 2025 PWL current profile files for each surface. Generating these PWL files manually would have been time prohibitive so the calculations and output of these files was automated using Matlab. Formulas that calculate between specified limits of triangle height and on-time were used. Nested Matlab loops were used to generate all combinations of pulse-height and on-time within the specified limits.

3.2.1 Step 3: Running and Exporting

To run the model, click the button that looks like a person running. The massless thermocouple model takes a few seconds to run. There are various factors that affect the time required to run the model. These factors are, the real world time simulated, the maximum time step chosen, the solver used, the reltol SPICE setting, and the performance of the computer running the software. For this simulation it was found by experimentation that going below 0.0001 on reltol doubled simulation run time for every order of magnitude smaller reltol. The alternate solver increased simulation-time by about 36%. Every order of magnitude decrease in time step increased simulation run time by about 10 X.

Once the simulation is complete, it is time to export the data. To export the data generated by the simulation, click the "scope" window that displays the voltage and

current waveforms after the simulation is done. Next click the "File" menu, then "Export". A dialog window appears. In this window, select the voltages and currents to be exported. The names that are selectable are either voltages or currents. Voltages are named for the node at which there are measured. Currents are named for the component for which they travel through. Click the export "Browse" button and choose a location to export the data. Click "ok" after the file save directory. LTSPICE now exports a text file to the desired directory.

As mentioned, these surface plots were made with 2025 combinations of pulse-height and pulse on-time. Even though the massless thermocouple model runs quickly, it was time prohibitive to run each simulation manually. To automate this task, a free software called AutoIt was used. This software records screen motions and clicks that can be played back. Having access to the program code that AutoIt creates allows these screen motions and clicks to be entered into a loop and repeated as many times as needed. For each of 2025 SPICE simulations, a new Piecewise Linear (PWL) current profile for which to operate the thermoelectric devices needs to be used. The PWL file name used was `file1.txt`, `file2.txt` ...`file2025.txt`. This naming convention allowed for loop operation. This is the same file naming convention used for exporting the data from LTSPICE. This export file naming convention permitted for the exported data file to be read into the post processing Matlab script with a loop.

3.2.2 Step 4: Post processing

Post processing of the massless thermocouple data consisted of processing the output data from the SPICE model in Matlab. Matlab calculates parameters used to characterize transient thermoelectric pulse cooling. The parameters and a description of how they were calculated in Matlab is below.

Holding Time

In Matlab, Holding Time was calculated first by finding the steady state temperature. In order to do this, Matlab code was created to find the start of the first current pulse. This code first finds every unique current value in the data file. The minimum value of all unique values is then found. The code then looks at all of the electrical current data that is larger than the minimum unique value plus a small tolerance. The data points that meet this criteria are defined to be when the current pulse is on. The code finds the minimum index value for all points while the pulse is on. The minimum index value is used to index the time vector to find the start of the first current pulse. One time step is subtracted from the start of the pulse and its index value is used to index the T_c vector to find the steady temperature just prior to the pulse.

Once T_c prior to the pulse is known, a steady state temperature vector is created to span the length of the data set. The vector will be used for several different calculations from here forward. This steady state temperature vector was made by creating two vectors, one with x-coordinates and one with y-coordinates. The y-coordinates are the steady temperature found just prior to the pulse and the x-coordinates are time values starting from the data point prior to the pulse and spanning a specified number of points to the last data point in the file.

An available third party Matlab function finds the intersections between the T_c data and the steady data vector that was created. This Matlab function provides both the x (time coordinate) and the y (temperature coordinate) for each intersection between the two vectors. The first intersection is the end of Supercooling time. Knowing the end of Supercooling time and the time of the start of the current pulse, the Holding Time can be calculated. The Holding Time is the difference between the start of the first current pulse and the end of Supercooling. The end of Supercooling occurs after the minimum temperature is achieved and T_c returns to the steady state temperature where it started just prior to the current pulse. The difference between the start of the current pulse and the end of Supercooling is the Holding Time.

Supercooling

Minimum temperature achievable can be found using the Matlab built in "min" function that searches the data to find this the smallest value. Since LTSPICE does not export even time step data, accuracy finding the minimum in Matlab may be decreased. To increase accuracy of finding the minimum, a subset of the full data set during the Supercooling event was interpolated using spline interpolation. Next the minimum of this interpolated subset was found. This subset used is all of the data in the file that occurs during Supercooling. The time period at which this occurred is also known as the "Holding Time" as described above. The subset was used rather than the full set because it provided a better curve fit and used less memory when interpolation at very small time steps was used.

Maximum temperature difference (ΔT_{Pulse}) is the difference between steady state T_c temperature before the pulse and the minimum T_c temperature achieved during transient pulse operation. In Matlab this was calculated by first finding the minimum temperature and then finding the steady state temperature as described in the Holding Time section above. The maximum temperature difference is calculated as the difference between these two temperature values.

Pulse cooling enhancement was calculated as ΔT_{Pulse} divided by ΔT_{max}. ΔT_{max} is the maximum temperature difference that can be sustained by a given device during steady state operation. The hot side temperature of the device T_h is part of the

exported LTSPICE data. The device is operating at steady state ΔT_{max} prior to the pulse. With this ΔT_{max} data and ΔT_{Pulse}, Pulse Cooling Enhancement is calculated in Matlab

Time to reach minimum temperature:

Time to reach minimum temperature is the time required after the start of the current pulse for T_c to reach the minimum temperature. If the minimum temperature is known per the calculation in the section above, the index of this temperature value can be found with the Matlab "find" function. This index value can then be used to index the time vector and find the time value at which that minimum temperature occurs. The start time of the current pulse is known from the Holding Time calculation above. The time to reach minimum temperature is calculated as the time at minimum temperature minus the time at the start of the current pulse.

Superheating

Similarly to Supercooling, Superheating is characterized in two different ways. One way is called "Maximum Overshoot Temperature" and the other ΔT_{Pulse}.

Similarly to minimum temperature achievable, the maximum temperature overshoot is found by obtaining a subset of data in Matlab, using spline interpolation and the Matlab "max" function can be used to find the peak temperature. To find the subset of data that is then interpolated, intersections are found between the steady temperature vectors and the T_c vectors. The first intersection is the end of Holding Time. The second intersection is the Settling Time. The x and y-coordinates between these two intersections are extracted with the third party Matlab function. Logic statements are used to find all the data between the end of Holding Time and the Settling Time. Once the data points of interest are found, the find function finds the index number for each point. Next the time vector and the temperature vector are indexed to extract the temperature and time data. These two new shorter vectors, along with the new smaller time step are used with the Matlab spline interpolation to find a more accurate maximum temperature.

ΔT_{Pulse} is found by subtracting the steady temperature (found in the holding time section above) from the maximum temperature overshoot.

Time to maximum temperature overshoot

Time to reach maximum temperature is the time required after the start of the current pulse until T_c reaches the maximum temperature. If the maximum temperature is known per the calculation in the preceding section, the index of this temperature value

can be found with the Matlab "find" function. This index value can then be used to index the time vector and find the time value at which that maximum occurs. Since the start time of the current pulse is known, the time to reach maximum temperature is the time at maximum temperature minus the time at the start of the current pulse. The method used to find the start of the current pulse was described in the Holding Time section.

Settling Time

Settling time is the time required for T_c to decay back to steady state starting from the end of Holding Time. In Matlab, the time at return to steady state is calculated with the third party function that finds the intersections between the steady state temperature and T_c. The return to steady state is the last intersection found in the data.

Transient Advantage

Transient Advantage is defined as the area contained between the steady state temperature vector and the area above T_c during Holding Time. To find this area, a Matlab function called "trapz" is used. This function uses numerical integration to find the area under a curve. First the area under the steady state temperature vector is found during holding time. Next the area under T_c is found during holding time. The difference in these two areas is the Transient Advantage. Subset vectors are used to find the start and end of these areas. The subset vectors are defined by the data that falls within the Holding Time.

Transient Penalty

Similarly to Transient Advantage, Transient Penalty is defined as the area between T_c and the steady temperature during the time period of the end of Holding Time and the end of Settling Time. Subset vectors are again defined between these time periods and the "trapz" Matlab function finds the areas. This time the area under the steady temperature vector during Settling Time is subtracted from the area under the T_c curve during the Settling Time.

Transient Advantage over Transient Penalty

Transient Advantage over Transient Penalty is the ratio of the two quantities. Knowing the Transient Advantage and the Transient Penalty calculated in the preceding sections, a simple ratio of the two values is calculated in Matlab.

Net Transient Advantage

A new metric defined herein, Net Transient Advantage is the difference between Transient Advantage and Transient Penalty. This is calculated with a subtraction in Matlab once the values of Transient Advantage and Transient Penalty are known.

3.3 System model

After the massless thermocouple model described in the previous section was built and demonstrated, it was time to study the effect of using a full scale pulse cooler module in contact with a heat generating mass. This module, a heat spreader and mass combine to form a system. The system model consists again of networked electrical components using electrical-thermal analogies. These electrical circuits are numerically solved simultaneously for transient responses using SPICE software. The thermocouple model is used in the system model however the inputs to the components that make it up have been scaled up and additional features that take it from a thermocouple to a module have been added.

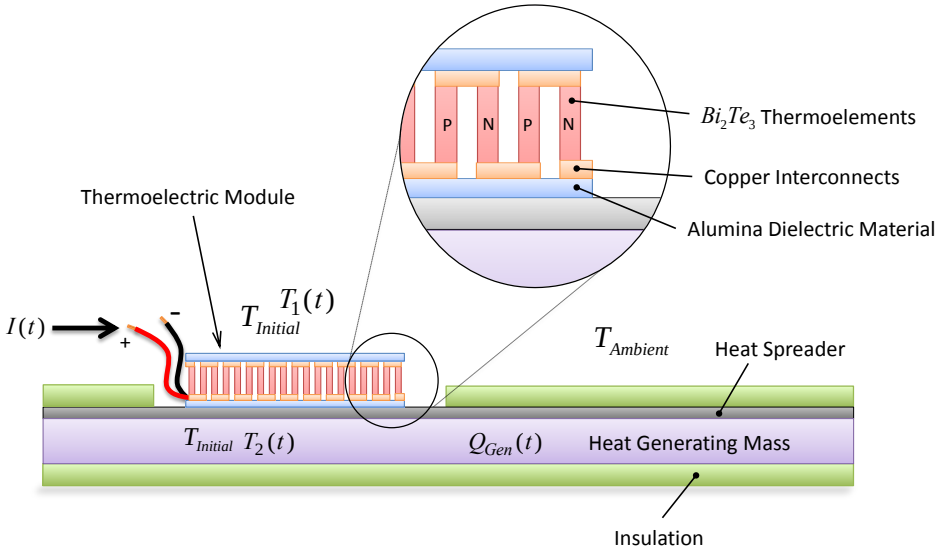

Figure 3.2. System Model

The physical components of the system model consist of a thermoelectric pulse cooler module, a heat spreader, the mass, grease thermal interface material and insulation. The mass generates heat internally. The heat spreader is mounted to one face of the mass and is in thermal contact with it via a grease joint. See figure 3.2.

A thermoelectric cooler module is attached to the heat spreader by use of another grease joint. The face area of the heat spreader opposite to the mass side that is not covered by the cooler module is covered by insulative material. The face of the mass opposite of the heat spreader side is also covered by insulative material. The perimeter of the mass is not insulated; it is exposed to the ambient air temperature. The face area of the mass that is attached to the heat spreader is much larger than the area of the edges of the mass. The dimensions of the system model components can be found in table 3.2.

Table 3.2. System Model Properties; Excluding Thermoelement Properties

	Component	Dimension [mm]	Number of Nodes	Thermal Conductivity [W/m K]	Density [kg/m^3]	Specific Heat [J/kg K]
Cold Side	Al Heat Spreader	165 X 230 X 1	25	204 [64]	2700 [64]	900[64]
	Mass	165 X 230 X 9	125	32 [65]	2323 [65]	1605 [65]
	Alumina Dielectric	0.70	6	230 [64]	3260 [66]	740[66]
	Cu Interconnects	0.3000	6	386 [64]	8960 [64]	385[64]
	Tin/lead Solder Joint	0.0500	6	48 [64]	not modeled	not modeled
	Thermal Grease	0.0235	6	3.7 [67]	not modeled	not modeled
Hot Side			constant temperature			
Both Sides	Polyurethane Foam Insulation	165 X 230 X 25.4	25	0.35 [68]	39 [69]	1450 [70]

The physics captured by addition of the new components in the system model are Joule heat, internal heat generation, thermal capacitance, thermal conduction, thermal interface resistance, and convection resistance.

When building the system model, the new development was addition of the mass, heat spreader, interface resistances, items to convert the couple model to a module model and boundary conditions. The thermoelement model remained the same with exception of scaling the model up to module size with additional preprocessing inputs.

Building the system model, there were many similarities to building the couple model. Placing components, inputting variables to components, inputting the SPICE directives, Initial conditions, and using the "edit simulation command" were all the same as described in the couple model section. These items were the same because they are the items required to operate LTSPICE. LTSPICE is again used for the system model.

The system model development was split into two main tasks. One task was to transform the thermocouple model into a module model and one was to build the model of the mass with heat generation, heat spreader, insulation and boundary

conditions. For the module model, the Mitrani et al. [56] model was scaled and additional components were added.

Studying three dimensional temperature gradients in the mass model was desirable. For this reason, the 1D couple model was connected to a 3D SPICE model of the mass. The insulation and heat spreader are 2D arrangements. The model of the mass, spreader and insulation are all distributed mass models with the model of the mass also containing distributed heat generation.

The system modeling process used the same four steps that were used for the thermocouple modeling. These steps are, the SPICE model build step, preprocessing, running and exporting and post processing.

3.3.1 Model Build

As said, the two main modeling tasks were converting the couple model to a module and the other task was adding the mass, spreader, insulation, interface resistances and convection boundary conditions.

Table 3.3. Thermoelectric Module Properties

number of couples	376
dimensions	82.5 X 57.5 X 6.5 mm
$I_{\max}$	4.874 A
I_{opt}	6.363 A
$V_{\max}$	45.650 V
$\Delta T_{\max}$	72.103 K
$Q_{\max}$ at I_{opt}	145.24 W
R	7.17 Ω

Starting with conversion of the thermocouple, the thermocouple was first scaled from one couple to 376 couples. This scaling capability comes without changing the design developed by Mitrani et al. [56]. Scalability comes by changing the variable SPICE component inputs for which the model is made. Next, the model was adapted by addition. Module level components were added. These additions include copper interconnects between the thermoelements and couples, a solder joint between the copper interconnects and the thermoelements, and alumina dielectric material. Heat generation was added to the copper interconnects to realistically capture internal Joule heating with passage of current through them. These module components were all captured in the SPICE model by use of resistors for thermal and interface resistance as well as current sources for heat generation. Capacitors were used to model the thermal effect of mass of each component.

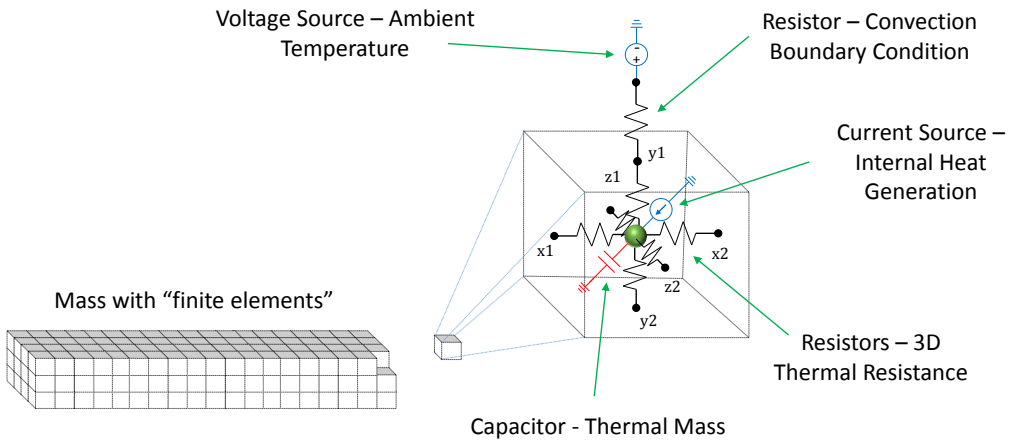

Figure 3.3. System Model Thermal-Electrical Analogy Schematic

The model of the mass alone is made up of 125 nodes. There are five nodes in the X dimension of the mass, 5 nodes in the Y dimension and 5 in the Z dimension. Each node of the mass is connected in a 3D arrangement of 6 resistors. See figure 3.3.

Table 3.4. Thermal Interface Resistance [m^2/K·W]

Cold Side: Alumina - Thermal Grease	0.0000063 [67]
Cold Side: Thermal Grease - Spreader	0.0000063 [67]
Cold Side: Spreader - Thermal Grease	0.0000063 [67]
Cold Side: Thermal Grease - Mass	0.0000063 [67]
Mass - Insulation	0.0800 [71]
Hot Side: Heat Exchanger	Constant Temperature

With the node in the center, resistors are attached in the positive and negative direction of each coordinate X, Y and Z-axis. Each node also contains one capacitor which provides a distributed mass effect. This arrangement was modified from [60]. This 3D arrangement of resistors and one capacitor was modified by connecting a current source to each node. This allowed for the study of variable distributed internal heat generation in the mass. Each 3D node of resistors, capacitor and current source can be viewed as a "finite element" as was done for the thermocouple model. Each finite element was connected to one another within LTSPICE. Resistors of each adjacent node were connected together in 3D. Each capacitor and current source at each node were connected to a ground. When two components interface for example the mass and the heat spreader, additional resistors are used to model thermal interface resistance (table 3.2). If the the edge of the component is touching the ambient air, additional resistors are used to model thermal resistance with the air. These resistors are connected to a voltage source which models ambient temperature. These voltage sources can be constant or variable temperature. For this modeling study they were constant.

The thermoelectric module length and width were sized based on the spacing between the nodes of the mass model. It was desirable for the thermoelectric cooler to touch a least four nodes. It was also desirable to have the device centered within the width of the mass. To achieve both of these goals, the module model was connected to six nodes that form the shape of a rectangle. Heat generation within the mass model was modulated to achieve a mass temperature of around 35 $^{\circ}C$ when the device is operating at steady state and stabilized heat transfer conditions.

The heat spreader uses the 2D resistor and capacitor node arrangement. This was done for simplicity and no desire to study 3D gradients in the heat spreader. The heat spreader is connected to the mass via resistors that capture thermal interface resistance between them.

The insulation was designed in the same way as the heat spreader; likewise it is also a 2D model. Insulation is attached to the mass and heat spreader by resistors that simulate the thermal interface resistance.

The nodes on the perimeter of the mass not covered by insulation are connected to resistors that simulate thermal resistance generated by a combination or area and a calculated heat transfer coefficient. On the side of these convection thermal resistors opposite of the mass, voltage sources are connected to simulate the ambient temperature. The free side of these voltage sources are connected to ground. This voltage source arrangement is the same arrangement used for the nodes exposed to the ambient on the insulation. This model also has the capability to use adiabatic or radiative boundary conditions, anisotropic mass or spreader materials and non-uniform heat generation. These features however were not used for this work.

Due to the 3D arrangement and large number of components in the mass, spreader, insulation and boundary condition components, the system model was more complex to build than the thermocouple model. Care was needed to connect each component properly and not cross wires that would result is short circuits. In LTSPICE, a wire that inadvertently crosses a node will short and it may not be immediately apparent due to the large amount of components used in the model.

3.3.2 Preprocessing

Just like for the thermocouple model, the system model preprocessing step consists of calculating values to use for all of the variables set in the LTSPICE model components. These calculations were performed in Matlab. Below is a list of all 34 variables that are inputs to the system model. This list excludes inputs that were already covered in the previous thermocouple modeling section.

Ambient Temperature $[K]$

1. `Ambient`: Ambient temperature

Thermal Capacitance $[\frac{J}{K}]$

2. `CapSpread`: Thermal capacitance of the heat spreader per capacitor
3. `CapMass`: Thermal capacitance of the mass per capacitor
4. `CapInsul`: Thermal capacitance of the insulation per capacitor
5. `CapAluminaCold`: Thermal capacitance of the alumina on the cold side of the module per capacitor
6. `CapCopperHot`: Thermal capacitance of the copper interconnects on the hot side per capacitor

Thermal Resistance $[\frac{K}{W}]$

7. `RspreadX`: Thermal resistance of the heat spreader in the x direction per resistor
8. `RspreadY`: Thermal resistance of the heat spreader in the y direction per resistor
9. `RspreadZ`: Thermal resistance of the heat spreader in the z direction per resistor
10. `RmassX`: Thermal resistance of the mass in the x direction per resistor
11. `RmassY`: Thermal resistance of the mass in the y direction per resistor
12. `RmassZ`: Thermal resistance of the mass in the z direction per resistor
13. `RInsulX`: Thermal resistance of the insulation in the x direction per resistor
14. `RInsulY`: Thermal resistance of the insulation in the y direction per resistor
15. `RInsulZ`: Thermal resistance of the insulation in the z direction per resistor
16. `RSolderCold`: Thermal resistance per resistor of the solder on the cold side

Electrical Resistance $[\Omega]$

17. `RCopperCold`: Electrical resistance per resistor of the copper on the cold side
18. `RinterconnectCold`: Electrical resistance of the copper interconnect on the cold side per resistor
19. `RinterconnectHot`: Thermal resistance of the copper interconnect on the hot side per resistor

Heat Generation $[Watts]$

20. `HeatGen`: Heat generation per node in the mass

Thermal Interface Resistance $[\frac{K}{W}]$

21. `InsulContact`: Interface resistance per resistor between the mass and the insulation

22. `GreaseContactResistanceCold`: Interface resistance of the grease per resistor between the grease and the alumina on the cold side.

23. `GreaseContactResistanceCold6b`: Interface resistance of the grease per resistor between the grease and mass on the cold side.

24. `SinkCnt`: Thermal interface resistance between the heat sink and the mass per resistor. Includes two thermal interface resistances and one thermal resistance of a grease layer. All resistors in series.

Convection resistance $[\frac{K}{W}]$

25. `RconvecMassSide`: Thermal convection resistance on the side of the mass per resistor

26. `RconvecMassBottom`: Thermal convection resistance on the bottom on the mass per resistor

27. `RconvecMassTop`: Thermal convection resistance on the top of the mass per resistor

28. `RConvSpreadBottom`: Thermal convection resistance on the bottom of the spreader per resistor

29. `RConvSpreadSide`: Thermal convection resistance on the side of the heat spreader per resistor

30. `RConvSpreadTop`: Thermal convection resistance on the top of the heat spreader per resistor

31. `RConInTop`: Thermal convection resistance on the top of the insulation per resistor

32. `RConInSide`: Thermal convection resistance on the vertical side of the insulation per resistor

33. `RConInBottom`: Thermal convection resistance on the bottom of the insulation per resistor

34. `RConInFac`: Thermal convection resistance on the vertical face of the insulation per resistor

The total thermal capacitance for each component can be calculated per equation (3.12). Before inputting the thermal capacitance variable, the total capacitance must be divided by the number of nodes in the part. This allows the model to capture the distributed mass effect.

Thermal resistance for the mass was calculated for all three coordinate directions.

$$R_{thermalx} = (\frac{L_x}{k_x A_{yz}})(\frac{N_{parastrings}}{R_{count}}) \tag{3.16}$$

Equation (3.16) is an example of the calculation for the x-direction. $\frac{L_x}{k_x A_{yx}}$ is the total thermal resistance in the x-direction of the 3D mass. Here L_x is the length of the mass in the x-direction. k_x is the thermal conductivity of the mass in the x-direction. A_{yz} is the area normal to heat flow in the x direction. This is the area made up of the y and z dimensions of the mass. This portion of the equation could stand alone if the mass was modeled with one large resistor. The mass however is modeled with multiple parallel strings of resistors for which heat flows in the x-direction. For this reason, this total resistance must be multiplied by the number of parallel strings of resistors that run in the x-direction of the mass and terminate on the yz-plane ($N_{parastrings}$). This gives the total resistance of each parallel string. Once this is found, it must be divided by the number of resistors in one of the strings (R_{count}). This process is repeated for the y and z direction thermal resistance.

Multiplying the total thermal resistance by the number of parallel strings may sound counter intuitive. This is analogous to using 10 pipes to flow water rather than one pipe. Each pipe has a resistance to flow that is 10 times higher than the one pipe yet there are 10 pipes in parallel so the same water flows.

Table 3.5. Boundary Conditions

Boundary Conditions T_c	Variable	[K]
Ambient Temperature	358	[K]
T_h	308.15	[K]
Initial System Temperature	358	[K]
Internal Heat Generation	15.054	[W]
Exposed Surface Condition	Natural Convection	

$$R_{convection} = \frac{1}{hA} \tag{3.17}$$

Equation (3.17) is the convection resistance. Here A is the area exposed to ambient air and h is the convective heat transfer coefficient. Like the thermal resistance calculation above, the total resistance must be multiplied by the number of nodes on the surface. No division is required since each "string" of resistors in this case is only one resistor. This also applies to thermal interface resistance.

For this model, a simplified method of finding convection heat transfer coefficients was used [72]. Different heat transfer coefficients were used depending if the surfaces exposed to ambient were vertical, horizontal facing up or horizontal facing down. Ambient temperature can be changed as desired. Heat generation is entered as desired but must be divided by the number of nodes on the mass model.

3.3.3 Running and Exporting

The process of running the model and exporting data is the same for the system model as it was for the thermocouple model. The main difference come from additional run time and many more variables to choose before exporting the data.

3.3.4 Post Processing

Post processing was divided up into two parts. The first part was model validation and the second is making the plots. In the validation stage, an energy balance was performed on the model. This double checked that all nodes in the model were connected correctly. Two dimensional plots were generated from the 3D arrangement of nodes, see figure 3.4. These were also used to confirm the nodes were connected correctly.

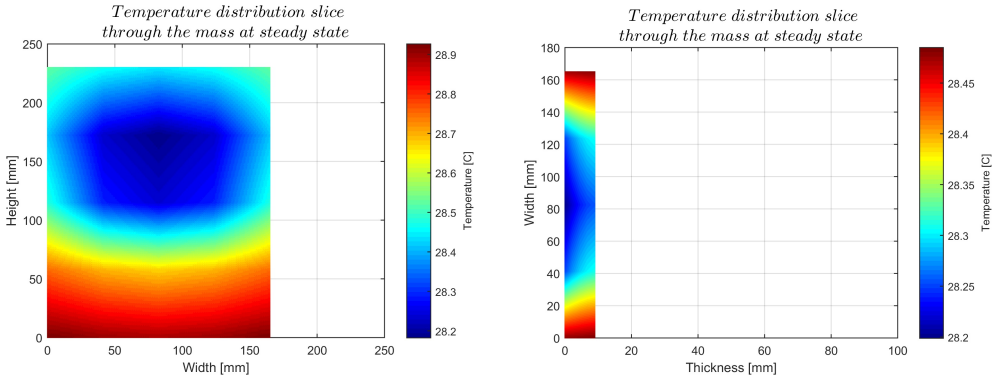

(a) $XY - Plane$ **(b)** $ZY - Plane$

Figure 3.4. Temperature distribution in the Mass

Chapter 4. Parametric Study of the Thermocouple Model

The results in this section were found by generating response surfaces. Response surfaces were created for each of the parameters that describe pulse cooling in figure 4.1. The independent variables for the response surfaces are pulse on-time and pulse height. All surfaces were generated using isosceles triangle shaped pulses. For each parameter, a surface was generated starting pulses from I_{max} and another surface generated starting from I_{opt} for comparison.

4.1 Time to Minimum Temperature

Time to minimum temperature in figure 4.2 is the longest when pulse on-time is maximum and $I_{\mathrm{P}}/I_{\max}$ is minimum. Time to minimum temperature is the minimum with minimum pulse on-times throughout the range of pulse-heights. The two charts

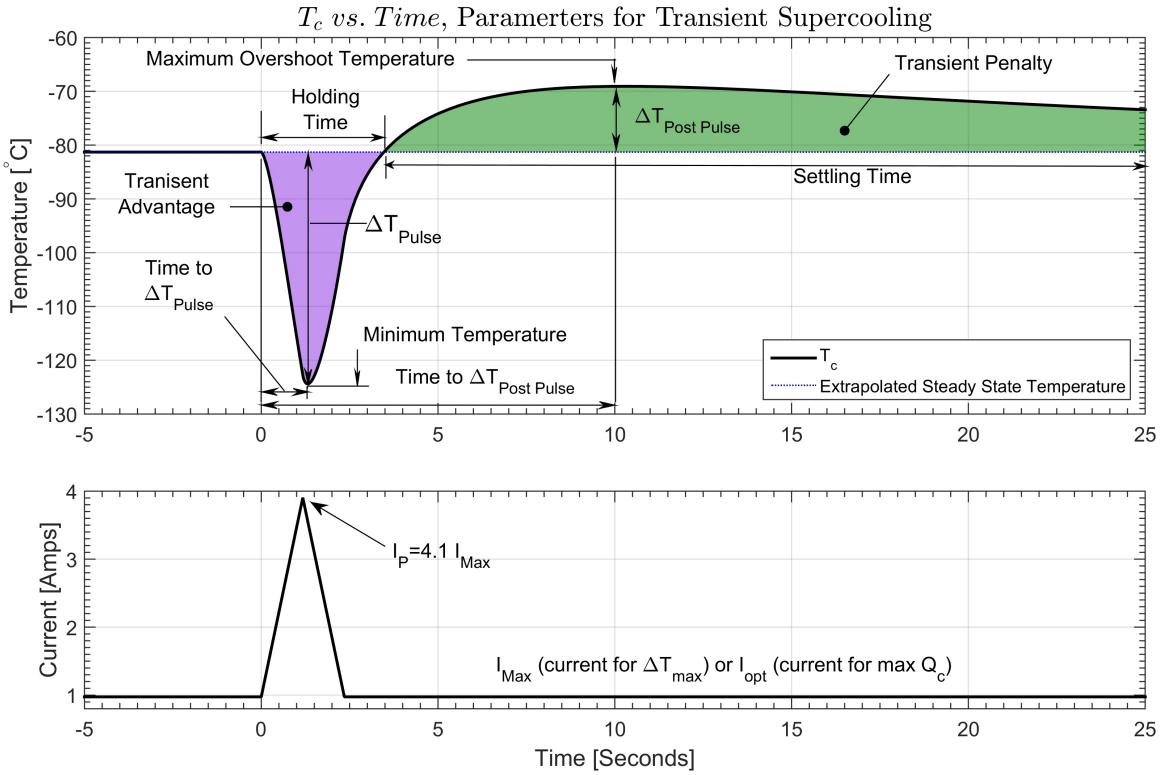

Figure 4.1. Cold side Temperature, T_c, during a Transient Pulse (Triangle Wave)

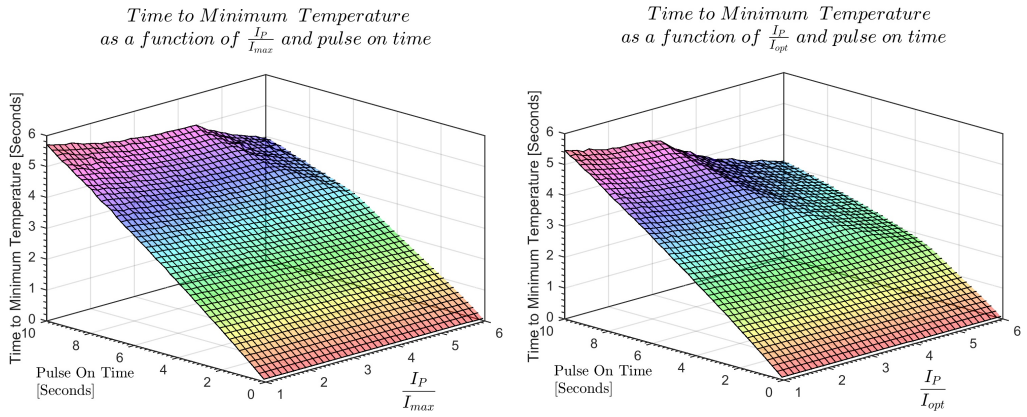

(a) $I_{\max}$ **(b)** I_{opt}

Figure 4.2. Time to Minimum Temperature

of Figure 4.2 are very similar with exception of the area of the plots in the upper right hand corner where a transition occurs. For $I_{\max}$, the time to minimum temperature does not change with $I_{\text{P}}/I_{\max}$, but linearly increases with pulse on-time up until about six seconds. Above six seconds of on-time, and higher than $I_{\text{P}}/I_{\max}$ of four, the time to minimum temperature surface becomes non linear. The same behavior is seen for pulses starting at I_{opt}, however the transition occurs at a lower $I_{\text{P}}/I_{\max}$.

The minimum temperature during a pulse event depends on how much heat is pulled from the thermoelement. The time to minimum temperature is an interplay between rate of heat subtracted by Peltier cooling and rate heat added by internal Joule heat. Temperature will always become lower at T_c as long as net amount of heat is being removed. When the bulk of the time delayed Joule heat reaches the T_c at such magnitude equal to the heat being removed by Peltier cooling, temperature will no longer continue to decrease and minimum temperature will be reached. The time at which this occurs depends on the magnitude of current pulse and current pulse on-time. Based on this, shorter times to minimum temperature indicate Joule heating has overtaken Peltier cooling faster.

In steady state operation analysis, Peltier cooling is a linear function of device input current. Joule heating is a function of current squared. If a linear function and a square function of current are plotted together, it can be seen there are different zones that explain device behavior. On this chart (figure 2.3), at zero current, Peltier cooling and Joule heating are both zero. As current increases, Joule heat and Peltier cooling will diverge and at some point be at maximum separation. The two curves will converge again and at some point be equal. After this point, Joule heat will exponentially diverge from Peltier cooling. The current at maximum separation between Joule heat and Peltier cooling is I_{opt}. The point where the two curves converge

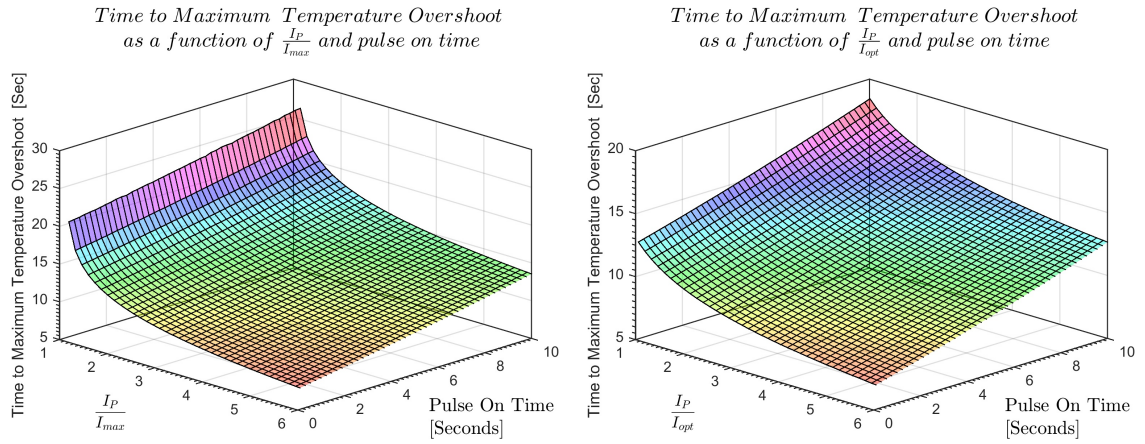

(a) $I_{\max}$ **(b)** I_{opt}

Figure 4.3. Time to Maximum Temperature

is zero Q_c. Above this convergence point, the device could be considered a heater, not a cooler, because the magnitude of Joule heat conducting to T_c is larger than the Peltier cooling leaving it.

It is proposed that the transition zone occurs in figure 4.2 at the point where the magnitude of current produces a net zero Q_c. Time to minimum temperature is a transient phenomenon, so there is still a time separation between Joule heat and Peltier cooling and thus it still takes time to get to minimum temperature, however, at the transition point, the time is reduced at a greater rate because the net rate of Q_c is dropping faster due to exponential separation between Peltier and Joule heating magnitudes.

For design purposes, if a maximum time to minimum temperature was desired, longer pulse on-times and pulse-heights tending toward $I_{\text{P}}/I_{\max} = 1$ are desirable. In effect, one would tend toward steady state $I_{\max}$ operation.

4.2 Time to Maximum Temperature Overshoot

Time to maximum temperature overshoot is the time to maximum temperature during the transient pulse event. This maximum temperature can occur after or during the pulse, depending on the pulse on-time.

In Figure 4.3 the Time to Maximum Temperature is a linear function of pulse on-time and a non-linear function of $I_{\text{P}}/I_{\max}$. The maximum Time to Maximum temperature occurs at maximum pulse on-time and minimum $I_{\text{P}}/I_{\max}$. The minimum Time to

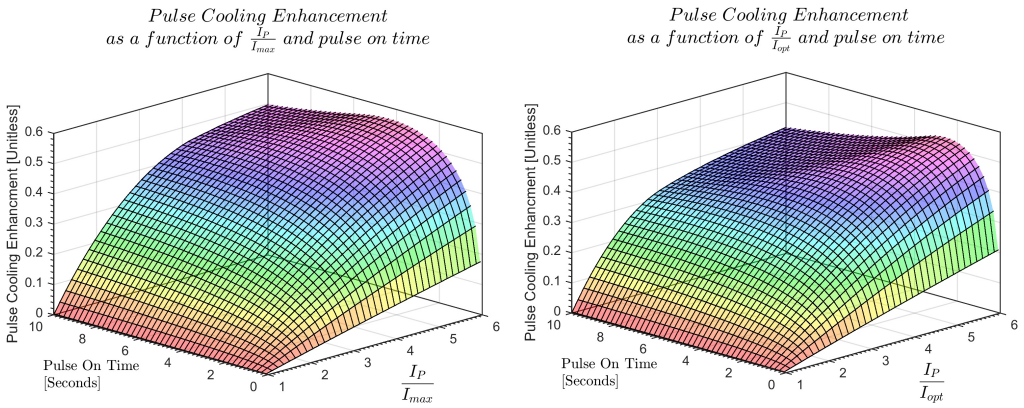

(a) $I_{\max}$ **(b)** I_{opt}

Figure 4.4. Pulse Cooling Enhancement

Maximum temperature occurs at the shortest pulse on-time and largest $I_{\text{P}}/I_{\max}$. For the same range of dependent variables, the Time to Maximum Temperature is longer starting from $I_{\max}$ than from I_{opt}.

This maximum temperature occurs at maximum difference between Joule heat added to T_c and Peltier cooling subtracted. For pulses starting from $I_{\max}$, below an $I_{\text{P}}/I_{\max}$ of 1.146, there is no Maximum Temperature overshoot. This is not shown in the figure. At these pulse-heights, the Peltier cooling from $I_{\max}$ operation is enough to absorb the Joule heat created by the pulse without an increase in temperature above that of steady state operation. In effect, there is always a net greater Peltier cooling at T_c. This behavior is not seen for pulses starting from I_{opt}. The joule heat created when starting a pulse from I_{opt} always overtakes Peltier cooling during a pulse event.

4.3 Pulse Cooling Enhancement

Pulse cooling enhancement is the ratio of ΔT_{Pulse} to ΔT_{max}. A Pulse cooling enhancement of 0.4 means the reduction in temperature due to the pulse is 40% more reduction in temperature compared to $I_{\max}$ steady state operation. In effect this measures how much improvement can be had with a pulse over $I_{\max}$ steady operation.

In Figure 4.4 there is a definitive maximum pulse cooling enhancement for a given design for the independent variable ranges studied here. Additional gains may be obtained in parametric ranges beyond that investigated herein.

Since pulse cooling enhancement is a reduction in temperature, it is helpful to consider that greater reductions in temperature are achieved by increasing the rate at which

heat is removed from T_c. Thus maximum pulse cooling enhancement occurs when the rate of Q_c is the highest. For transient operation, this occurs early on during the pulse before Joule heat has a chance to reach the T_c. In the case of the studied thermoelement design and independent variables, this occurs around the four second pulse on-time mark for $I_{\max}$ operation and around two seconds pulse on-time for I_{opt} operation. This occurs sooner for I_{opt} operation because increasing the current from I_{opt} immediately operates the device with a current that produces less steady state Q_c. That is, there is a higher ratio Joule heat to Peltier cooling from the start.

In a design situation, if one were looking for the maximum pulse cooling enhancement, the use of these surfaces would be one way of finding the optimum combination of $I_{\text{P}}/I_{\max}$ and pulse on-time.

4.4 Transient Penalty

Transient penalty is described in the background section as the area between two curves. This area is constrained between the temperature vs. time curve for the overshoot portion of a transient pulse event and an imaginary straight line that is T_c for steady state operation.

In Figure 4.5, it can be seen that the Transient Penalty increases linearly with pulse on-time and exponentially with $I_{\text{P}}/I_{\max}$. The surface is a result of the two effects. Transient penalty can be seen to approach zero at very small pulses and very small pulse on-times. These operating points are essentially steady state operation. This is expected because Transient Penalty is a result of transient operation and the time delay for Joule heating to reach T_c.

Transient penalty is proportional to the amount of Joule heat generated within the volume of the thermoelement during the pulse. Joule heat increases with the square of input current. Also, more heat is generated linearly as the pulse is left on longer. From a design standpoint, transient penalty may be difficult to eliminate. It is possible the Transient Penalty may be reduced by using material properties with an optimum mix of Seebeck coefficient, resistivity and thermal conductivity.

It was seen early on in the model development that holding the figure of merit Z constant while variably mixing the ratios of Seebeck coefficient, resistivity, and thermal conductivity can change the time required to return to steady state. Optimizing the material for minimum Transient Penalty or optimizing any of the transient characterization could be a topic of future study.

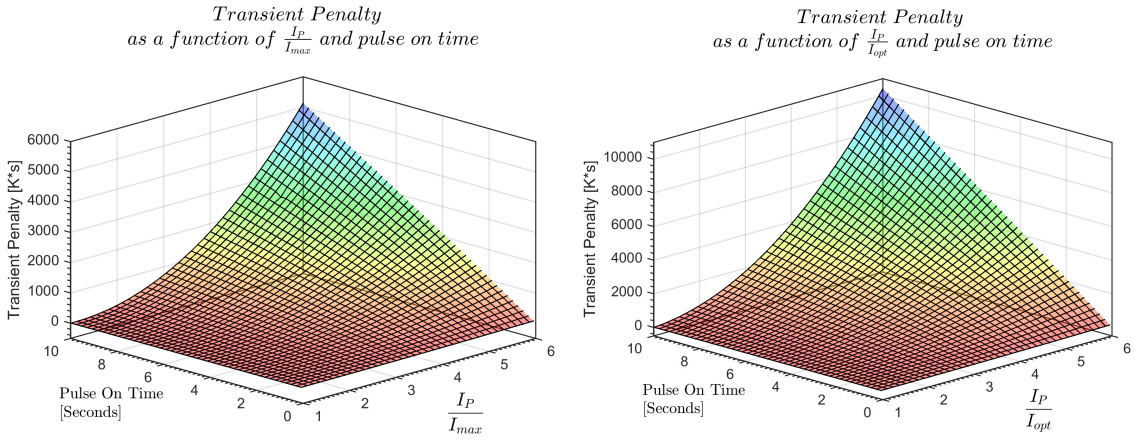

(a) $I_{\max}$ **(b)** I_{opt}

Figure 4.5. Transient Penalty

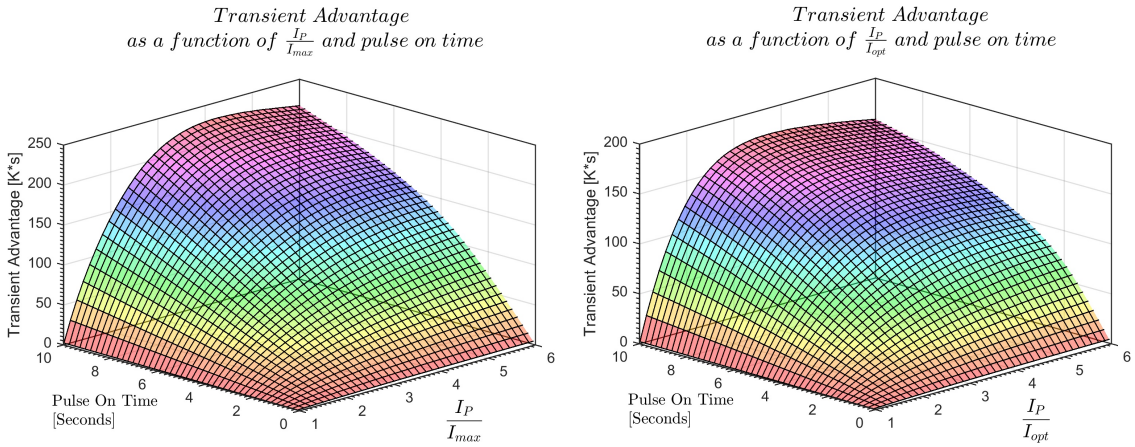

(a) $I_{\max}$ **(b)** I_{opt}

Figure 4.6. Transient Advantage

4.5 Transient Advantage

Transient Advantage is described in the background section as the area between two curves. One curve is the temperature produced by steady current operation and the other curve is temperature vs. time curve for the supercooling portion of a transient pulse event.

From Figure 4.6, the effects of both pulse on-time and $I_{\text{P}}/I_{\max}$ are observed to be nonlinear. A clear maximum occurs at approximately $I_{\text{P}}/I_{\max} = 4$ for both $I_{\max}$ and I_{opt}. Additional transient advantage may be gained with additional pulse on-times

that are beyond the limits of what was studied here. The peak transient advantage is around $225Ks$ for $I_{\max}$ operation and around $175Ks$ for I_{opt} operation.

Transient advantage is an aggregate of both minimum temperature achieved and time spent below $I_{\max}$ steady state temperature. The peak Transient Advantage is the point that has the best combination of Minimum Temperature achieved and time spent below $I_{\max}$ steady temperature.

The minimum temperature achieved and the time spent below $I_{\max}$ steady temperature are both related to the relative rates of Peltier cooling and Joule heating reaching T_c. The minimum temperature will continue to go lower as long as the Peltier cooling is larger in magnitude than Joule heating at T_c. Likewise the time spent below $I_{\max}$ steady state temperatures can be prolonged by having a very small net difference between Peltier cooling and Joule heating. Temperatures drops quickly when Peltier cooling has a large difference from Joule heating and rise quickly if Joule heating has a much larger magnitude than Peltier cooling. Bringing these rates closer to each other would provide a temperature drop or rise that changes very slowly and prolongs time spent below $I_{\max}$ steady temperature.

In Figure 4.6, $I_{\max}$ operation has a higher peak Transient Advantage than I_{opt}. For a transient temperature vs. time event, starting from $I_{\max}$ or I_{opt} early on in the pulse event, Peltier cooling is the dominant effect thus the temperature drops very quickly. Time delayed Joule heat generated internally in the thermoelement quickly catches up to T_c. Due to Joule heat being the square of operating current, I_{opt} operation should start out with a higher proportion of Joule heat than $I_{\max}$ operation. As time into a pulse progresses, this proportion will become higher for both operating currents yet increase faster for I_{opt} operation based on its squared relationship with current.

Even if the pulse from I_{opt} was to reach an initially lower temperature than a pulse from $I_{\max}$, the time spent there would be less than the pulse from $I_{\max}$ operation. The net effect is a Transient Advantage that is larger for $I_{\max}$ operation under the same dependent variables. The dominant factor in Transient Advantage is Joule heat. Since starting a Pulse from I_{opt} will always create a disproportional increase of Joule heat, pulses from $I_{\max}$ operation with the same independent variables will have a higher advantage.

From a design perspective, it is helpful to understand the above discussed factors that control minimum temperature and time below steady state $I_{\max}$ operation. With these in mind, an optimal combination of $I_{\text{P}}/I_{\max}$ and pulse on-time can be found. This information could also help design a pulse shape that has characteristics that could initially bring temperature down to a desired minimum and then control the relative

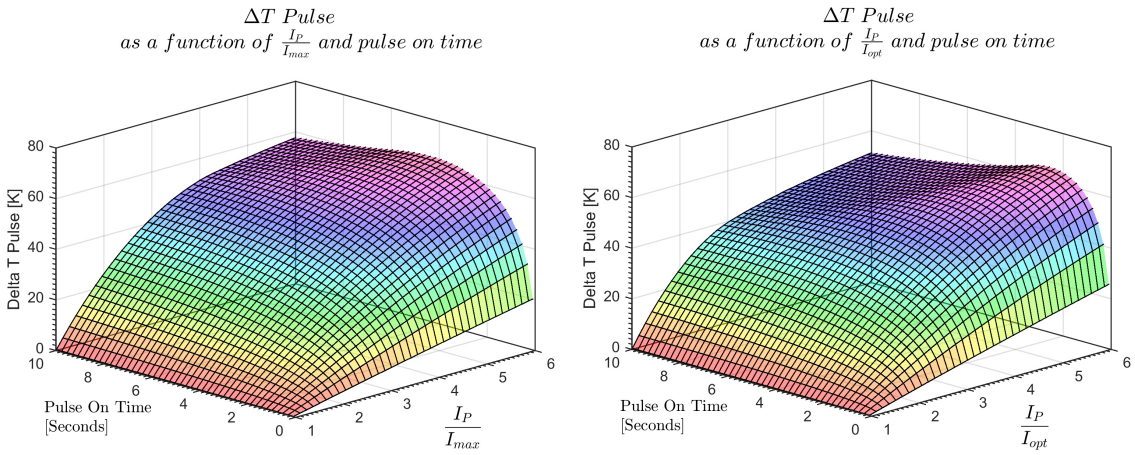

(a) $I_{\max}$ **(b)** I_{opt}

Figure 4.7. ΔT_{Pulse}

rates of Peltier and Joule heating to maximize time below $I_{\max}$ steady operation temperature. In effect a pulse shape is a designed combination of $I_{\text{P}}/I_{\max}$ and pulse on-time.

4.6 ΔT_{Pulse}

ΔT_{Pulse} is very similar to Pulse Cooling Enhancement with exception that it is a difference rather than a ratio. ΔT_{Pulse} may be more of an interest for those comparing absolute ΔT, while Pulse Cooling Enhancement could be more of an interest to those that want a normalized perspective. The analysis between the two is the same.

4.7 $\Delta T_{\text{post pulse}}$

$\Delta T_{\text{post pulse}}$ is the magnitude of the delta between the maximum temperature achieved and the temperature achieved by steady state operation. $\Delta T_{\text{post pulse}}$ happens after the pulse has occurred and the bulk of the Joule heat arrives at T_c during Superheating. $\Delta T_{\text{post pulse}}$ is a normalized method of reporting the effect of superheating during a transient pulse event. A normalized method allows for comparison of performance between two different devices or hot side temperatures.

In Figure 4.8, $\Delta T_{\text{post pulse}}$ is a linear function of pulse on-time and a non-linear function of $I_{\text{P}}/I_{\max}$. For the same independent variables, the magnitude of $\Delta T_{postpulse}$ is double for I_{opt} operation than for $I_{\max}$ operation.

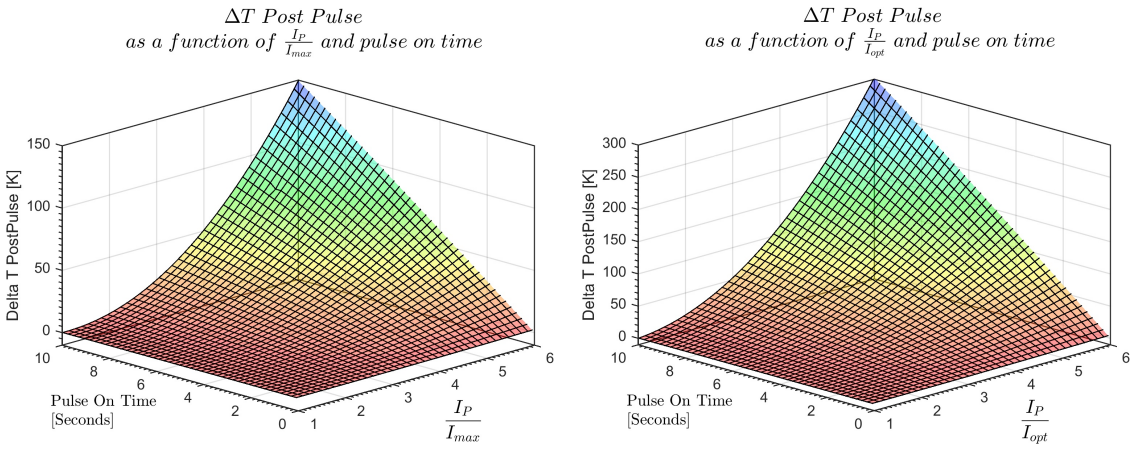

(a) I_{max} **(b)** I_{opt}

Figure 4.8. $\Delta T_{\text{post pulse}}$

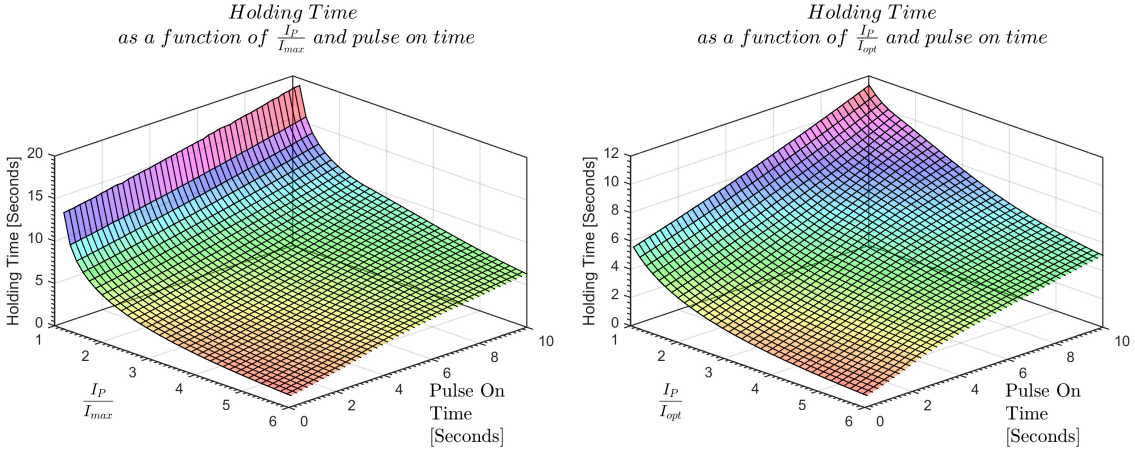

(a) I_{max} **(b)** I_{opt}

Figure 4.9. Holding Time

The reason $\Delta T_{\text{post pulse}}$ is higher for I_{opt} operation is due to the maximum temperature reached being primarily a function of the magnitude of Joule heat reaching T_c. The Joule heat created is much higher for I_{opt} because Joule heat is a function of current squared and I_{opt} operation is at a higher current.

4.8 Holding Time

Holding Time is defined as the amount of time during a transient pulse event that T_c spends below the temperature at which it would have been during steady state operation.

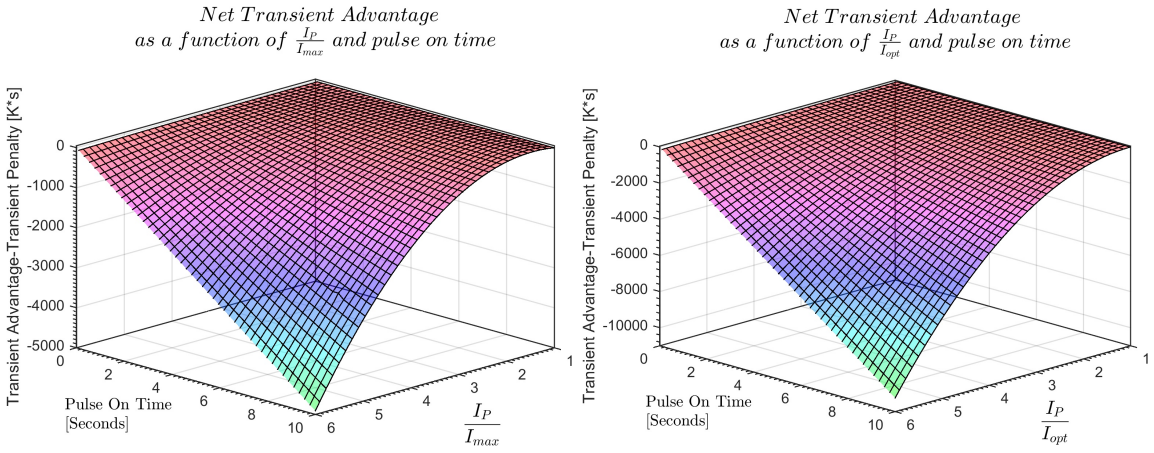

(a) $I_{\max}$ **(b)** I_{opt}

Figure 4.10. Net Transient Advantage - Full Study Range Surface

Holding Time is a linear function of pulse on-time and a nonlinear function of $I_{\text{P}}/I_{\max}$. Although not shown on figure 4.9a for clarity, for $I_{\max}$ operation and $I_{\text{P}}/I_{\max}$ smaller than 1.146, Holding Time increases to approximately 300 to 400 seconds with pulse on-times ranging from 0 to approximately 10 seconds. Peak Holding Time for $I_{\max}$ operation is much higher than that of I_{opt} operation. The explanation of why Holding Time is larger for $I_{\max}$ operation is the same as that of Transient advantage and was discussed previously. See figure 4.6 analysis for details.

4.9 Net Transient Advantage

Net Transient Advantage is the difference between Transient Advantage and Transient Penalty. A positive difference is considered a net advantage and a negative difference is a net penalty. A net advantage indicates a net increase in Q_c for a transient pulse event over steady state operation.

From figure 4.10, it can be seen that for both $I_{\max}$ and I_{opt} operation, Net Transient Advantage approaches zero. Upon closer inspection of the $I_{\max}$ operation chart and zooming closer on the scale, a net advantage is found. See figure 4.11.

Figure 4.11 shows a zoomed in version of 4.10a. It can be seen that $I_{\max}$ operation contains a net advantage between a $I_{\text{P}}/I_{\max}$ of 1 and 2.

Additional gains may be seen by simulating additional pulse on-time past 10 seconds. At some point adding pulse on-time would no longer be considered transient operation. Steady state may be defined as when Joule heat from a increase in current is

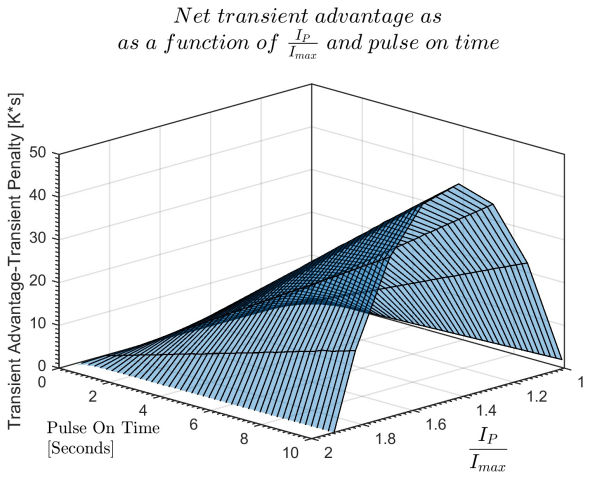

Figure 4.11. Net Transient Advantage - Advantage Portion, $I_{\max}$ Surface

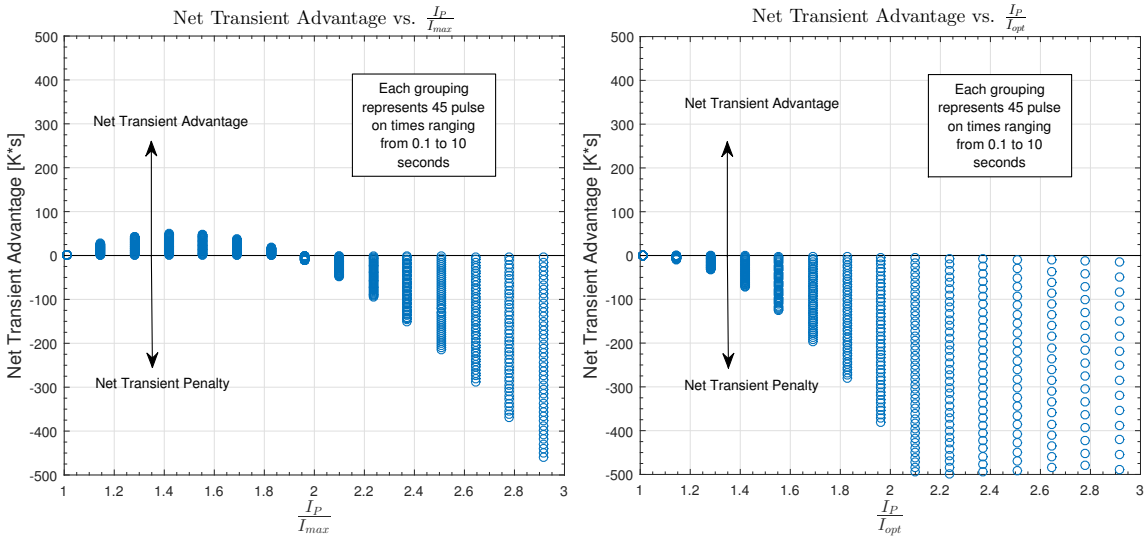

(a) $I_{\max}$ **(b)** I_{opt}

Figure 4.12. Net Transient Advantage - Partial Study Range, Alternate View

no longer delayed from effecting T_c.

Figure 4.12 shows the same data as the two plots in figure 4.10, however the figures are now viewed from the side and without surface. Figure 4.12 clearly shows the area where $I_{\text{P}}/I_{\max}$ creates a net transient advantage for $I_{\max}$ operation and the same $I_{\text{P}}/I_{\max}$ for I_{opt} creates a net transient penalty.

The reason pulses from I_{opt} operation provide no net Transient Advantage is related to steady state operation. As discussed previously, I_{opt} steady state operation is the

point of maximum separation between the magnitude of Joule heating and Peltier cooling. Any additional increase in current, serves to provide more Joule heat than Peltier cooling. The net Q_c for steady state operation goes down in this case. For the transient case, the pulse is the additional current over steady state I_{opt} current. As in steady state operation, the Joule heat is now larger than Peltier cooling. For transient operation, the only difference is the time separation between the two factors.

Chapter 5. Performance Measures of the System Model

The previous results presented in the previous chapter were obtained by modeling a single thermocouple with no attached mass. In this chapter a complete thermoelectric cooler module connected to a heat generating mass is used to study the effect of current pulses on performance while varying system parameters. The analysis also looks at the effect of starting pulses from both $I_{\max}$ and I_{opt} operation.

5.1 Effect of Pulse Height, $I_P/I_{\max}$

Figure 5.1 shows the effect of variable $I_P/I_{\max}$ on temperature for pulses starting from both $I_{\max}$ and I_{opt} steady current. It is seen that some of the pulses provided a net heat removal compared with steady operation as shown by the lasting temperature reduction for pulses starting from $I_{\max}$. All pulses starting from I_{opt} provide a net heating effect over steady state operation that can be seen from the lasting increased average temperature of the mass.

The dip in temperature is due to Peltier cooling that happens instantly at the cold junction. The time delayed Joule heat then arrives at T_c raising the average temperature of the mass. Some current pulses provide a net cooling because the magnitude of

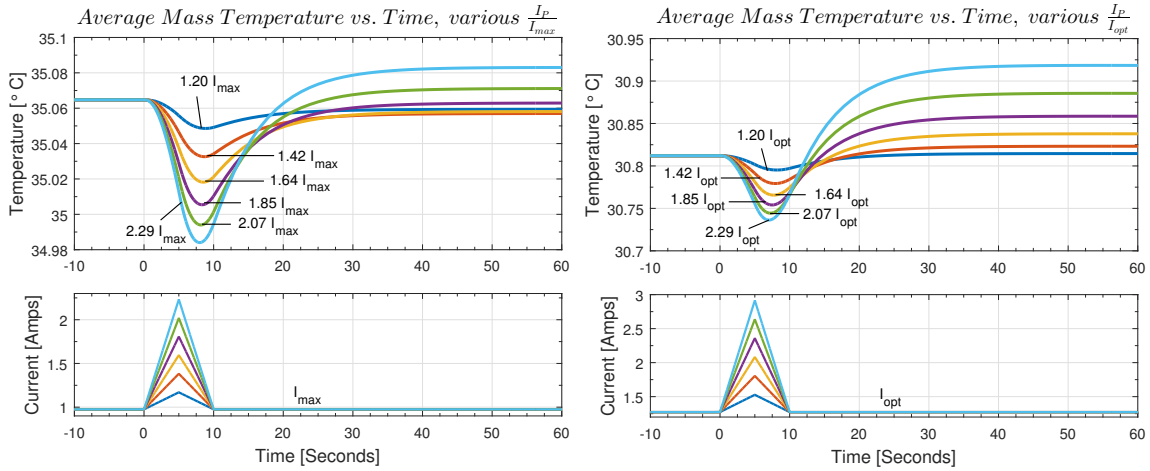

(a) $I_{\max}$ **(b)** I_{opt}

Figure 5.1. Effect of Pulse Height, $I_P/I_{\max}$ on Average Mass Temperature

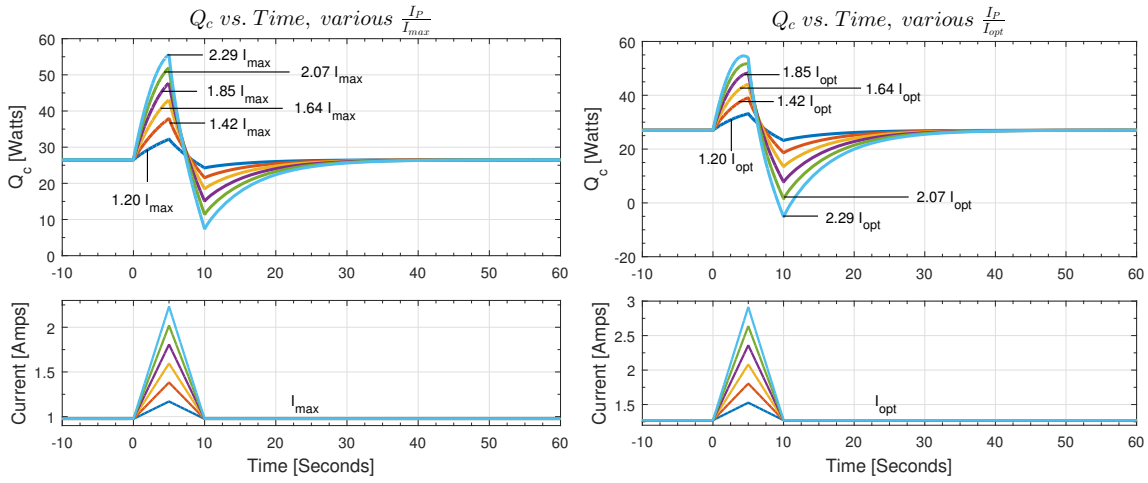

(a) $I_{\max}$ **(b)** I_{opt}

Figure 5.2. Effect of Pulse Height, $I_{\text{P}}/I_{\max}$ on Q_c

Peltier cooling is greater than that of Joule heating. Some pulses provide net heating over steady state operation because the Joule heating over the pulse event is higher than the Peltier cooling.

Now looking at the effect of the pulse-height on Q_c, figure 5.2 confirms the finding from figure 5.1. The delay in Joule heat is clear. After an initial spike in Q_c, a rapid drop in Q_c follows. As pulse-heights become larger, the net amount of energy removed during the entire transient event becomes lower than it would have otherwise been had the steady state operation continued without a pulse. As expected, some of the pulses are net lower cooling than steady state when starting from $I_{\max}$ current. When starting from I_{opt} operation, the net cooling is lower for all pulse-heights than it would be had steady state operation continued.

P_{in}, shown in Figure 5.3 is approximated by the steady state equation (2.14). Each term of the equation, however, are time delayed from one another for transient operation. Electrical current happens instantly. The temperatures of T_h and T_c take time to change. This explains the nonlinear shape of the P_{in} curve.

Figure 5.4 shows the effect of various $I_P/I_{\max}$ on COP. Interestingly, COP drops for all $I_P/I_{\max}$. COP is defined by equation 2.15. One may expect that an increase in P_{in} and a roughly proportional increase in Q_c initially during the pulse would keep the COP almost constant or the same as in steady state operation, however there is a drop in COP. The reason this happens is again the time separation between Q_c and P_{in}. The current and for the most part power in the equation for COP happens instantly. The Q_c is time delayed. For COP this means a fast increase in P_{in} before

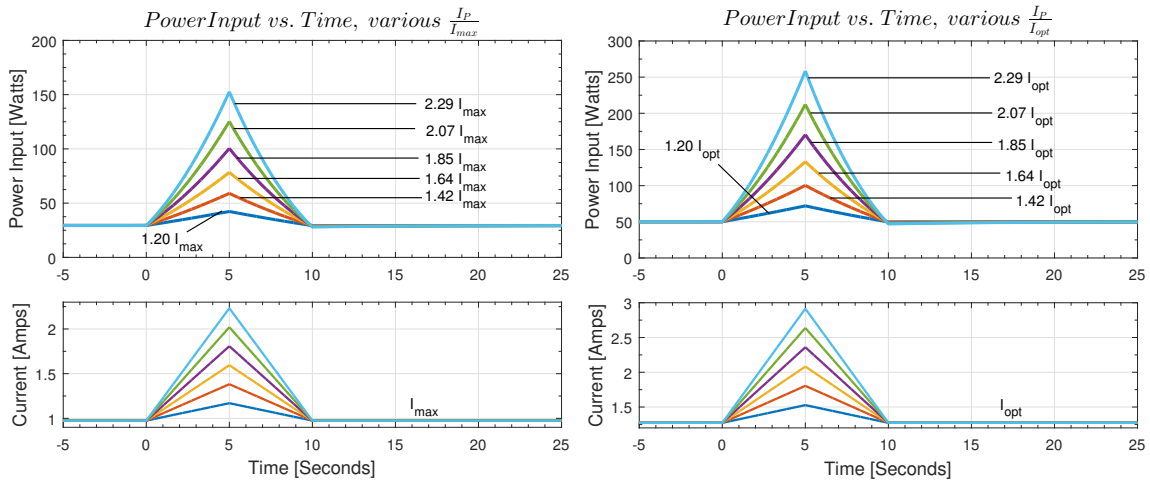

(a) $I_{\max}$ **(b)** I_{opt}

Figure 5.3. Effect of Pulse Height, $I_{\text{P}}/I_{\max}$ on P_{in}

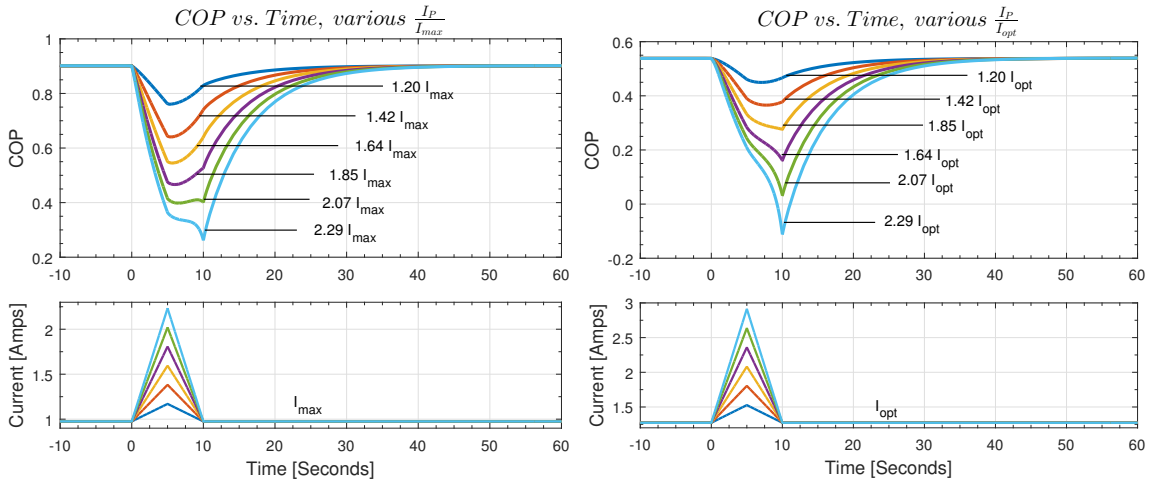

(a) $I_{\max}$ **(b)** I_{opt}

Figure 5.4. Effect of Pulse Height, $I_{\text{P}}/I_{\max}$ on COP

Q_c can react proportionally. Thus the reduction in COP.

For current pulses starting from I_{opt}, COP drops below zero. In addition to the time delay that lowers COP, the addition of Joule heat greater than Peltier cooling causes Q_c to become negative, further dropping COP. Knowledge of this transient effect on COP can help designers optimize device operation for transient applications. The design that allows for faster heat transfer may be the most efficient.

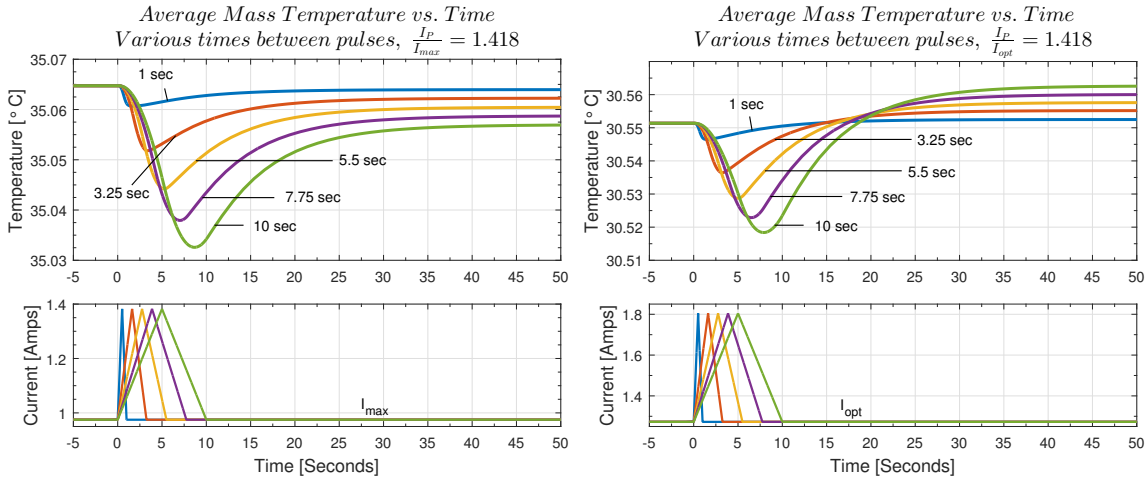

(a) $I_{\max}$ **(b)** I_{opt}

Figure 5.5. Effect of Pulse On-Time to Mass Temperature

5.2 Effect of Pulse On-Time

Figure 5.5 shows the effect of leaving the same magnitude current pulse on for a longer time. For the current pulse starting from $I_{\max}$, average mass temperature during and after the pulse is lower than that of steady state. This suggests a net heat removal from the mass during the pulse event.

For the current pulses starting from I_{opt}, average mass temperature becomes lower with longer pulse on-time however the average mass temperature recovers to a temperature higher than it otherwise would have been in the absence of a pulse. This suggests the heat removal with a current pulse starting from I_{opt} has a lower net Q_c than steady state operation.

If the current pulses are left on longer or for a infinite time period, the device would simply be operating at a new steady state current. Operating the device at a current higher than $I_{\max}$ will provide a higher Q_c, however, operating at a current higher than I_{opt} will not due to the higher proportion of Joule heat relative to Peltier cooling at those current levels.

In Figure 5.6, additional pulse on-time increases net Q_c over steady state operation during the pulse event for some pulses starting from $I_{\max}$ operation. This is difficult to see in the figure but it is known from the study of Net Transient Advantage in figure 4.12. Net Transient Advantage uses the approach of temperature over time. Analysis of Q_c can tell the same story as analysis of transient temperatures because

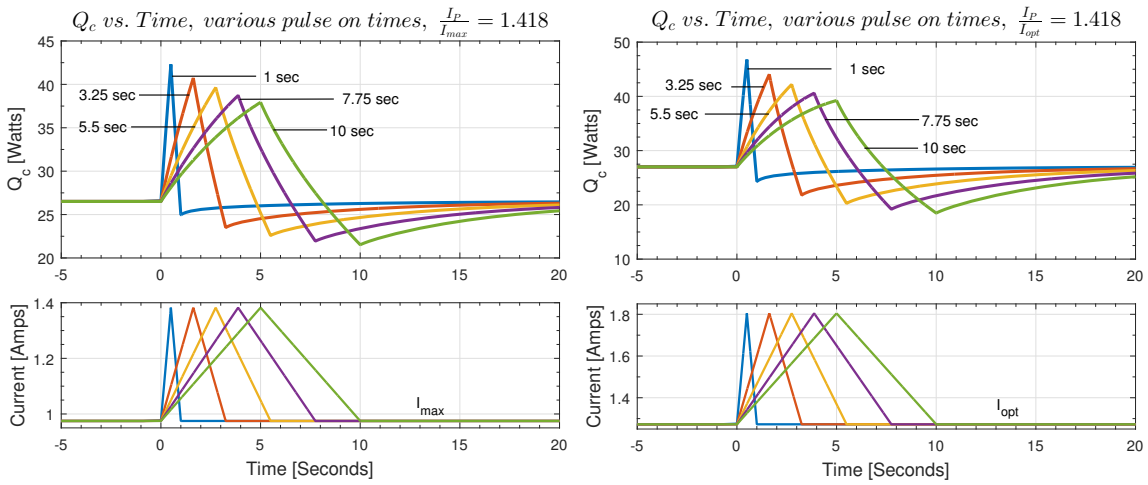

(a) $I_{\max}$ **(b)** I_{opt}

Figure 5.6. Effect of Pulse On-Time on Q_c

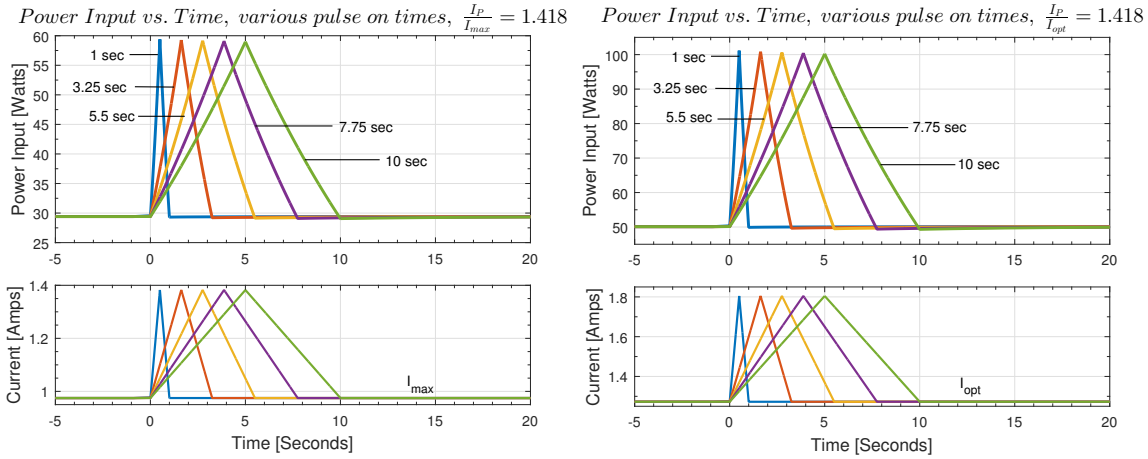

(a) $I_{\max}$ **(b)** I_{opt}

Figure 5.7. Effect of Pulse On-Time on P_{in}

they are directly related.

The power scales as expected with increases in pulse on-time as observed in Figure 5.7. Figure 5.8 shows a trend of COP decreasing with each successive increase in pulse on-time. This happens for the current pulses starting from I_{opt} and $I_{\max}$. The reason this happens is because the time spent at higher current levels is longer for the longer pulse on-times. This increases the amount of Q_c, however again the Q_c is on a slower time scale than the current input. As Q_c increases, there may be an inability for the mass to transfer the heat to the device. Localized temperature gradients could

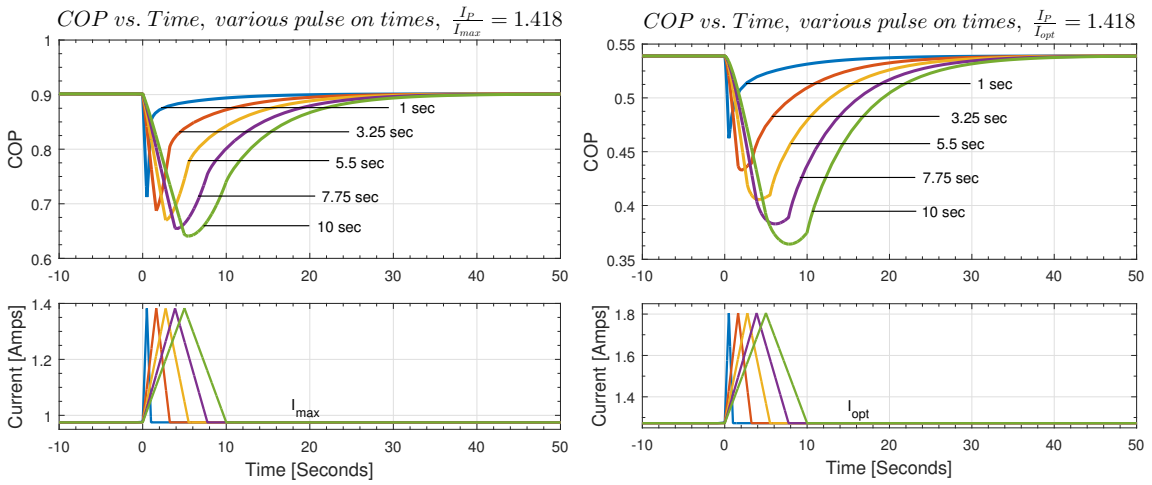

(a) $I_{\max}$ **(b)** I_{opt}

Figure 5.8. Effect of Pulse On-Time on COP

develop around the device and slow the driving force for heat transfer to the device. The additional heat transfer proportional to current may not be able to be obtained due to other limiting thermal resistances in the system.

5.3 Effect of Interface Resistance between Heat Spreader and Thermoelectric Cooler

Figure 5.9 compares the effect on average mass temperature of linearly changing thermal interface resistance for the cold side of the device. This figure also compares the effect of starting pulses from I_{opt} and $I_{\max}$. The lowest thermal interface resistances produced the lowest average mass temperature. The temperature drop during the pulse is proportional to changes in thermal interface resistance for I_{opt} and $I_{\max}$ operation.

As expected and seen from previous data, temperatures remain lower than initial steady operation after the pulse starting from $I_{\max}$. Starting from I_{opt} shows an increase in temperature after a pulse. This reflects a higher net Q_c provided over the pulse event from pulses starting from $I_{\max}$.

Figure 5.10 compares the effect on Q_c of linearly changing thermal interface resistance for the cold side of the device. This figure also compares the effect of starting pulses from I_{opt} and $I_{\max}$. Looking at steady state alone for both $I_{\max}$ and I_{opt} operation, the highest Q_c thermal interface resistance is the lowest thermal interface resistance. This might be expected because the lower thermal resistance would be less likely to

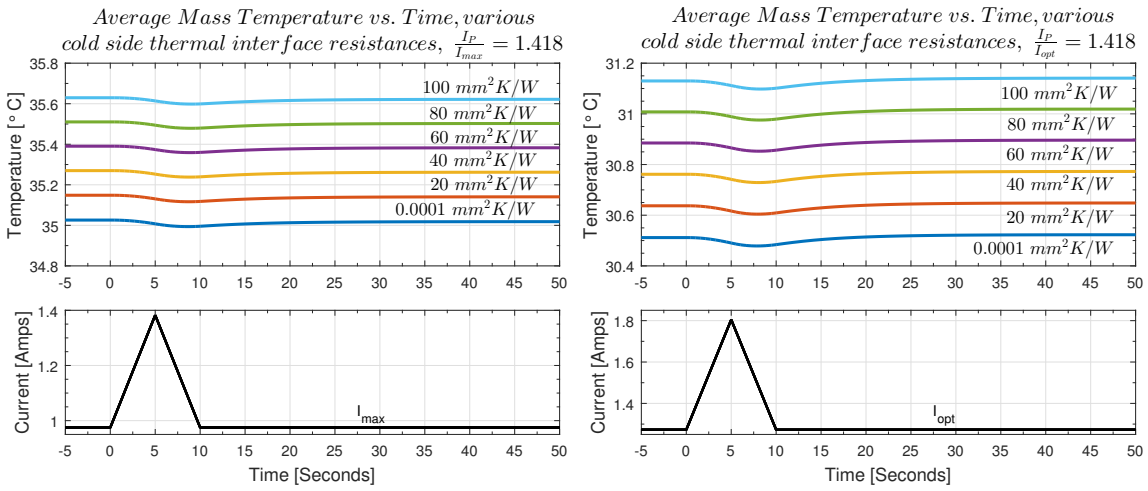

(a) Cold Side - I_{max} **(b)** Cold Side - I_{opt}

Figure 5.9. Effect of Changing Device Cold Side Interface Resistance on Mass Temperature

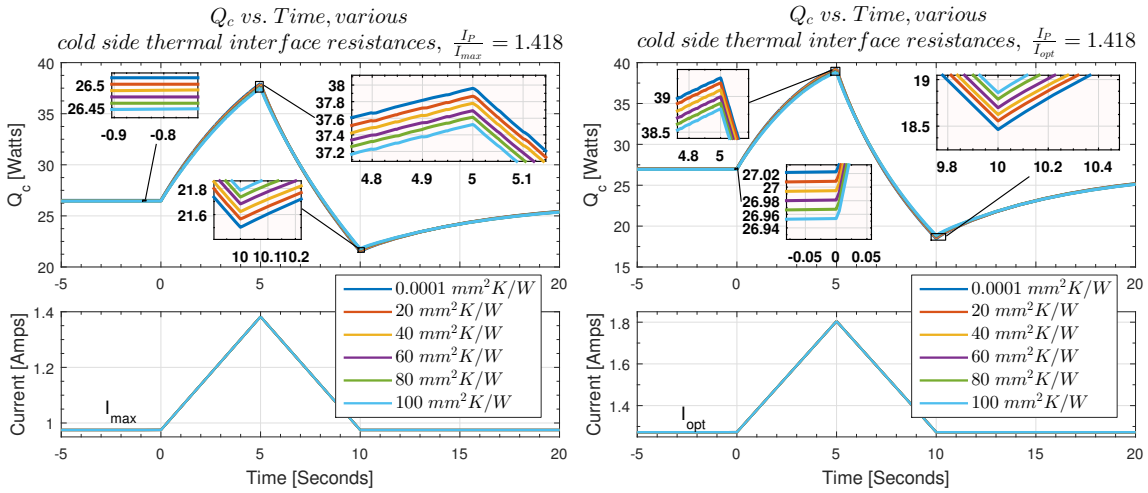

(a) Cold Side - I_{max} **(b)** Cold Side - I_{opt}

Figure 5.10. Effect of Changing Device Cold Side Interface Resistance on Q_c

limit the heat flow to the thermoelement. Interestingly, this changes for transient operation while current input is decreasing during the pulse and for a time after. During this time the highest Q_c is seen for the highest thermal interface resistance.

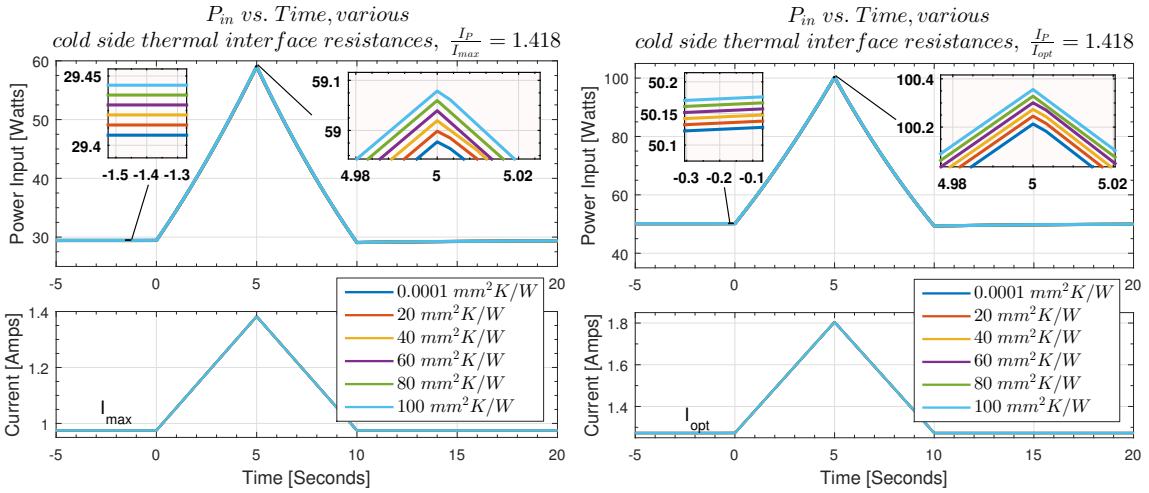

(a) Cold Side - $I_{\max}$ **(b)** Cold Side - I_{opt}

Figure 5.11. Effect of Changing Device Cold Side Interface Resistance on P_{in}

Consider the case of higher thermal interface resistance on the cold side of the device. Relative to low interface resistance, heat is limited from flowing into T_c from the mass by the higher interface resistance. In this case, T_c will be colder during the the initial Peltier cooling that happens instantly during the pulse. This is because more heat is pulled from the immediate surroundings and thermoelement and less through the high interface resistance. The temperature gradient between T_c and the center of the thermoelement is now a driving force for conduction heat transfer in the thermoelement. Because of the initially lower T_c with the high thermal interface resistance, the rate of thermal conduction is higher for this case inside the thermoelement. This draws the bulk of the Joule heat from the thermoelement faster for the higher thermal interface resistance case. As the current pulse starts to decrease on the down slope, the magnitude of Joule heat reaching T_c is now smaller than the low thermal interface resistance case because there is not as much left. It was pulled out by the higher rate of conduction. Q_c being the net sum of the Joule heat entering T_c by thermal conduction and the heat leaving T_c by Peltier cooling is now higher than the low thermal interface resistance case.

A future study might look a the net impact of thermal interface resistance over a transient cycle. Rather than assume that lower thermal interface is better, there may be an optimal thermal interface resistance that depends on the amount of transient operation in a given time. Knowledge of optimal thermal interface rather than assuming lower is better could save unneeded expense of using exotic thermal interface materials.

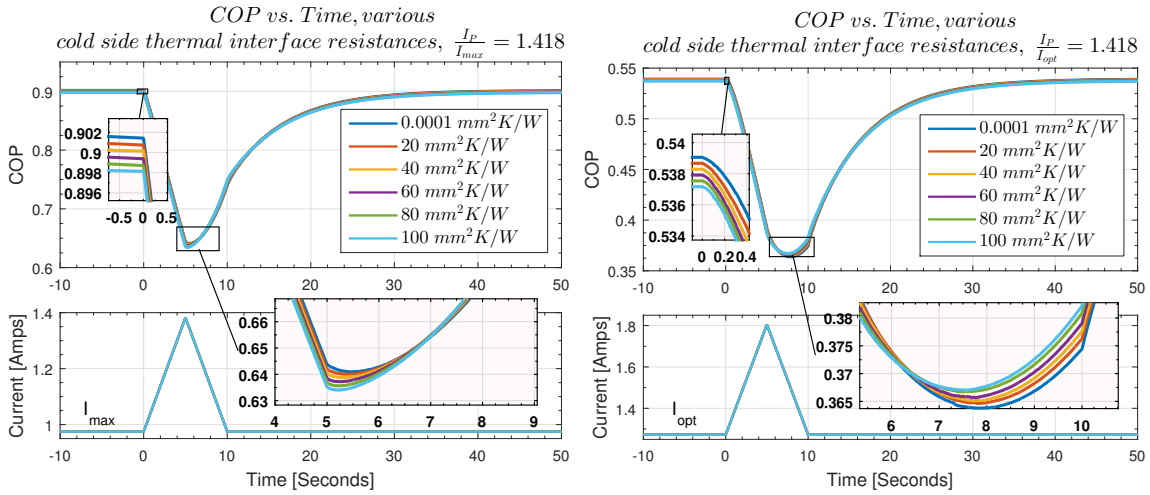

(a) Cold Side - $I_{\max}$ **(b)** Cold Side - I_{opt}

Figure 5.12. Effect of Changing Device Cold Side Interface Resistance on COP

From Figure 5.11, the lowest thermal interface resistance is observed to be that which requires the least power input. This can be explained through equation 2.14. The Joule heating portion of this equation is constant. The Seebeck term changes with thermal interface resistance. This happens because the Seebeck term is a function of T_h and T_c. With smaller thermal interface resistance, the cold side does not get as cold and the hot side does not get as hot. If a thermocouple was placed in free air for example, simulating a high interface resistance, the hot side would become very hot and the cold side would become very cold. If the same thermocouple was placed between two highly conductive plates simulating a low thermal interface resistance, the thermoelement could potentially not change temperature at all. Since equation 2.14 is a function of the delta between T_h and T_c, and the situation of high thermal interface resistance increase this ΔT, power required goes up. In effect this Δ creates a Seebeck voltage, and increases the work required to push current through the device.

Looking at figure 5.12, interesting behavior was seen again starting at around 6 seconds. This shows a reversal in which interface resistance has the highest COP at a given time. At about 6 seconds, the highest thermal interface resistance started heading toward the highest COP. We know from the analysis of figure 5.10, that the Q_c for the highest thermal interface went from lowest during steady state and increasing current to the highest Q_c during the down slope of the pulse and for a time there after. This effect can be seen in figure 5.12 with a reversal in COP.

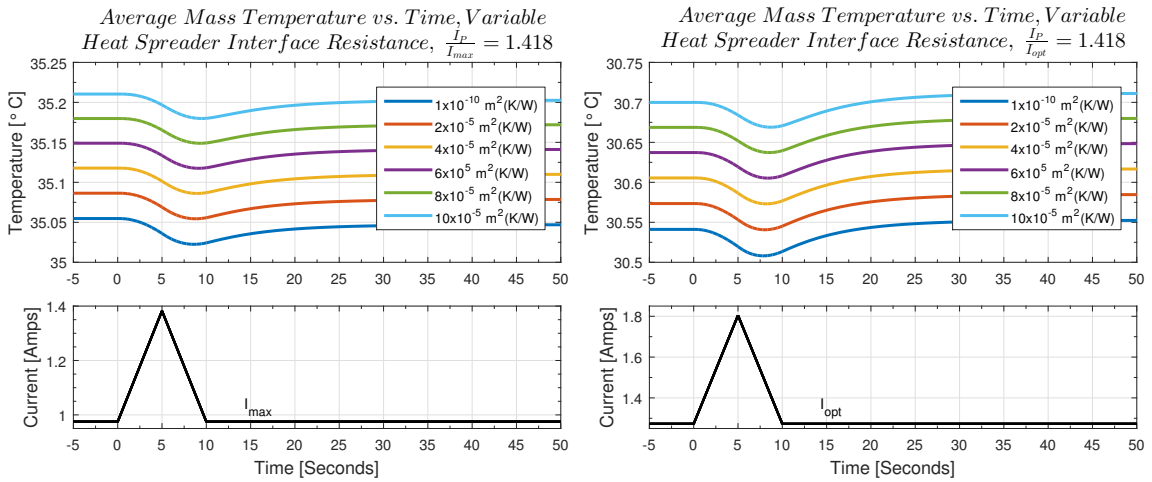

(a) $I_{\max}$ **(b)** I_{opt}

Figure 5.13. Effect of Heat Spreader-Mass Interface Resistance on Mass Temperature

5.4 Effect of interface Resistance between Heat Spreader and the Mass

Figures 5.13 through 5.16 illustrate the effect that the thermal resistance between the heat spreader on the mass has on average mass temperature, Q_c, P_{in}, and COP, respectively.

The trends seen are similar as that of heat spreader thermal conductivity without the diminishing returns. The effect of changing thermal interface resistance is very small during the pulse and during steady state operation. Lower thermal interface resistance allowed for the lowest temperature, highest Q_c, lowest power consumption and highest COP even though the effect was very small. The scale is so fine that some defects in the numerically found results can be see. This is most prominent in the zoomed in portion in the upper right hand corner of figure 5.15.

5.5 Effect of Mass Thermal Effusivity

Figure 5.17 shows the average mass temperature effect of changing the thermal effusivity of the mass with linearly spaced values. The change in average temperature of the mass during the pulse is difficult to see in this figure due to a relativly wide scale compared with previous figures. The largest thermal effusivity values allow for the most cooling during the steady state operation. This is expected because a larger

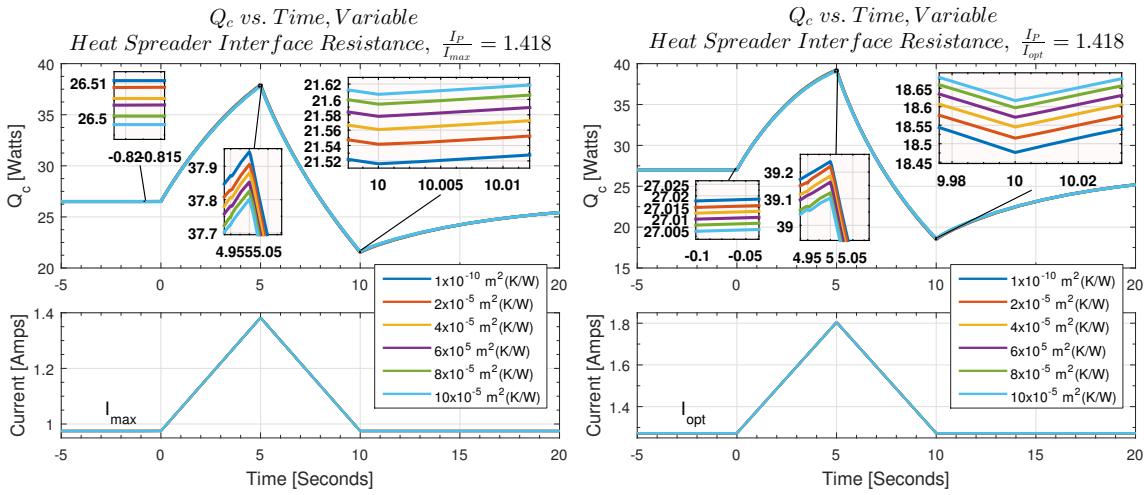

(a) I_{max} **(b)** I_{opt}

Figure 5.14. Effect of Heat Spreader-Mass Interface Resistance Q_c

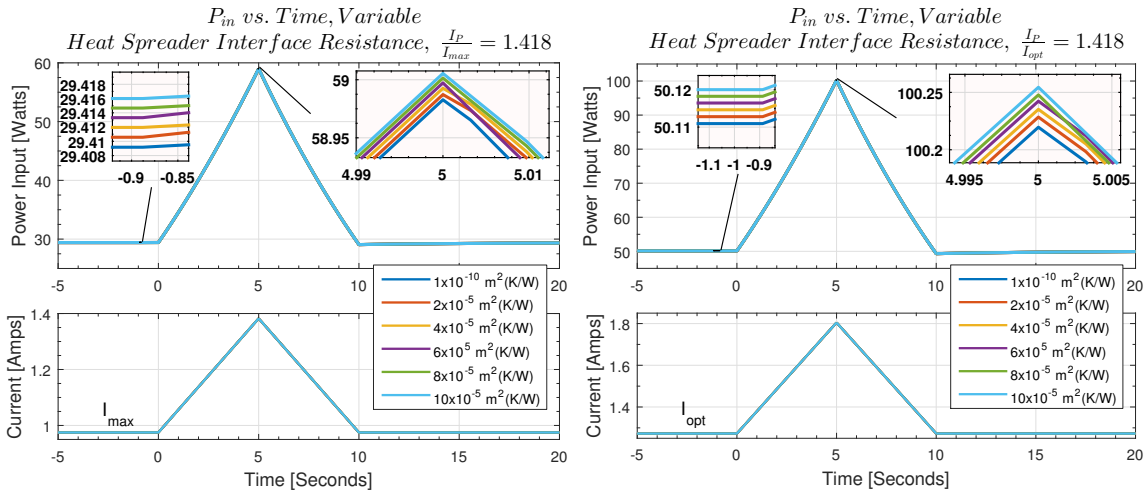

(a) I_{max} **(b)** I_{opt}

Figure 5.15. Effect of Heat Spreader-Mass Interface Resistance on P_{in}

effusivity value means heat can be transfered through the mass with less thermal resistance. This means a greater amount of heat can be transferred. It is notable that increasing the effusivity meets a point of diminishing returns. It may be the highest thermal resistance in the system is limiting the flow of heat through the mass and therefore any increases in thermal effusivity of the mass no longer increase heat flow.

Figure 5.18 shows the effect on Q_c of linearly changing the thermal effusivity of the mass. The change in Q_c follows expectedly with what was seen with changes in

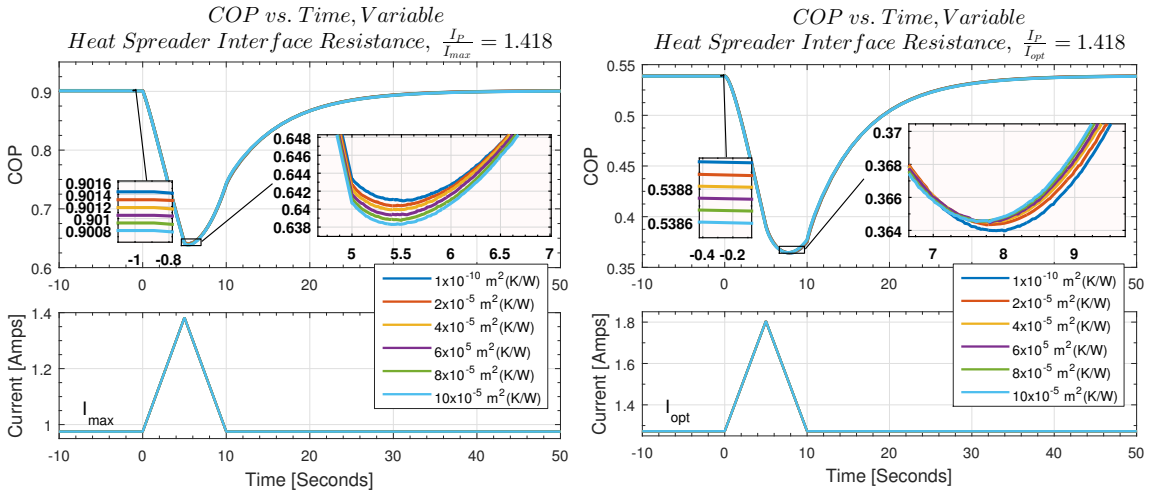

(a) $I_{\max}$ **(b)** I_{opt}

Figure 5.16. Effect of Heat Spreader-Mass Interface Resistance on COP

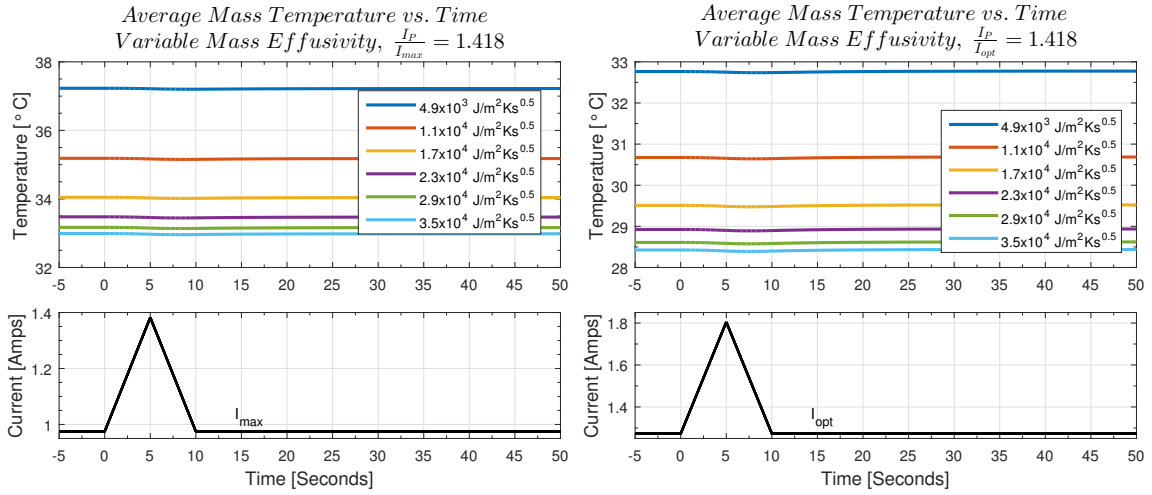

(a) $I_{\max}$ **(b)** I_{opt}

Figure 5.17. Effect of Mass Thermal Effusivity on Mass Temperature

temperatures. Larger values of thermal effusivity allow for more Q_c up to a limit. This very small change in Q_C showed a more than expected change in average mass temperature.

Figure 5.19 shows the effect on P_{in} of linearly changing the thermal effusivity of the mass. The same trend of seeing a point of diminishing returns with changes in thermal effusivity is seen when looking at the power consumption.

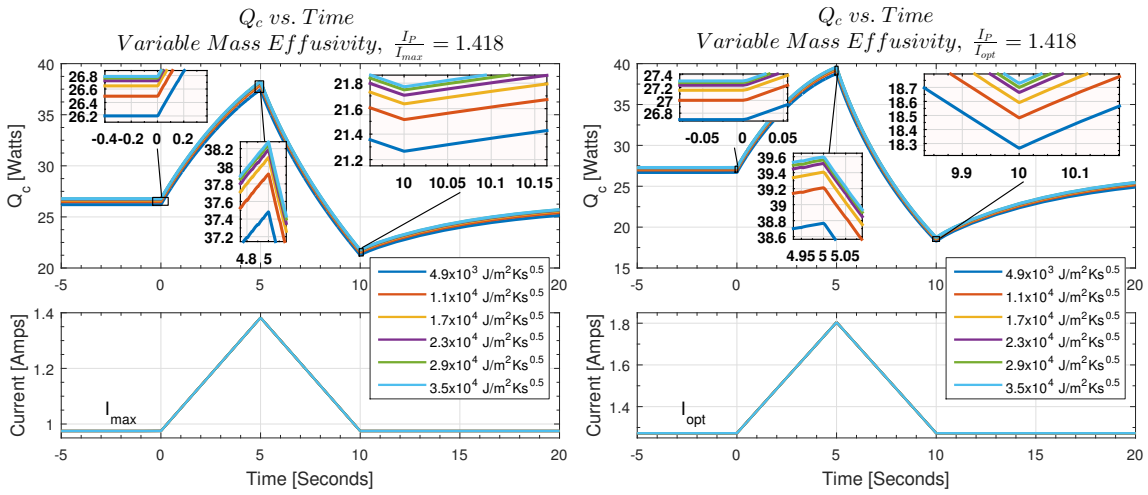

(a) $I_{\max}$ **(b)** I_{opt}

Figure 5.18. Effect of Mass Thermal Effusivity on Q_c

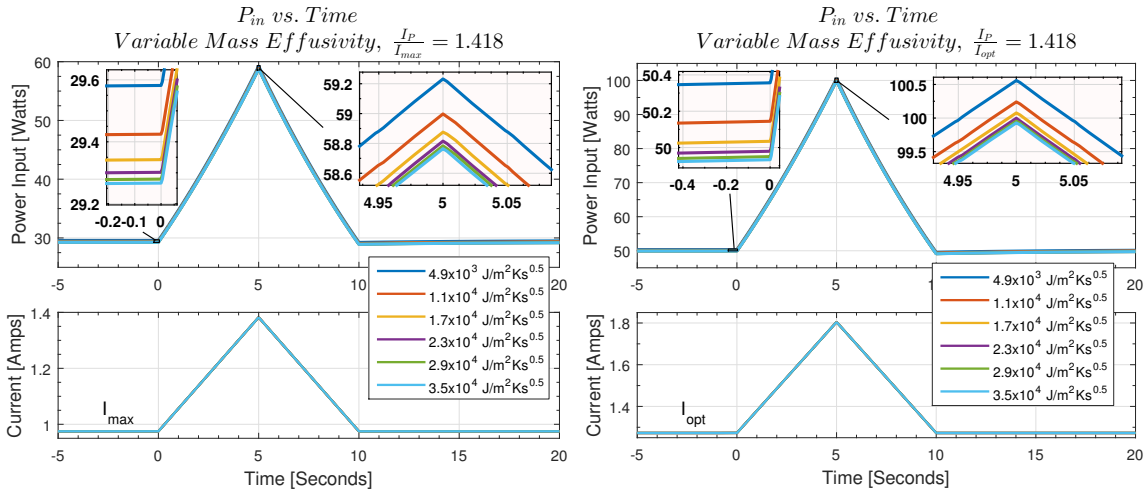

(a) $I_{\max}$ **(b)** I_{opt}

Figure 5.19. Effect of Mass Effusivity on P_{in}

Although all values of power consumption are very close to one another, the highest thermal effusivity allows for lower power consumption. This follows equation 2.14. The higher effusivity values allow for a lower ΔT across the thermoelement and therefore less Seebeck voltage is created and less power is required to overcome this voltage which is impeding desired current flow. The magnitude of the effect of changing thermal effusivty on power consumption does not appear to change significantly during the pulse from where it is during steady state operation.

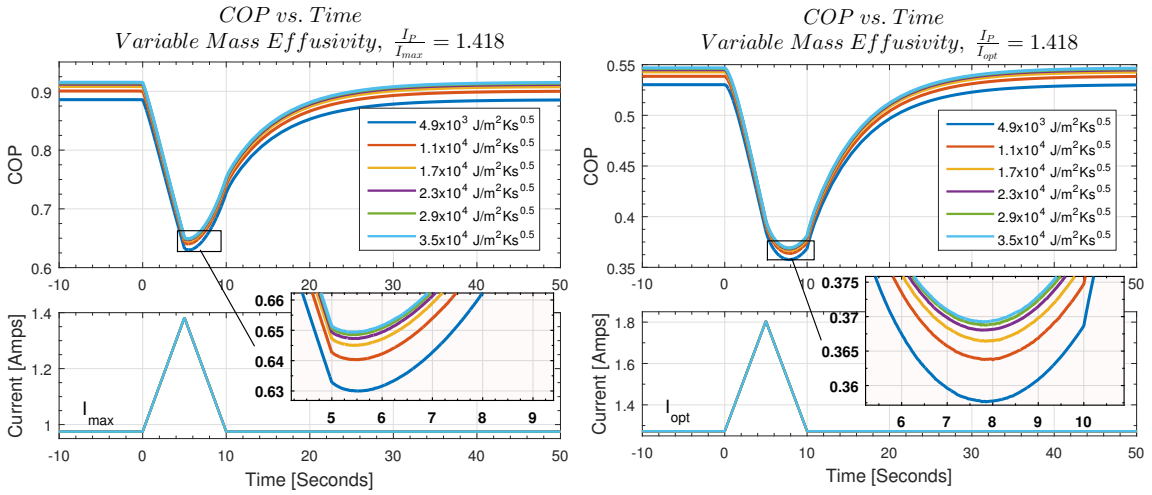

(a) $I_{\max}$ **(b)** I_{opt}

Figure 5.20. Effect of Mass Thermal Effusivity on COP

Figure 5.20 shows the effect on COP of linearly changing the thermal effusivity of the mass. The shape of the COP curves between $I_{\max}$ and I_{opt} follows the shapes seen in previous plots. During steady state operation, the highest COP is achieved with the highest mass thermal effusivity. This trend continued during the pulse.

5.6 Effect of Heat Spreader Thermal Conductivity

Figure 5.21 shows the effect on average mass temperature of changing the thermal conductivity of the heat spreader. The effect of the pulse does not show well due to the relativly large scale compared with the change in average mass temperature during the pulse.

Figure 5.21 also shows a point of diminishing returns when increasing heat spreader thermal conductivity. With linearly spaced thermal conductivity values, a non-linear effect on average mass temperature occurs. This may be due to another heat limiting factor in the system.

Figure 5.22 shows the effect on Q_c of changing the thermal conductivity of the heat spreader. The impact is quite small in the range of thermal conductivity values used. It is possible that the mass or interface resistance is a limiting factor and therefore not enough heat can flow to make a difference by changing the thermal conductivity of the heat spreader. Figure 5.22 does show that higher thermal conductivities increase Q_c for both steady state and transient pulse operation.

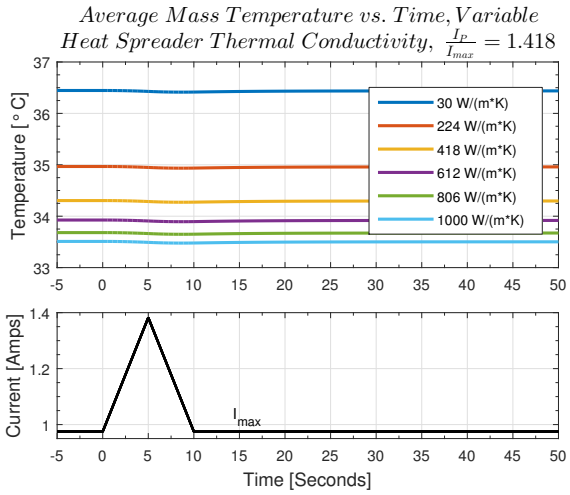

(a) $I_{\max}$

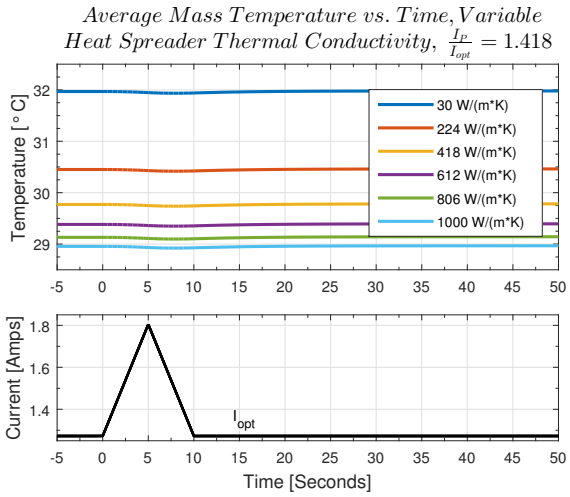

(b) I_{opt}

Figure 5.21. Effect of Heat Spreader Thermal Conductivity on Mass Temperature

Figure 5.23 shows the effect of changing the thermal conductivity of the heat spreader on P_{in}. P_{in} is effected only by a very small amount by changing spreader thermal conductivity. The highest thermal conductivity allows for the lowest power consumption, however, only by a small amount. The linearly spaced thermal conductivities show diminishing returns.

Figure 5.24 shows the effect on COP of changing the thermal conductivity of the heat spreader. The effect of heat spreader thermal conductivity on COP during steady state operation and during the pulse was very small. The results show the highest thermal conductivity spreader will perform the best but only by a very small amount.

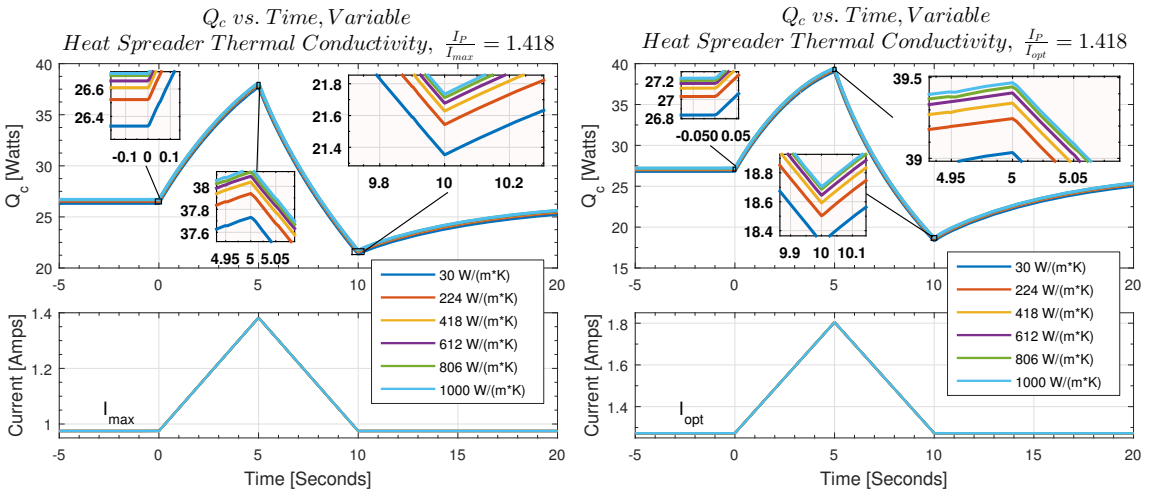

(a) $I_{\max}$ **(b)** I_{opt}

Figure 5.22. Effect of Heat Spreader Thermal Conductivity on Q_c

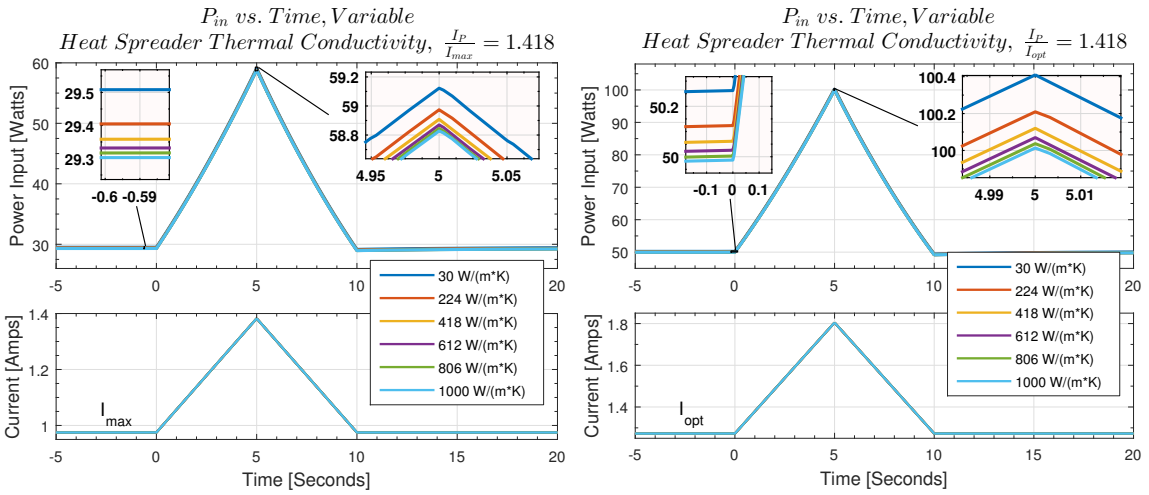

(a) $I_{\max}$ **(b)** I_{opt}

Figure 5.23. Effect of Heat Spreader Thermal Conductivity on P_{in}

This result may be dependent on what else is happening in the system. For example, the effusivity of the mass or interface resistance may be limiting heat to the spreader so any decrease in thermal resistance of the spreader may not help.

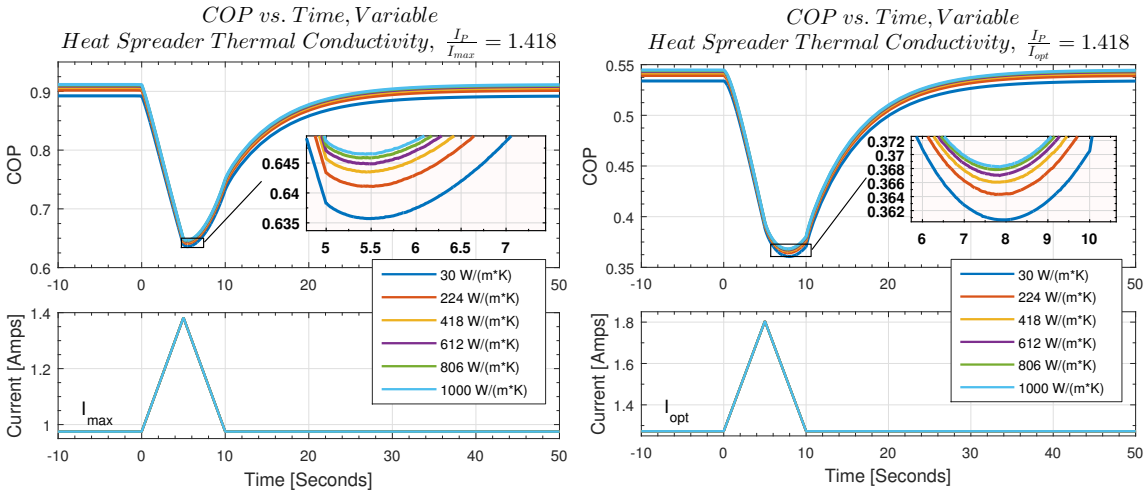

(a) $I_{\max}$ **(b)** I_{opt}

Figure 5.24. Effect of Heat Spreader Thermal Conductivity on COP

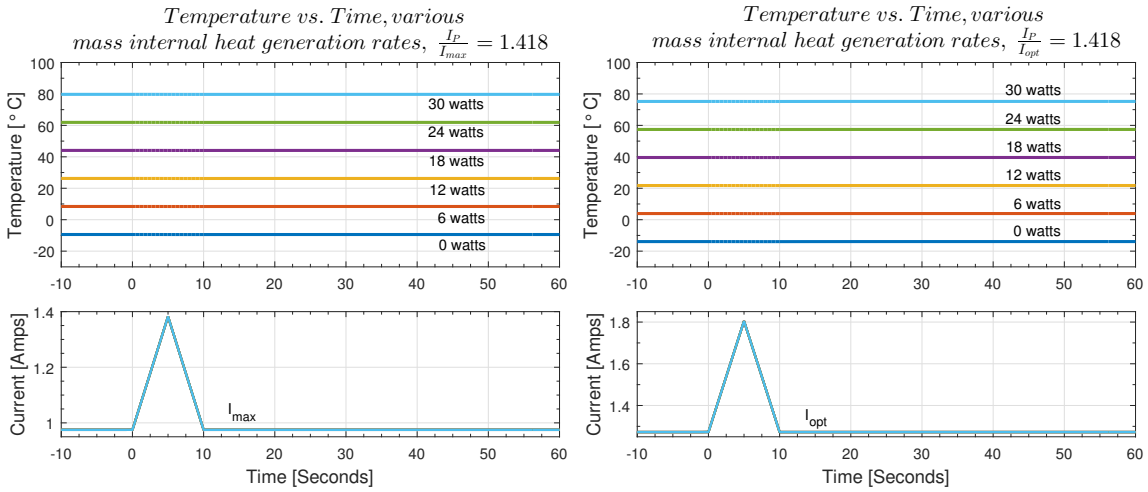

(a) $I_{\max}$ **(b)** I_{opt}

Figure 5.25. Effect of Variable Heat Generation in the Mass on Mass Temperature

5.7 Effect of Internal Heat Generation in the Mass

Figure 5.25 shows the effect of variable heat generation in the mass on the average temperature of the mass. The effect of variable mass heat generation has a relatively large effect compared with the other variables studied. Linearly spaced heat generation values produce a linearly spaced result. The effect on temperature is large enough that the scale does not allow for changes in temperature during the pulse to

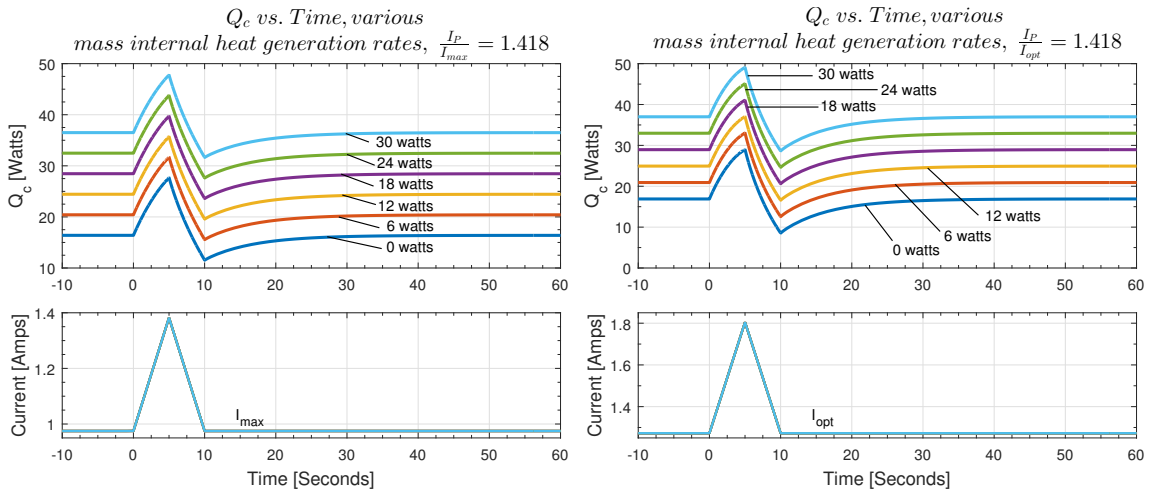

(a) $I_{\max}$ **(b)** I_{opt}

Figure 5.26. Effect of Variable Mass Heat Generation on Q_c

be seen. The average mass temperature change during the pulse is too small.

The reason variable heat generation has a large effect is due to a change in the ΔT between T_h and T_c. When the heat generation in the mass is increased, the temperature of T_c increases. When the ΔT term of equation 2.1 is increased, Q_c decreases. When the ΔT term is decreased, Q_c is increased. This is due to either increased or decreased thermal conduction across the thermoelement.

Figure 5.26 shows the effect of increased heat generation in the mass and its effect on Q_c. The highest heat generation rates have the highest amount of Q_c during steady state operation and during pulse operation. As explained for figure 5.25, this is due to less thermal conduction through the thermoelement, which leads to increased Q_c.

Figure 5.27 shows the effect of increased heat generation in the mass and its effect on P_{in}. Clearly the highest heat generation rates in the mass reduce power consumption to the lowest levels. Equation 2.14 shows increasing T_c, and keeping T_h constant reduces the power required for the device. When T_c is higher than T_h, the Seebeck effect lowers power consumption. When T_c is the same as T_h, the net Seebeck effect is zero so it does not change power consumption. When T_c is lower than T_h the Seebeck effect increases power consumption. Equation 2.14 is typically used for steady state. This equation can be used for transient operation as well, however it is important to note there is a time delay between the two terms of the equation. The Joule heating term is an instant effect due to electrical current happening instantly. The Seebeck term happens more slowly as it is a function of temperature and temperature changes

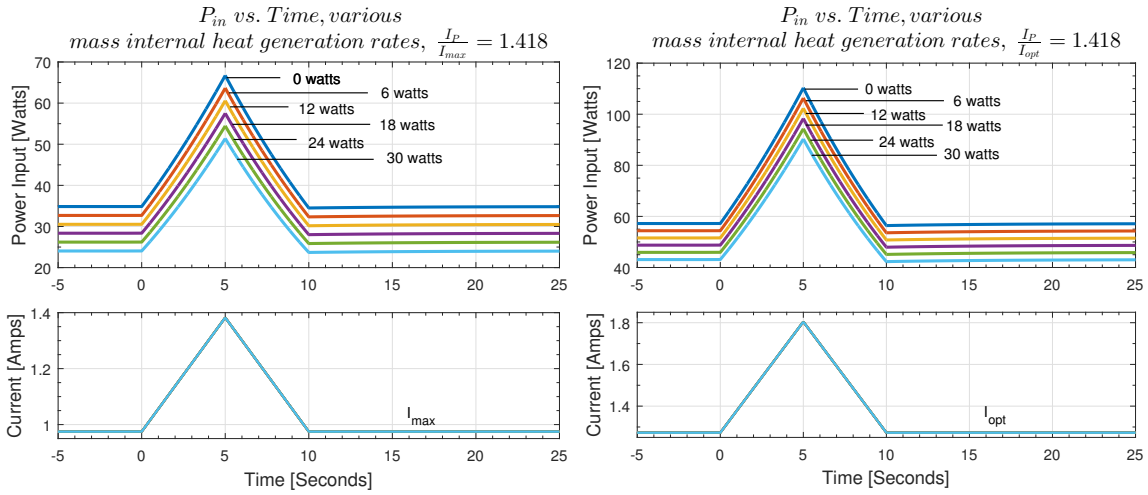

(a) $I_{\max}$ **(b)** I_{opt}

Figure 5.27. Effect of Variable Mass Heat Generation on P_{in}

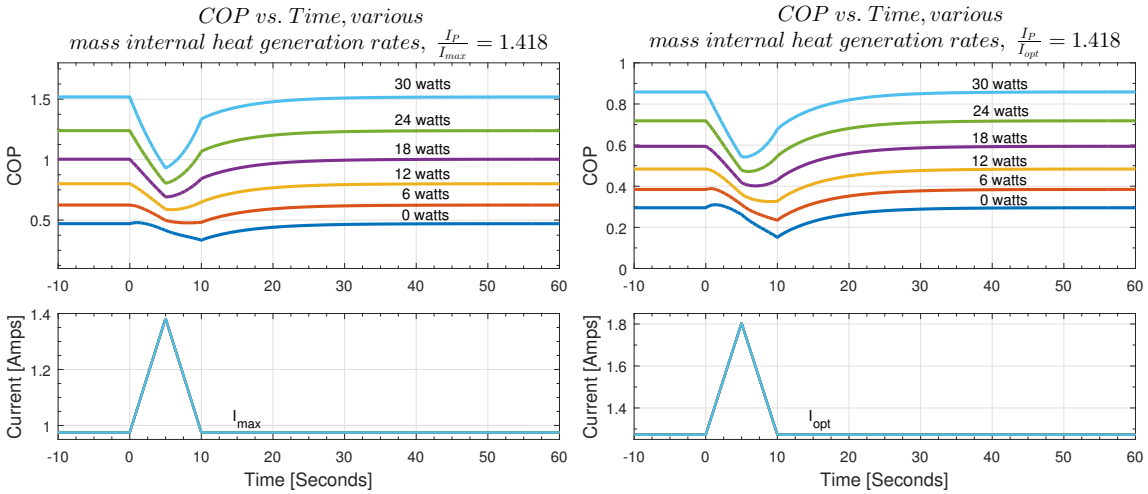

(a) $I_{\max}$ **(b)** I_{opt}

Figure 5.28. Effect of Variable Mass Heat Generation on COP

more slowly. The effect on power consumption is seen with some non-linearity during the power pulse as can be seen in the figure.

Figure 5.28 shows the effect of increased heat generation in the mass and its effect on COP. Linearly spaced changes in heat generation in the mass cause a non-linear spacing of steady state COP values. The shape of the COP curve during the pulse is significantly effected by changing heat generation within the mass.

Under the modeled scenario, 18 to 30 watts represents a negative ΔT across the thermoelement. That is, $T_c > T_h$. A positive ΔT is observed for 0 to 12 watts. At approximately 15 watts, the ΔT is zero. The effect of the pulse on COP is much greater when starting from a negative ΔT than it is for a positive ΔT. For some of the positive ΔT runs, there is an observable increase in COP for the first 0.5 to 1 second of the pulse. In this region, the rate of increase of Q_c is outpacing the rate change in P_{in}. Why this happens for these conditions is not well understood at this time. When the pulse turns off, there is an immediate start of recovery in COP.

5.8 Temperature Distribution in the Thermoelement During Pulsing

Figure 5.29 shows the temperature distribution in a thermoelement during steady state and during a current pulse. This figure also shows the effect of changing the temperature difference between T_h and T_c. There is one parabolic line curve for every time step of data. The first and lowest temperature line is the steady state operation line. During the pulse, temperature increases. When all lines are plotted together, the figure appears as a continuous filled shape.

The parabolic shape is due to the volumetric heat generation within the thermoelement. For this system model, the temperature of T_h and T_c are for the most part constrained. It can be seen that the center of the thermoelement becomes the hottest and varies the most in temperature. Although not shown, pulses starting from I_{opt} have a larger temperature variation within the center due to increased volumetric Joule heating at higher current.

Figure 5.29a is operating at zero ΔT. For this case the peak temperature is in the center of the thermoelement. Figure 5.29b is operating at +6 ΔT ($T_h > T_c$). It is observed that the peak temperature shifts toward T_h in this case. This means for more than half the thermoelement, the temperature gradient is biasing heat transfer toward T_c

Operating at negative ΔT, $T_c > T_h$ (Figure 5.29c and 5.29d) shifts the peak temperature toward T_h and therefore a greater percentage of heat is transferred through the thermoelement to T_h by conduction. Increasing the temperature of T_c shifts the peak temperature, however further increases in T_c appear to have a limited effect on the shift. As an example going from -6K ΔT to -12K ΔT did not change the shift as much as going from zero ΔT to -6K ΔT.

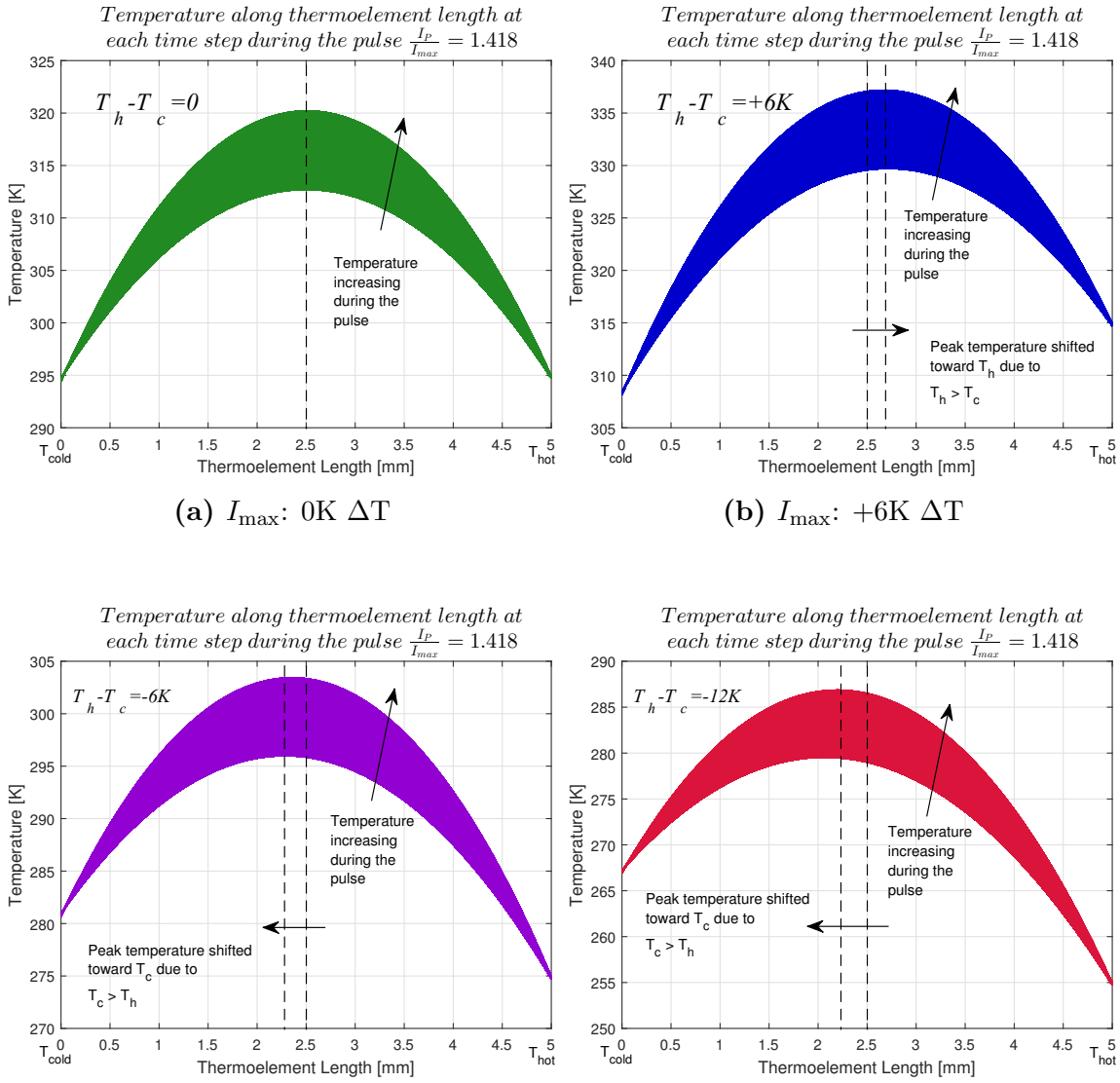

(a) $I_{\max}$: 0K ΔT

(b) $I_{\max}$: +6K ΔT

(c) $I_{\max}$: -6K ΔT

(d) $I_{\max}$: -12K ΔT

Figure 5.29. Effect of the Pulse and Changing ΔT on Thermoelement Temperature Distribution

5.9 Effect of Continuous Pulsing

Figure 5.30 shows the effect of various times between current pulses and its effect on average mass temperature. The model was allowed to run to quasi-steady state before taking the data. The time constant used is the time constant for temperature to decay back to steady state after $\Delta T_{postpulse}$. This was found during thermoecouple modeling. It can be seen that for pulses starting from $I_{\max}$, continuous pulsing provided the most cooling, even more so than steady state $I_{\max}$ operation.

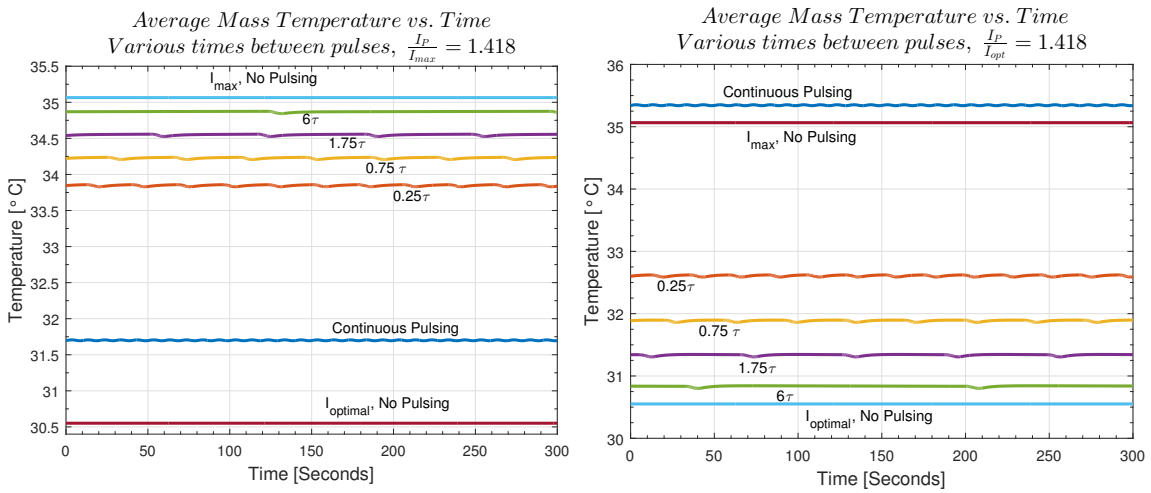

(a) Starting from $I_{\max}$ **(b)** Starting from I_{opt}

Figure 5.30. Effect of Time Between Pulses on Mass Temperature

For pulses starting from I_{opt}, the opposite effect is seen. Continuous pulsing from I_{opt} provides the least cooling. The reason for this has to do with the net Q_c provided over the pulse event. It is known that for steady state operation, I_{opt} operation is the maximum Q_c achievable. Going over I_{opt} current reduces Q_c.

In transient pulse operation, Q_c temporarily goes above that achievable during steady operation. This is true for both $I_{\max}$ and I_{opt} operation. However, after Q_c rises above steady operation, it falls below steady operation Q_c. For pulses starting from $I_{\max}$, the time and magnitude of Q_c being above steady operation is greater than the time and magnitude below steady operation, thus an advantage is seen.

For pulses starting from I_{opt} the time and magnitude of the fall in Q_c below steady operation is larger than the time and magnitude above steady operation. Thus a net cooling advantage is seen for current pulses starting from $I_{\max}$ but not I_{opt}. This rise in Q_c above steady operation in both cases is due to Peltier cooling that is linearly proportional to input current. The fall in Q_c is due to the time delayed Joule heat. Joule heat dominates the end result since it is proportional to the square of current. It is possible that pulsed current operation starting from $I_{\max}$ could provide a net decrease in cooling. For pulses that use an average current greater than I_{opt} this would be the case.

Figure 5.31 through 5.36 shows the effect of various time spacing between current pulses and its effect on COP, Q_c, and P_{in}. These effects are shown for pulses starting from both $I_{\max}$ and I_{opt} operation. It is difficult to visualize the average effect of pulse

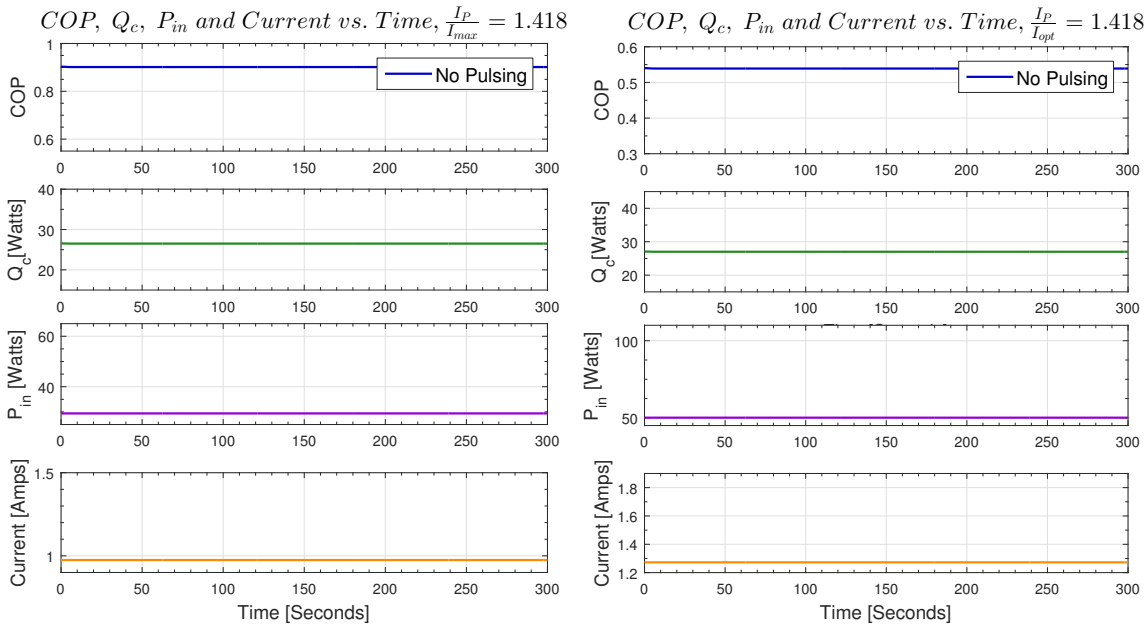

(a) $I_{\max}$ **(b)** I_{opt}

Figure 5.31. Effect of Pulse Spacing - Baseline, No Pulsing

spacing from these plots. Figures 5.37 through 5.38 assist with assessing the effect of pulse spacing.

Figure 5.37 shows the average P_{in} for various pulse spacing. For a series of repeating pulses, there is power consumption during the pulse and power consumption during the steady state current between the next pulse. The averages calculated here are the average for one pulse and one steady state period following the pulse. The exception is the steady operation runs that do not have pulsing ($I_{\max}$ and I_{opt}).

For each pulse spacing run, the average power during the pulse is the same since the same pulse is used for all runs. The difference is the time between the pulses. This steady state P_{in} averages in with a pulse P_{in}. Therefore as can be seen from Figure 5.37, the more steady state time, the more the average power consumption approaches steady state power consumption.

Steady state power consumption is the lowest because power consumption is primarily a function of current squared. If there is no pulsing, current is the lowest. Power consumption is secondarily a function of the Seebeck effect. The larger the temperature difference between T_h and T_c, the larger the contribution of the Seebeck effect to power consumption.

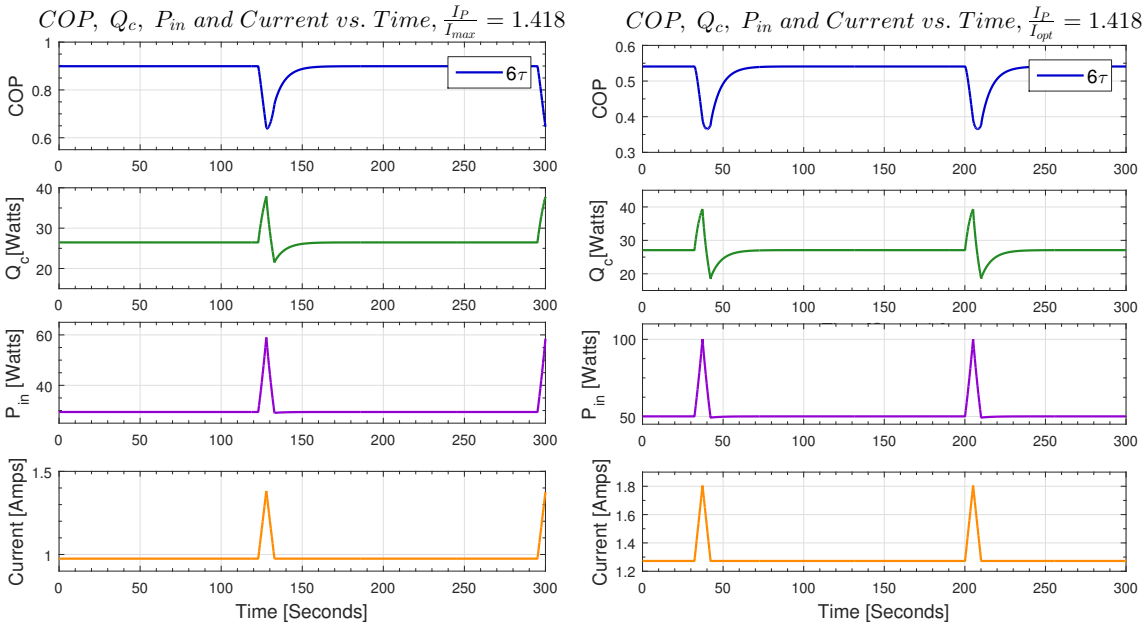

(a) $I_{\max}$ **(b)** I_{opt}

Figure 5.32. Effect of Pulse Spacing - 6τ Spacing

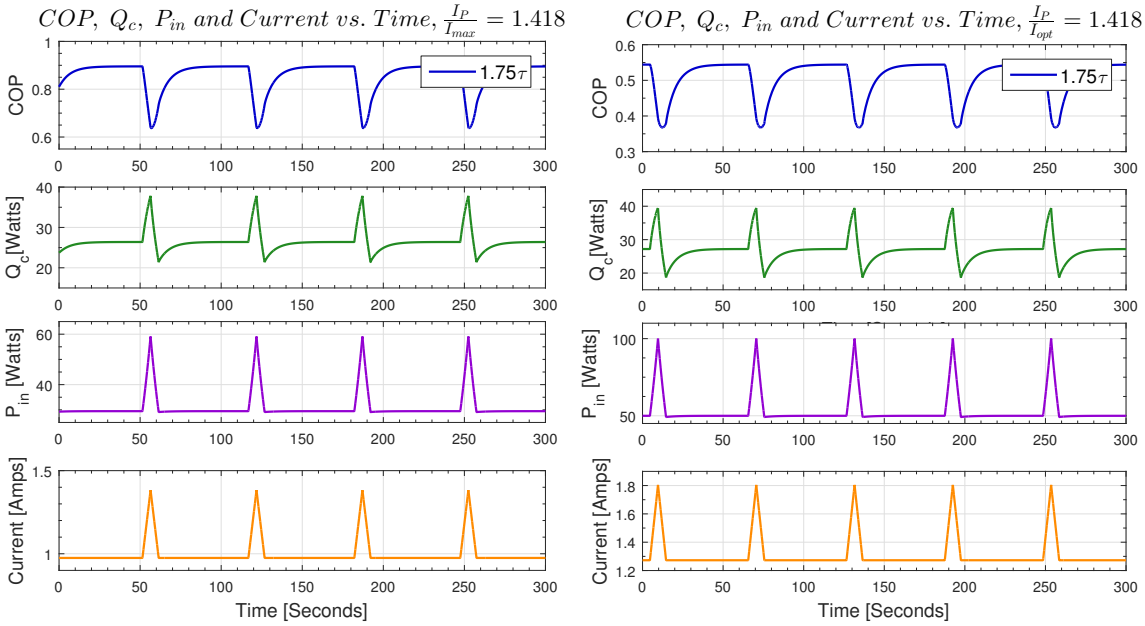

(a) $I_{\max}$ **(b)** I_{opt}

Figure 5.33. Effect of Pulse Spacing - 1.75τ Spacing

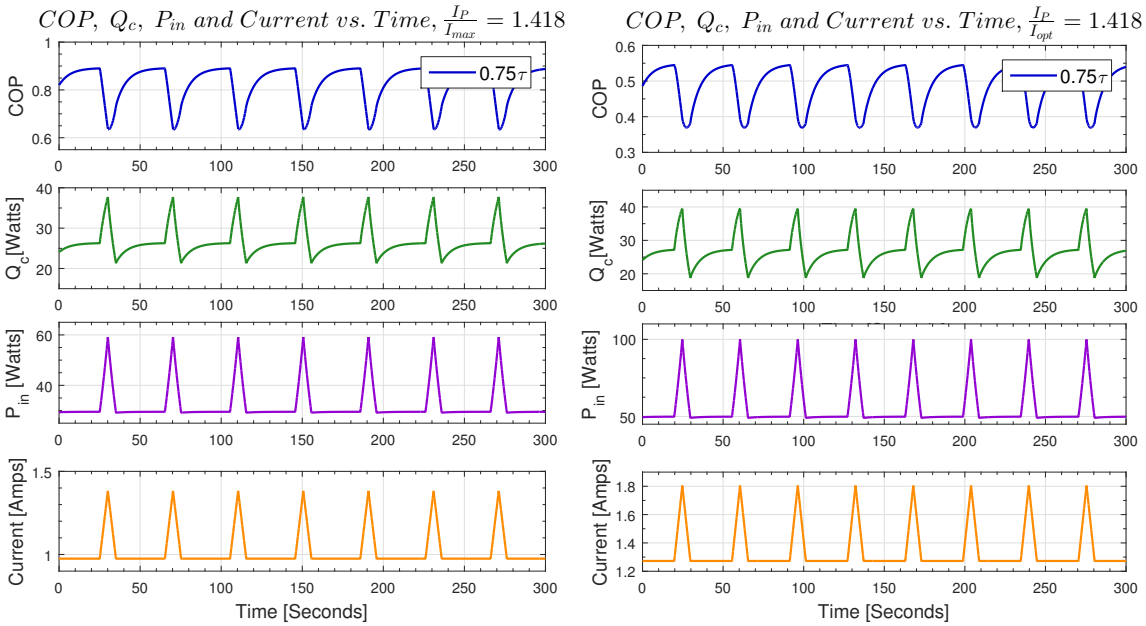

(a) $I_{\max}$ **(b)** I_{opt}

Figure 5.34. Effect of Pulse Spacing - 0.75τ Pulse Spacing

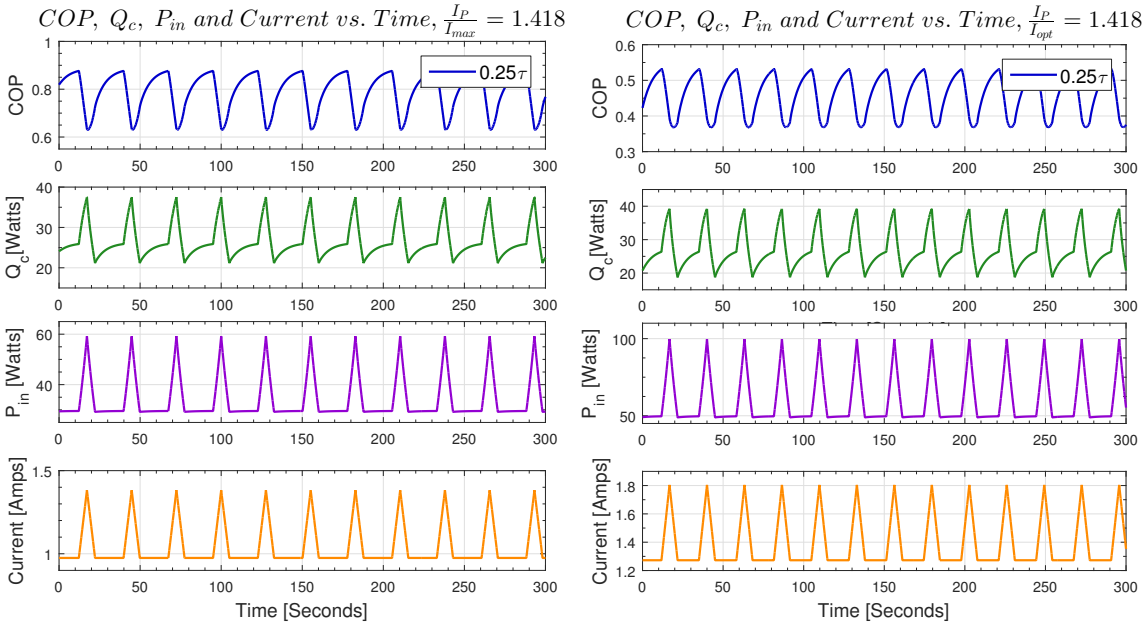

(a) $I_{\max}$ **(b)** I_{opt}

Figure 5.35. Effect of Pulse Spacing - 0.25τ Pulse Spacing

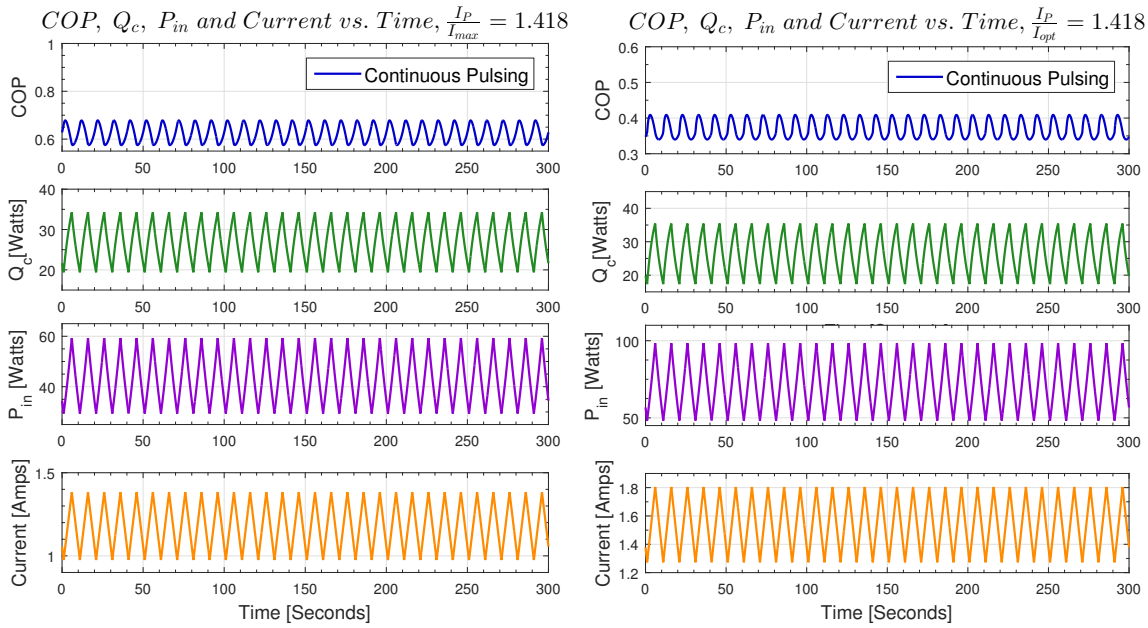

(a) $I_{\max}$ **(b)** I_{opt}

Figure 5.36. Effect of Pulse Spacing - Continuous Pulsing, No Spacing

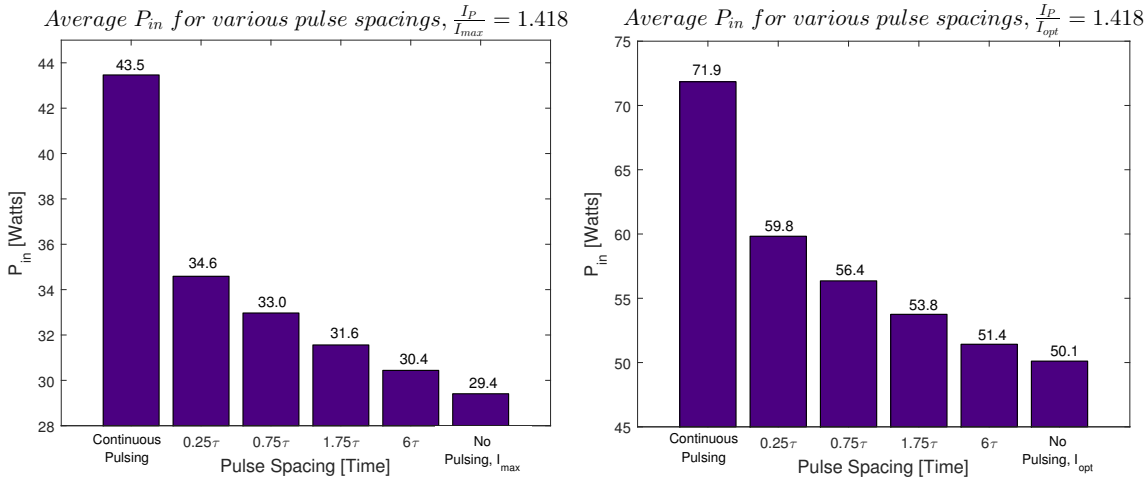

(a) $I_{\max}$ **(b)** I_{opt}

Figure 5.37. Average Effect of Pulse Spacing on P_{in}

Figure 5.38 shows the average Q_c for various pulse spacing. For a series of repeating pulses, there is Q_c during the pulse event and Q_c during the steady state current between the next pulse. The averages calculated here are the average for one pulse and one steady state period following the pulse. The exception is the steady operation runs that do not have pulsing ($I_{\max}$ and I_{opt}).

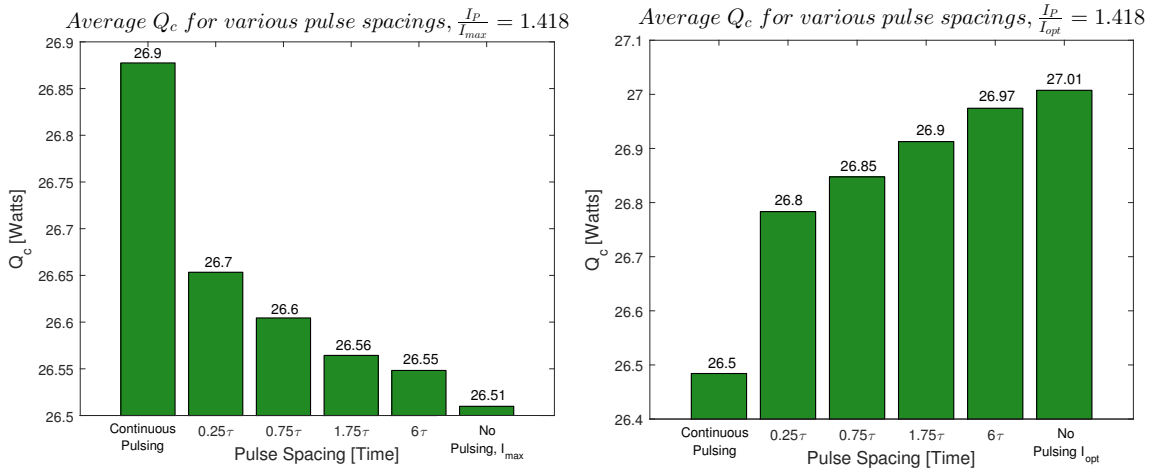

(a) $I_{\max}$ **(b)** I_{opt}

Figure 5.38. Average Effect of Pulse Spacing on Q_c

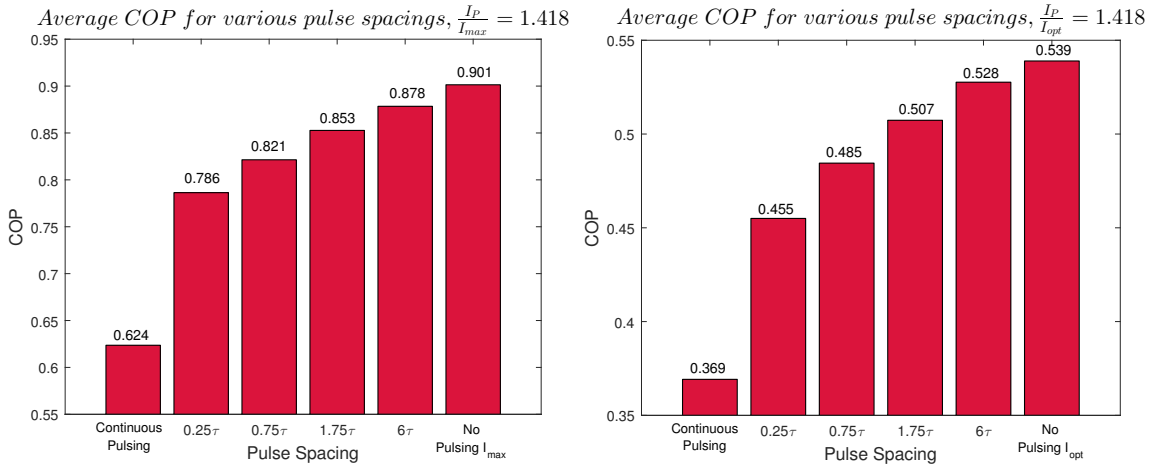

(a) $I_{\max}$ **(b)** I_{opt}

Figure 5.39. Average Effect of Pulse Spacing on COP

It is known that during transient current pulses starting from $I_{\max}$, the net Q_c over the pulse event is increased over steady state operation. Likewise it is known that during transient current pulses starting from I_{opt}, the net Q_c over the pulse event is decreased over steady state operation. Therefore, subsequent pulses with less steady time between them will have higher Q_c for those pulses starting from $I_{\max}$ and lower Q_c for those pulses starting from I_{opt}.

Figure 5.39 shows the average COP for various pulse spacing. For a series of repeating pulses, there is a COP during the pulse event and COP during the steady state

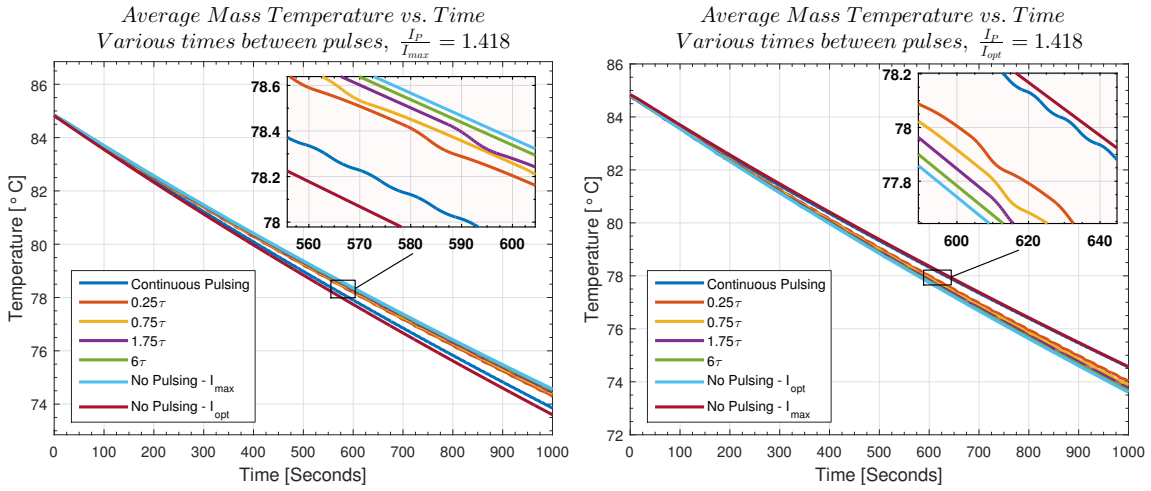

(a) $I_{\max}$ **(b)** I_{opt}

Figure 5.40. Continuous Pulsing Pull Downs Effect on Mass Temperature

current between the next pulse. The averages calculated here are the average for one pulse and one steady state period following the pulse. The exception is the steady operation runs that do not have pulsing ($I_{\max}$ and I_{opt}).

Figure 5.39 shows that whether the pulses start from $I_{\max}$ or I_{opt}, decreasing the time between pulses leads to lower COP. This is expected as from previous figures, it was found that COP decreases during the pulse. So more pulses and less steady operation leads to a lower COP.

5.10 Effect of Continuous Pulsing on Mass Temperature

Figure 5.40 shows the effect of continuous pulsing over time on average mass temperature. For this section the average mass temperature was not stabilized but cooling down from a higher temperature. This will be called "pull down" from here forward. The time constant used is the time constant for temperature to decay back to steady state after $\Delta T_{postpulse}$ found during thermocouple modeling.

The same trends hold for temperature "pull down" as did with quasi-steady state temperature. Continuous pulsing provides the most cooling and fastest "pull down" for pulses starting from $I_{\max}$ and steady state operation provides the most cooling and fastest "pull down" for pulses starting from I_{opt}.

Looking at Figures 5.41 through 5.46 some trends can be seen. COP and Q_c are generally higher than has been seen previously. COP and Q_c are decreasing over

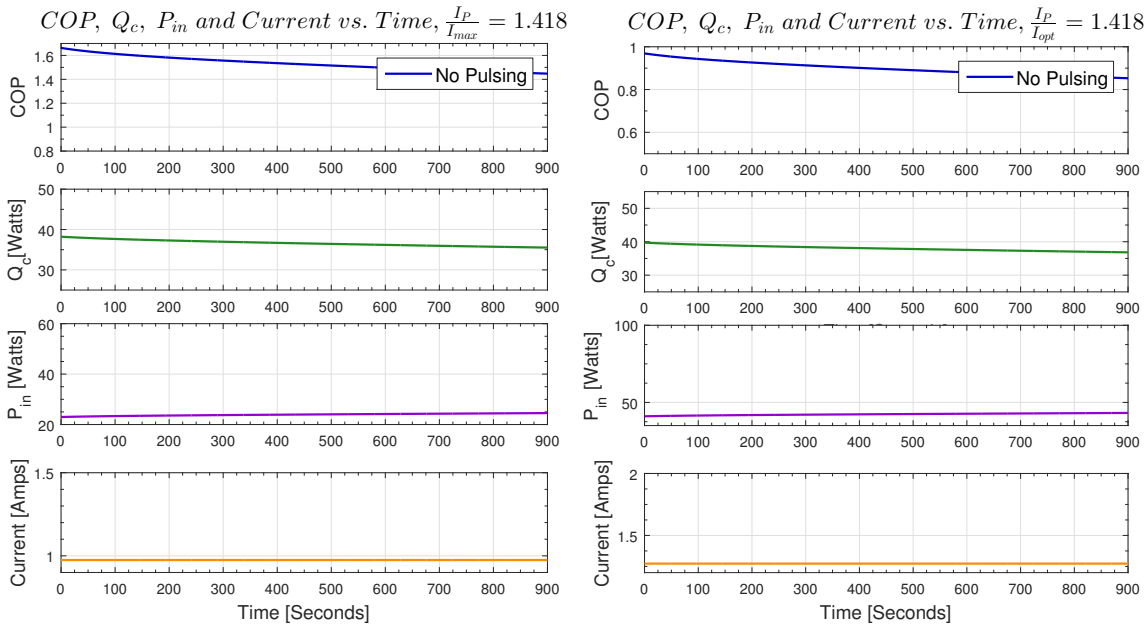

(a) $I_{\max}$ **(b)** I_{opt}

Figure 5.41. Effect of Pulse Spacing, Pull Downs - Baseline, No Pulsing

time. Power consumption is increasing. All of these trends are driven by T_c being at a higher temperature than T_h. In this case equation 2.1 says that as the ΔT in the third term of the equation becomes negative, Q_c will increase. Equation 2.14 shows that if T_c is a higher temperature than T_h, the Seebeck effect will be negative and the power consumption will be reduced. COP is decreasing over time. This is due to Q_c decreasing as well as power consumption decreasing, however, since Q_c is decreasing faster than P_{in}, COP goes down.

5.11 Output Sensitivity to Input Parameter Significant Digits

It was found during the model development process that recreating the model would not be accurate if the material properties provided were rounded. Tables 5.1 through 5.3 are the results of a parametric sensitivity study for the massless thermal couple model. These tables provide a guideline for reporting significant figures on thermoelectric thermoelement or module data. The data in tables 5.1 through 5.3 was obtained by varying the number of significant figures in the input data one at a time until the output parameters stabilized at one decimal place. Knowing the number of significant figures in the model input that will provide desired accuracy on the output will allow enhanced communication from a technical paper.

Table 5.2 and 5.3 use input data for intrinsic properties of a thermoelement. Table

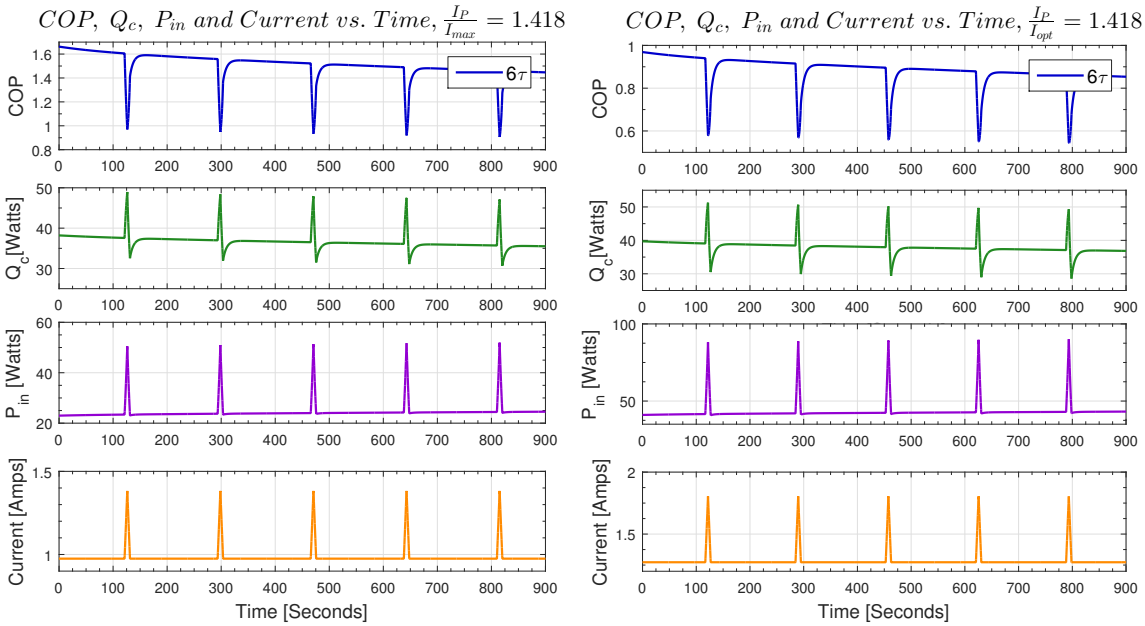

(a) $I_{\max}$ **(b)** I_{opt}

Figure 5.42. Effect of Pulse Spacing, Pull Downs - 6τ Pulse Spacing

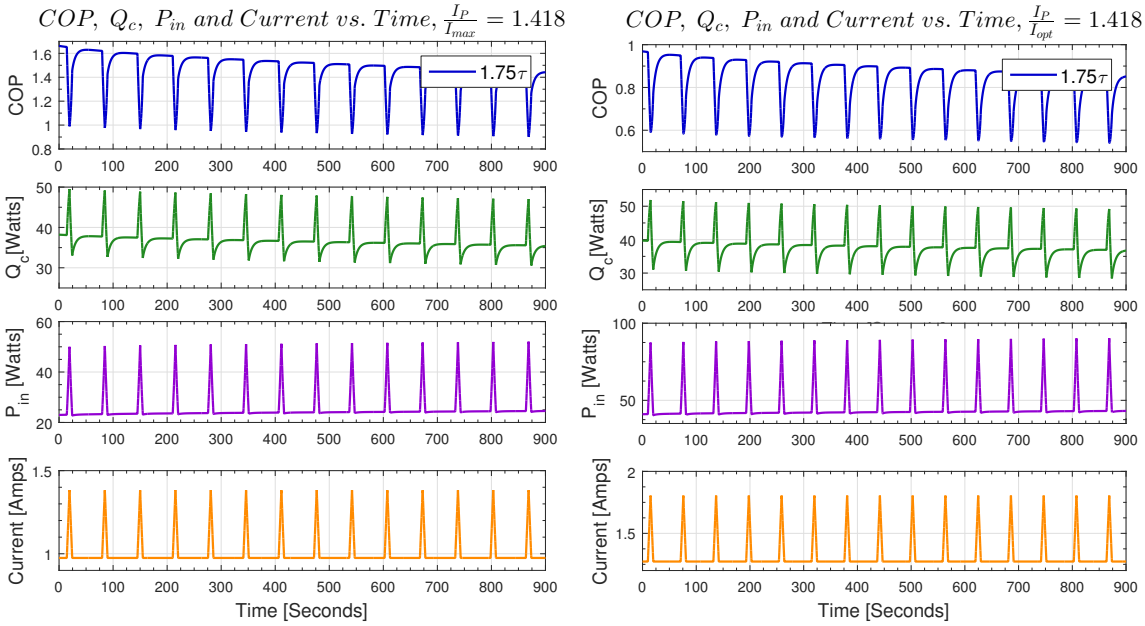

(a) $I_{\max}$ **(b)** I_{opt}

Figure 5.43. Effect of Pulse Spacing, Pull Downs - 1.75τ Pulse Spacing

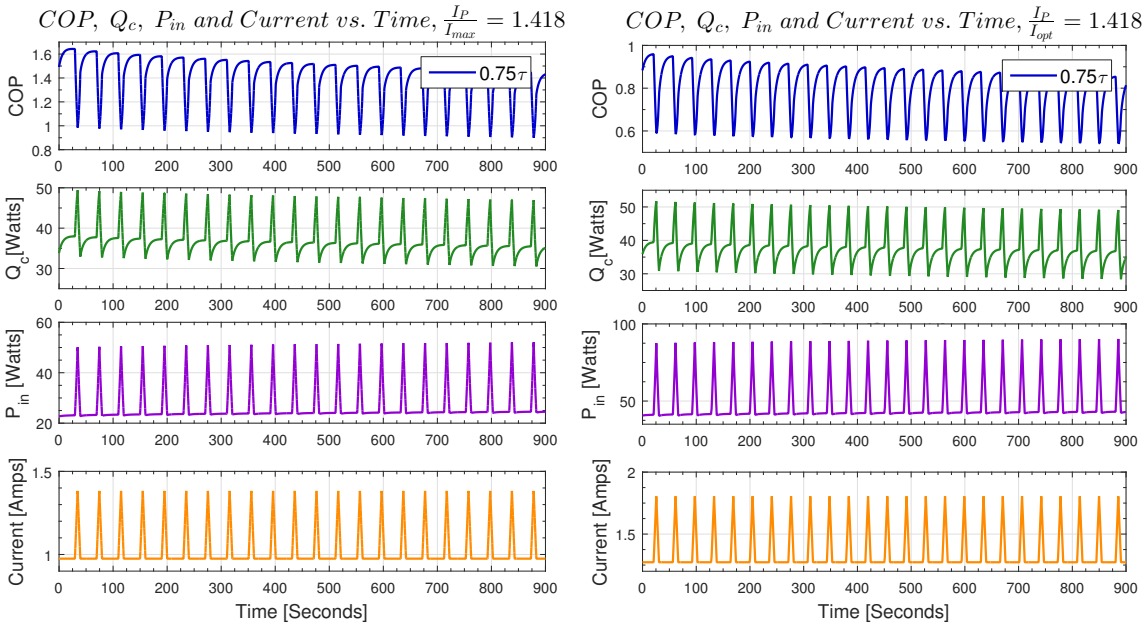

(a) $I_{\max}$ **(b)** I_{opt}

Figure 5.44. Effect of Pulse Spacing, Pull Downs - 0.75τ Pulse Spacing

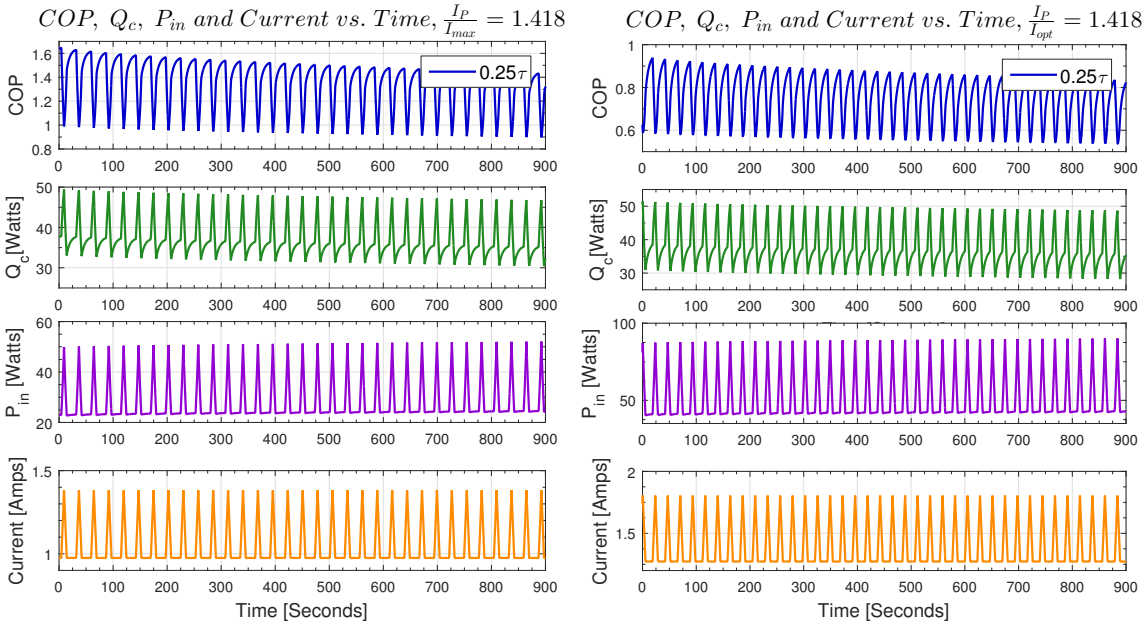

(a) $I_{\max}$ **(b)** I_{opt}

Figure 5.45. Effect of Pulse Spacing, Pull Downs - 0.25τ Pulse Spacing

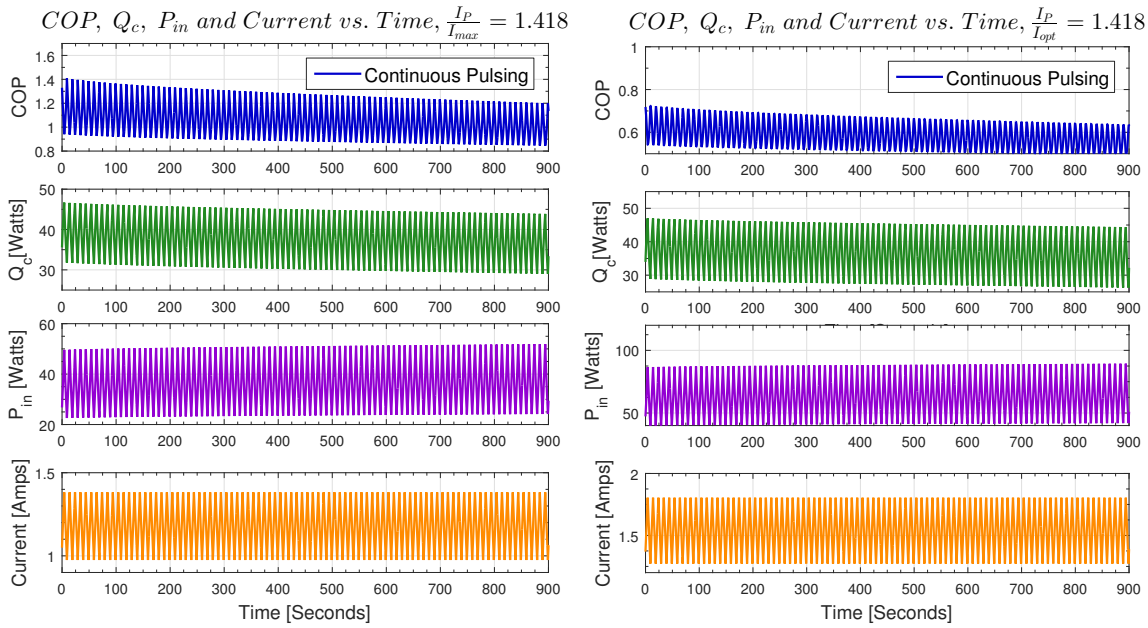

(a) $I_{\max}$ **(b)** I_{opt}

Figure 5.46. Effect of Pulse Spacing, Pull Downs - Continuous Pulsing, No Spacing

5.1 uses module level data. Both types of input data are used as inputs to thermoelectric models. As a example, in Table 5.2, for reporting a Seebeck coefficient used for modeling ΔT_{Pulse}, Table 5.2 says to report three significant figures. This will provide the reader of the reported data one decimal place of accuracy on the output. All numbers in the tables are the number of significant figures needed for a particular model input that would provide one decimal place of accuracy on the output. Additional significant figures would be needed but not reported in these tables if more than one decimal place of accuracy on the output is desired. Without these guidelines it may be tempting to round the input data in a technical report, which will render reproduction of results difficult.

Table 5.1. Module Properties Sensitivity

	Module Properties (Input Data)			
	$I_{\max}$ [amps]	T_h [K]	V_{max} [V]	$\Delta T_{\max}$ [K]
Steady State Temperature [K]	2	2	2	3
$\Delta T_{\max}$ [K]	2	2	2	NA
Min Temperature [K]	2	2	2	4
ΔT_{pulse} [K]	1	1	1	3
Time to Min Temperature [s]	2	2	2	3
Holding Time [s]	3	2	2	2
Transient Advantage [K s]	4	4	3	4
Maximum Temperature Overshoot [K]	2	3	2	3
$\Delta T_{\text{post pulse}}$ [K]	1	3	1	3
Time to Maximum Temperature Overshoot [s]	3	2	3	3
Settling Time [s]	2	3	2	2
Transient Penalty [K s]	5	4	4	5
Pulse Cooling Enhancement [unitless]	1	1	1	1

Table 5.2. Thermoelement Properties Sensitivity - 1 of 2

	Thermoelement Properties (Input Data)					
	Seebeck Coeff. [V/K]	Resistivity [ohm-m]	Thermal Conduct. [W/m-K]	Figure of Merit [K^{-1}]	Length, Width [m]	Height [m]
Steady State Temperature [K]	3	3	3	1	1	1
$\Delta T_{\max}$ [K]	3	3	3	1	1	1
Minimum Temperature [K]	3	3	4	1	1	1
ΔT_{pulse} [K]	3	3	3	1	1	1
Time to Minimum Temperature [s]	1	1	2	1	1	2
Holding Time [s]	2	2	3	2	1	3
Transient Advantage [K·s]	3	4	4	3	1	4
Maximum Temperature Overshoot [K]	3	3	3	2	1	1
$\Delta T_{\text{post pulse}}$ [K]	3	3	3	2	1	1
Time to Maximum Temperature Overshoot [s]	2	2	3	2	1	3
Settling Time [s]	3	3	4	2	1	4
Transient Penalty [K·s]	2	4	5	4	1	5
Pulse Cooling Enhancement [–]	4	1	1	1	1	1

Table 5.3. Thermoelement Properties Sensitivity - 2 of 2

	T_h [K]	$I_{\max}$ [A]	$I_p/I_{\max}$	Density [kg/m^3]	Heat Capacity [J/kgK]
Steady State Temperature [K]	2	2	1	3	1
$\Delta T_{\max}$ [K]	2	2	1	3	1
Minimum Temperature [K]	2	2	3	1	1
ΔT_{pulse} [K]	1	1	3	1	1
Time to Minimum Temperature [s]	2	2	4	2	2
Holding Time [s]	2	3	3	2	2
Transient Advantage[K·s]	4	4	3	3	3
Maximum Temperature Overshoot [K]	3	3	3	1	1
$\Delta T_{\text{post pulse}}$ [K]	3	3	3	1	1
Time to Maximum Temperature Overshoot [s]	2	3	3	3	3
Settling Time [s]	3	3	3	4	4
Transient Penalty [K·s]	4	4	5	5	5
Pulse Cooling Enhancement [–]	1	2	1	1	1

Chapter 6. Conclusions and Recommendations

Thermoelectric cooling has many advantages over vapor compression cooling. Typically cost is not an advantage when looking at thermoelectric systems that provide more than approximately 200-600 watts of cooling power. If the efficiency or capacity of thermoelectric coolers could be improved, they would become more competitive with vapor compression systems. The possibility of a wider range of new and exciting thermal management applications could be realized.

Much research is focused on improving thermoelectric performance with enhanced semiconductor materials. Recent research points to a potential cooling capacity increase with pulsed operation. The study of pulsed transient operation could lead to performance gains that are synergistic with materials research.

6.1 Originality of Work

For this work, transient thermoelectric pulse cooling research was performed with modeling studies. Two main focuses where the modeling of a single free standing thermocouple and modeling of a system. The system consisted of a full sized pulse cooler module interfaced with a heat generating mass.

Previous studies have focused on pulse cooling of a couple from the perspective of changing one variable at a time. This work looks at pulse cooling from the perspective of response surfaces and how multiple variables interact over a wide range of variation. These interactions are not always intuitive. The interaction of the independent variables pulse-height and pulse on-time were studied.

Previous studies start the current pulse from a steady state current of I_{max}. This thermocouple study looked at the effects of starting pulses from I_{max} and I_{opt} and compared the two.

A previous study defined the terms Transient Advantage and Transient Penalty. This study defines Net Transient Advantage to find the combination of pulse-height and pulse on-time that provides the largest positive difference between Transient Advantage and Transient Penalty.

A previous study touched on the impact of pulse cooling with an isosceles triangle shaped current pulse. This pulse shape was the main focus of this study.

From a system modeling standpoint, previous studies looked at the effect of cooling small masses with no internal heat generation. New features of this work include looking at the effects of changing system variables: continuously repeated pulse cooling analysis, addition of convection boundary conditions, a relatively large mass compared with the cooler, thermal insulation, interface resistance, heat spreader and internal heat generation in the mass.

This study also looked at pulse cooling from a new perspective. Rather than defining performance parameters from a temperature vs. time perspective, this study characterized performance from a Q_c, P_{in} and COP standpoint. Additional knowledge was gained by operating at I_{opt} steady current before the pulse. Previous studies used only I_{max} operation.

The models for this study used electrical-thermal analogies with SPICE electrical circuit simulation software. These models used distributed mass and heat generation and 1D, 2D and 3D arrangements to model the thermocouple, module and system.

6.1.1 Key Findings - Thermocouple Model

There is not always a temperature overshoot with transient operation. The same pulse shape can provide a transient operation with and without a temperature overshoot. Previous studies attributed the lack of a temperature overshoot to the pulse shape alone. No overshoot occurs when the heat leaving T_c stays greater than the heat entering T_c throughout the pulse event. If the Joule heat reaching T_c is greater than the magnitude of Peltier cooling leaving T_c, the temperature at T_c increases. If this happens for a long enough time, the temperature will increase above the steady state temperature and by definition cause and overshoot. The overshoot is a function of pulse shape and the magnitude of current and pulse on-time.

With the response surfaces generated, a desired outcome can be chosen for one surface and the trade offs required will be seen from other surfaces at the same combination of independent variables.

For the independent variables studied, sometimes pulse on-time has a linear effect to the dependent variable and sometimes a nonlinear effect. The effect of changing pulse-height always has a non-linear effect for the parameters studied here.

Studying Net Transient Advantage, there was found a range of transient operating

conditions where Q_c is improved over steady operation. The advantage came from pulses starting from I_{max} steady current. Starting current pulses from I_{opt}, did show increased Q_c early in the pulse but a larger decrease in Q_c later in the pulse, therefore, there was no net advantage.

6.1.2 Key Findings - System Model

The main physics of the steady state equations still apply to transient operation, however each term in the steady state equations has a variable amount of time separation from one another for transient operation. The steady state equations are also lumped equations. To capture the effects of transient operation, it is necessary to use distributed mass and heat generation 1D models.

COP drops when electrical current increases sharply. During this electrical current increase, power input to a device takes place instantly. Q_c is time delayed due to thermal resistance limited heat transfer. Since COP is defined by Q_c/P_{in} this causes a large drop in COP under transient conditions. A further COP drop comes when Q_C is reduced by Joule heat that ramps up throughout the pulse. The bulk of the Joule heat is time delayed from reaching T_c.

COP can be negative during a pulse if the magnitude of the pulse is such that the magnitude of Joule heat reaching T_c is higher than the magnitude of Peltier cooling leaving T_c.

Low thermal interfaces resistance between the device and the heat spreader and heat spreader to the mass are known to improve heat transfer due to less resistance to heat flow. These are not always the highest Q_c and highest COP during transient pulsed operation. When high interface resistances are used, T_c becomes colder during the first part of the pulse due to the inability to pull heat from a farther distance. At this point Joule heat is pulled from the thermoelement. More Joule heat pulled out earlier translates to less Joule heat pulled later. This increases Q_c and COP later in the pulse.

Certain pulses starting from I_{max} can provide a net increase in Q_c over steady state operation. No pulse starting from I_{opt} steady operation can provide a net cooling increase over steady I_{opt} operation. The reason is, above I_{opt} current, the Joule heating produced is higher than the Peltier cooling heat removed over the full pulse event. Unlike steady operation, for transient operation Q_C can be increased over Q_c of steady operation but only for a short time.

Increasing the amount of time the pulse is left on increases the average current input

to the device. Q_c increases with more on-time if the average current of the pulse is below I_{opt}. Increasing the on-time indefinitely tends toward changing the input current to a higher and steady state value. Operating at higher currents, even if below I_{opt} provides a higher proportion of Joule heat to T_c. This decreases COP because Q_c goes down and P_{in} goes up.

The temperature distribution in the thermoelement is an upside down parabola with highest temperature at the center. This parabolic shape is due to internal heat generation. The temperature at the center increases with increased current flow through the thermoelement. For a module with good heat flow at T_h and T_c, the temperatures at T_h and T_c do not change significantly during the pulse. When T_h equals T_c, the parabolic temperature gradient is such that 50% of the Joule heat conducts to T_h and 50% conducts to T_c. If T_h is greater than T_c, the peak of parabolic temperature gradient shifts toward T_h. This changes the proportion of thermal conduction in the thermoelement that goes to T_h and what goes to T_c. There appears to be a limit for how far the peak of the parabola can be shifted by changing T_h or T_c.

Increasing the effusivity of the mass and thermal conductivity of the heat spreader within the range of the study meets a point of diminishing returns for Q_c. This may be a limitation of the heat transfer in the rest of the system. Changing the interface resistance between the heat spreader and the mass did not meet a point of diminishing returns. This may indicate a big opportunity for improving performance of the system.

Changes in system parameters have a similar effect to steady state operation as they have during a current pulse in terms of average mass temperature change.

Increasing the internal heat generation of the mass increases the temperature at T_c. T_h stays relatively constant. Raising the temperature of T_c raises the amount of Q_c, lowers the amount of P_{in} and raises COP.

Changes in the internal heat generation of the mass were studied. For some of the lower heat generation rates, a small increase in COP was seen during the first 0.5 to 1 seconds of the pulse. This behavior is not fully understood at this time. This does indicate that under the right conditions, COP for transient operation may be improvable over steady state operation. Finding this condition was one of the main goals of this study.

For quasi-steady-state operation of continuous pulsing current, performance parameters can be calculated as the aggregate of what happens during the transient pulse and what happens during steady state temperature operation between the pulses.

Average performance of a continuous pulsing cooler tends toward steady state with more steady state time in between pulses. Average performance tends toward transient performance as the steady state time between pulses decreases toward zero. If pulses are continuous from a current standpoint with no steady state time in between, Joule heat from the first pulse does not have time to fully diffuse. This increases the proportion of Joule heat reaching T_c for each pulse and Q_c decreases.

For continuous pulsing during pull-downs, Q_c and COP are increased over quasi-steady-state continuous pulsed operation and performance decreases as the mass cools with time. This happens because the temperature of the mass is warmer than T_h so thermal conduction through the thermoelement is in a favorable direction during pull-downs. P_{in} is reduced due to the Seebeck effect which helps lower power consumption under those conditions.

6.2 Future Work

It was seen that for higher interfaces resistance provided more Q_c and a higher COP for part of the transient pulse event than lower interfaces resistance. A future study might look at the net impact of thermal interface resistance over a transient cycle. Rather than assume that lower thermal interface resistance is higher Q_c and COP, there may be an optimal thermal interface resistance for transient operation that depends on the transient cycle. Knowledge of optimal thermal interface resistance during transient operation could save unneeded expense of using exotic thermal interface materials.

It was seen early on in the model development that holding the figure of merit Z constant while variably mixing the ratios of Seebeck coefficient, resistivity, and thermal conductivity can change the time required to return to steady state. From a design standpoint, transient penalty may be difficult to eliminate. It is possible the Transient Penalty may be reduced by using material properties with an optimum mix of Seebeck coefficient, resistivity and thermal conductivity. Optimizing the material for minimum Transient Penalty or optimizing any of the transient characterizations could be a topic of future study.

Future parallel paths to materials research should consider novel ways to decrease joule heat or preferentially send it to the hot side of the device.

There was seen a very small increase in COP within the first 0.5 to one second of the pulse during the study of variable internal heat generation of the mass connected to the thermoelectric module. This phenomenon should be studied in more detail. It is apparent that Q_c is increasing faster than P_{in} for this short time. Knowledge

of why this happens and under what range of conditions could lead to a transient performance increase over steady state operation.

The accuracy of the SPICE model could be improved by making the Peltier effect temperature dependent. Currently the model uses a predetermined T_c which is the desired steady state mass temperature. Including temperature dependence would improve the transient accuracy of the model. This is especially the case for the couple model because the change in T_c is much greater than for the system model.

Currently the convection heat transfer coefficients related to the mass and insulation are predetermined for the intended mass operating temperature. A future model improvement would be to design the convection coefficients to automatically update as mass and ambient temperatures change.

References

[1] Alfred Piggott, Dmitri Kossakovski, and Todd Barnhart. Thermoelectric-Based Thermal Management System, U.S. Patent No. 2015/0357692 A1, Dec. 10, 2015.

[2] Improving efficiency of a vehicle HVAC system with comfort modeling, zonal design, and thermoelectric devices, 2012 Deer Conference.

[3] Thermotek. Medical Devices, 2015. `http://www.thermotekusa.com/medical_devices.php`.

[4] Thermoelectric Air Conditioner Applications (TACA) http://www.thermoelectric.com/2010/applications/ac.htm.

[5] Hot spot cooling using embedded thermoelectric coolers, 2nd IEEE SEMI-THERM Symposium, 2006.

[6] Microsystems TEC. Bulk and tiny - world smallest bulk technology thermoelectric cooler, 2010. downloaded Sep. 2015, http://www.tec-microsystems.com/.

[7] Laird Technologies. Thermoelectric Handbook, 2014. http://www.lairdtech.com/temhandbook/.

[8] M. Manno, Wang Peng, and A. Bar-Cohen. Pulsed thermoelectric cooling for improved suppression of a germanium hotspot. *Components, Packaging and Manufacturing Technology, IEEE Transactions on Components, Packaging, and Manufacturing Technology*, 4(4):602–611, 2014.

[9] Douglas T. Crane and Lon E. Bell. Design to maximize performance of a thermoelectric power generator with a dynamic thermal power source. *Journal of Energy Resources Technology*, 131(1), 2009.

[10] Madhav Karri. *Thermoelectric Power Generation System Optimization Studies.* PhD Dissertation, Clarkson University, 2011.

[11] Caltech. Brief history of thermoelectrics. http://www.thermoelectrics.caltech.edu/thermoelectrics/history.html.

[12] T. J. Seebeck. *Magnetische Polarisation der Metalle und Erze durch Temperatur-Differenz (Magnetic polarization of metals and minerals by temperature differences).* Abhandlungen der Königlichen Akademie der Wissenschaften zu Berlin (Treatises of the Royal Academy of Sciences in Berlin), 1825.

[13] Daniel D. Pollock. *Physical Properties of Materials for Engineers 2nd Addition*. CRC Press, 1993.

[14] D.M. Rowe. *Thermoelectric Handbook, Macro To Nano*. Taylor & Francis Group, LLC, 2006.

[15] Leon van Dommelen. Thermoelectric Effects, last accessed 10/28/2015, `http://www.eng.fsu.edu/~dommelen/quantum/style_a/nt_pelt.html`.

[16] Gentherm. Climate Seats, http://www.gentherm.com/en/page/climate-seats.

[17] Gentherm. Thermal Convenience, http://www.gentherm.com/en/page/thermal-convenience.

[18] kryotherm. Thermoelectric coolers for domestic cooling devices. http://kryothermtec.com/thermoelectric-coolers-for-domestic-refrigerating-devices.html.

[19] Gentherm. Our revolutionary climate control sleep system (ccss), http://www.gentherm.com/en/page/bedding.

[20] Gentherm. Personalized microclimate technology, http://www.gentherm.com/en/page/furniture.

[21] V S Yadav. *Engineering Physics*. Tata McGraw-Hill Publishing Company Limited, 2009.

[22] Northwestern University. Thermoelectrics - Northwestern Materials Science and Engineering, 2015. http://thermoelectrics.matsci.northwestern.edu/thermoelectrics/index.html.

[23] Taylor Sparks. How do thermoelectrics work?, Found 10/28/2015. URL http://www.eng.utah.edu/ sparks/how-do-thermoelectrics-work.html. downloaded from http://www.eng.utah.edu.

[24] D. Zhao. A review of thermoelectric cooling: Materials, modeling and applications. *Applied Thermal Engineering*, 66(1):15, 2014. ISSN 1359-4311.

[25] T.C. Harman, M.P. Walsh, B.E. Laforge, and G.W. Turner. Nanostructured thermoelectric materials. *Journal of Electronic Materials*, 34, 2005.

[26] Lon E. Bell. Cooling, heating, generating power, and recovering waste heat with thermoelectric systems. *Science*, 321:1457–1461, 2008.

[27] G. Jeffrey Snyder, Jean-Pierre Fleurial, Thierry Caillat, Ronggui Yang, and Gang Chen. Supercooling of peltier cooler using a current pulse. *Journal of Applied Physics*, 92(3):1564, 2002.

[28] LS Stilbans and NA Fedorovich. Cooling of thermoelectric cells under nonstationary conditions. *Soviet Physics. Technical Physics*, 3:460–463, 1958.

[29] J. Parrott. The interpretation of the stationary and transient behaviour of refrigerating thermocouples. *Solid-State Electronics*, 1(2):135–143, 1960.

[30] K. Landecker Findlay and A.W. Study of fast transient behavious of peltier junctions. *Soild-State Electronics*, 3:239–260, 1961.

[31] Robert R Heikes and Roland W Ure. *Thermoelectricity: Science and Engineering*. Interscience Publishers New York, 1961.

[32] M. Idnurm and K. Landecker. Experiments with peltier junctions pulsed with high transient currents. *Journal of Applied Physics*, 34(6):1806, 1963.

[33] Babin VP. Enhancement of thermoelectric cooling in non stationary operation. *Soviet Physics*, 14:293–8, 1969.

[34] K Landecker. Some further remarks on the improvement of peltier junctions for thermoelectric cooling. *Energy Conversion*, 14(1):21–33, 1974.

[35] R. Field and H. Blum. Fast transient behavior of thermoelectric coolers with high current pulse and finite cold junction. *Energy Conversion*, 19(3):159–165, 1979. ISSN 0013-7480.

[36] A. Miner, A. Majumdar, and U. Ghoshal. Thermoelectromechanical refrigeration based on transient thermoelectric effects. *Applied Physics Letters*, 75(8):1176, 1999.

[37] A. Ravi Kumar, R.G. Yang, G Chen, and J.P. Fleurial. Transient thermoelectric cooling of thin film devices. *Materials Research Society Symosia Proceedings*, 626:Z11–4, 2000.

[38] A. Chakraborty. Thermodynamic formulation of temperature-entropy diagram for the transient operation of a pulsed thermoelectric cooler. *International Journal of Heat and Mass Transfer*, 49(11):1845, 2006.

[39] Q. Zhou, Z. Bian, and A. Shakouri. Pulsed cooling of inhomogeneous thermoelectric materials. *Journal of Physics D: Applied Physics*, 4014):4376–4381, 2007.

[40] M. Gupta, M. Sayer, S. Mukhopadhyay, and S. Kumar. Ultrathin thermoelectric devices for on chip peltier cooling. *IEEE Transactions on Components, Packaging and Manufacturing Technology*, 1(9):1395–1405, 2011.

[41] L. M. Shen, F. Xiao, H. X. Chen, and S. W. Wang. Numerical and experimental analysis of transient supercooling effect of voltage pulse on thermoelectric element. *International Journal of Refrigeration*, 35(4):1156–1165, 2012.

[42] I.V. Bezsudnov and A.A. Snarskii. Rotating thermoelectric device in periodic steady state, PACS No: 72.15.Jf, 72.20.Pa, Institute of Information Recording NAS, Kiev, Ukraine, 2014.

[43] M. Ma. A numerical study on the temperature overshoot characteristic of a realistic thermoelectric module under a current pulse operation. *International journal of heat and mass transfer*, 72:234, 2014.

[44] L. Shen. The step-change cooling performance of miniature thermoelectric module for pulse laser. *Energy Conversion and Management*, 80:39, 2014.

[45] Owen A. Sullivan. *Embedded Thermoelectric Devices For On-chip Cooling And Power Generation*. PhD Dissertation, Georgia Institute of Technology, 2012.

[46] Hao Lv, Xiao-Dong Wang, Tian-Hu Wang, and Jing-Hui Meng. Optimal pulse current shape for transient supercooling of thermoelectric cooler. *Energy*, 83: 788–796, 2015.

[47] T. Thonhauser, G. D. Mahan, L. Zikatanov, and J. Roe. Improved supercooling in transient thermoelectrics. *Applied Physics Letters*, 85(15):3247, 2004.

[48] Ming Ma, Jianlin Yu, and Jiaheng Chen. An investigation on thermoelectric coolers operated with continuous current pulses. *Energy Conversion and Management*, 98:275–281, 2015.

[49] Gabriel Eduardo Hoyos, KR Rao, and D Jerger. Fast transient response of novel peltier junctions. *Energy Conversion*, 17(1):45–54, 1977.

[50] *Geometric Effects on the Transient Cooling of Thermoelectric Coolers*, Thermoelectric Materials 2001 - Research and Applications: Symposium, vol 691, G8-G27, Boston, Massachusetts, USA, November 26-29, 2001.

[51] A . F. Robertson and Daniel Gross. An electrical-analog method for transient heat-flow analysis. *Journal of Research of the National Bureau of Standards*, 1958.

[52] L. W. Nagel and D. O. Pederson. Spice (simulation program with integrated circuit emphasis). Memorandum No. ERL-M382, University of California, Berkeley, 1973.

[53] J. A. Chavez, J. A. Ortega, J. Salazar, A. Twb, and M.J. Garcia. Spice model of thermoelectric elements including thermal effects. *IEEE*, 2000.

[54] *Spice Compatible Equivalent Circuit of the Energy Conversion Process in Thermoelectric Modules*, 2004.

[55] Simon Lineykin and Sam Ben-Yaakov. Analysis of thermoelectric coolers by a spice-compatible equivalent-circuit model. *IEEE Power Electronics*, 2005.

[56] Daniel Mitrani, Jordi Salazar, Antoni Turi, Miguel J. Garcia, and Juan A. Chavez. Transient distributed parameter electrical analogous model of TE devices. *Microelectronics Journal*, 40(9):1406–1410, 2009.

[57] G. Hoyos and D. Jerger. Numerical analysis of transient behavior of thermoelectric coolers. *Energy conversion*, 17(1):23–29, 1977.

[58] E.E. Looman and D. C. Antonova, *Finite Elements for Thermoelectric Device Analysis in ANSYS*, 2005. 2005 International Conference on Thermoelectrics.

[59] Martin Jaegle. Multiphysics simulation of thermoelectric systems - modeling of peltier-cooling and thermoelectric generation. *Excerpt from the Proceedings of the COMSOL Conference*, Hannover, 2008.

[60] Owen Sullivan, Borislav Alexandrov, Saibal Mukhopadhyay, and Satish Kumar. 3d compact model of packaged thermoelectric coolers. *Journal of Electronic Packaging*, 135(3):031006, 2013.

[61] Robert Simons. Calculation corner: Using vendor data to estimate thermoelectric module cooling performance in an application environment, July 2010. http://www.electronics-cooling.com/2010/07/using-vendor-data-to-estimate-thermoelectric-module-cooling-performance-in-an-application-environment/.

[62] Melcor. Melcor thermal solutions, email correspondence with Daniel Mitrani, March 2015.

[63] HoSung Lee. Thermoelectric Coolers, downloaded December 2014. `http://homepages.wmich.edu/~leehs/ME539/Thermoelectric%20Coolers%20for%20class.pdf`.

[64] Melcor. Thermoelectric Handbook, `https://home.zhaw.ch/~fusa/PSS_VLE_C/CHAPTER_03/CASES/Materials/Melcor_TE_Handbook.pdf`.

[65] S.J. Drakea, D.A. Wetz, J.K. Ostanek, S.P. Miller, J.M. Heinzel, and A. Jain. Measurement of anisotropic thermophysical properties of cylindrical li-ion cells. *Journal of Power Sources*, 252:298–304, 2014.

[66] Accuratus.com. Aluminum nitride, AIN Ceramic Properties, 2013. http://accuratus.com/alumni.html.

[67] *Thermal Interface Materials for Power Electronics Applications*, 2008. http://www.nrel.gov/docs/fy08osti/42972.pdf.

[68] Moran Wang and Ning Pan. Modeling and prediction of the effective thermal conductivity of random open-cell porous foams. *International Journal of Heat and Mass Transfer*, 51:1325-1331, 2008.

[69] Wit Witkiewicz and Andrzej Zielinski. Properties of the polyurethane (PU) light foams. *Advances in Materials Science*, 6(2):36–51, October 2006.

[70] Federation Of European Rigid Polyurethane Foam Associations. Thermal insulation materials made of rigid polyurethane foam (PUR/PIR) properties - manufacture, October 2006. `http://www.excellence-in-insulation.eu/site/fileadmin/user_upload/PDF/Thermal_insulation_materials_made_of_rigid_polyurethane_foam.pdf`.

[71] thermopedia.com. Thermal Contact Resistance. http://www.thermopedia.com/content/1188/ (2011).

[72] Robert E. Simons, Simplified formula for estimating natural convection heat transfer coefficient on a flat plate, August 2001 http://www.electronics-cooling.com/2001/08/simplified-formula-for-estimating-natural-convection-heat-transfer-coefficient-on-a-flat-plate/.